GUANIDINE-SULFONATE METAL COMPLEXES FOR OLEFIN POLYMERIZATION, ISOCYANIDE POLYMERIZATION, AND RING-OPENING POLYMERIZATION OF CYCLIC ESTERS

NICHOLAS LUIGI MICELI

THESIS SUBMITTED TO THE FACULTY OF GRADUATE STUDIES IN PARTIAL FULFILMENT OF THE REQUIREMENTS FOR THE DEGREE OF

MASTER OF SCIENCE

GRADUATE PROGRAM IN CHEMISTRY

YORK UNIVERSITY

TORONTO, ONTARIO

June 2026

© NICHOLAS LUIGI MICELI, 2026

Abstract

Herein are reported synthesis methods and structural elucidation of a novel ligand family of guanidine-sulfonates. These monoanionic chelating ligands were coordinated to palladium(II), nickel(II), and zinc(II) to form novel complexes which were applied for preliminary polymerization activity studies. Palladium(II) catalysts were tested for polymerization of norbornene and tert-butyl and 2,6-dimethylphenyl isocyanide, yielding oligomers as confirmed by NMR and mass spectrometry. Palladium(II) and zinc(II) bis-chelated catalysts were tested for ring-opening polymerization of lactide to polylactic acid under solventless conditions at 130 ºC, the most active catalyst yielding high tacticity control while rates remained within an order of magnitude of the industrial standard.

Computational chemistry was implemented to provide deeper insight into the structure and stability of guanidine-sulfonate ligands and palladium(II) complexes thereof. Single crystal X-ray diffraction was used in the structural elucidation of two guanidine-sulfonate ligands, as well as three palladium(II) complexes containing guanidine-sulfonate species and one guanidine-phenolate containing palladium(II) complex.

Acknowledgements

I would first like to acknowledge Dr. Gino G. Lavoie for providing me an opportunity to grow as a chemist. With his trust, guidance, and meticulousness, Dr. Lavoie created and atmosphere for the development of invaluable skills whose depth extends even beyond the field of chemistry. I hope to continue to embody the values the Lavoie lab has instilled within me as I move forward as a chemist. I would like to thank my supervisory committee, Professors Caputo and Baumgartner, for their patience and guidance throughout my time at York. I am very thankful for Dr. Howard Hunter and Dmitry Pichugin both for their help as NMR specialists and for their pleasant conversation that was always uplifting. I would also like to thank Dr. Ryan Hili for his help and support throughout my time at York.

I would also like to acknowledge the amazing work colleagues and friends that I was fortunate enough to meet during my time at York. My labmates, Víctor Flores-Romero and Lya Campos-Rivera, I am so grateful to have met you, not only for your mentorship but for the joy and calm that your presence provided me. While our paths have diverged, I hope to see you both again soon. To Jesse LeBlanc, I thank you for your crystallographic know-how, friendship, and willingness to discuss chemistry at any and all occasions. To my cohorts from the van Wijngaarden, Caputo, Orellana, and Lee labs, thank you all for your friendship and endless support.

Finally, to my family, words are not enough to describe all that you've done for me. All that I have achieved is a consequence of your help and sacrifice, I love you all.

Table of Contents

Abstract ii
Acknowledgements iii
Table of Contents iv
List of Abbreviations v
List of Figures vi
List of Schemes viii
List of Tables ix
1. Introduction 1
1.1 Polyolefins 1
1.1.1 Polyolefin Catalysis Methods 3
1.1.2 Transition Metal Based Polyolefin Catalysis 7
1.1.3 Polynorbornene 11
1.2 Polylactide 12
1.2.1 Polylactide Synthesis Methods 12
1.2.2 Polylactide Catalysts 16
1.3 Polyisocyanides 18
1.4 Guanidine-Containing Ligands 21
1.5 Scope of Thesis 23
2. Results and Discussion 26
2.1 Synthesis of Guanidinium-Sulfonate Ligands 26
2.2 Transition Metal Complexes of Guanidinium–Sulfonate Ligands 34
Section 2.3 Polymerization Studies 52
Section 2.3.1 Olefin Polymerization 52
Section 2.3.2 Isocyanide Polymerization 56
Section 2.3.3 Lactide Polymerization 58
3. Conclusions 61
4. Experimental 63
5. References 70
Appendix 75

List of Abbreviations

ADMET	Acyclic Diene Metathesis Polymerization
Alk	Alkyl
AMM	Activated Monomer Mechanism
Ar	Aryl
COD	Cyclooctadiene
DCM	Dichloromethane
DMIC	2,6-dimethylphenyl isocyanide
DMSO	Dimethylsulfoxide
DFT	Density Functional Theory
iPr	Isopropyl
LA	Lactic Acid
Lut	Lutidine
KOtBu	Potassium tert-butoxide
MeCN	Acetonitrile
MLC	Metal-Ligand Cooperation
Mn	Number-Average Molecular Weight
Mw	Weight-Average Molecular Weight
NB	Norbornene
NMR	Nuclear Magnetic Resonance
Nu	Nucleophile
ORTEP	Oak Ridge Thermal Ellipsoid Plot
PE	Polyethylene
PIC	Polyisocyanide
PLA	Polylacticacid
PNB	Polynorbornene
PO	Polyolefin
Py	Pyridine
ROMP	Ring-Opening Metathesis Polymerization
ROP	Ring-Opening Polymerization
XRD	X-Ray Diffraction
VT	Variable Temperature

List of Figures

Figure 1. Copolymers classified by their structure. Adapted from de Bruin B. et al., Chem. Soc. Rev. **2013**, 42 (13), 5809–5832. 1
Figure 2. Grubbs 1st-generation catalyst (left) and Hoveyda-Grubbs 2nd-generation catalyst (right).[10] 4
Figure 3. Coordination-insertion mechanism for ethylene. 5
Figure 4. Tacticity of polypropylene 7
Figure 5. Kaminsky catalysts, used with an MAO cocatalyst to polymerize olefins. While (a) exercises no polyolefin tacticity, (b) has shown to produce isotactic polypropylene. 7
Figure 6. Brookhart et al.'s diimine containing complex, M = Ni(II) or Pd(II) 8
Figure 7. Grubbs et al.'s neutral salicyldiminato containing complex. 9
Figure 8. Nozaki et al.'s phosphine-sulfonate containing complex. 9
Figure 9. Xu et al's phosphine-sulfonate containing complex. 10
Figure 10. One of Eisen et al.'s group 10 norbornene copolymerization catalysts. 11
Figure 11. Copolymers of norbornene (NB) with functionalized monomers. 11
Figure 12. L and D enantiomers of lactic acid. 12
Figure 13. Activated monomer mechanism for polymerizing lactide reproduced from literature. 13
Figure 14. Stereoisomers of Lactide. 14
Figure 15. Tacticity of PLA and the corresponding starting LA stereoisomers. 14
Figure 16. Representation of a homodecoupled ^{1}H-NMR experiment, removing scalar coupling of methyl and methine protons to yield singlets representative of different monomer arrangement patterns.[22] 15
Figure 17. Tin octanoate industrial standard. 16
Figure 18. One of Herres-Pawlis' zinc-based PLA catalysts. 17
Figure 19. Preparation of polyisocyanide. 18
Figure 20. Generic coordination-insertion mechanism for isocyanide. 18
Figure 21. Porphyrin bearing polyisocyanide. 20
Figure 22. Generic structures of guanidine and some derivatives. 21
Figure 23. One of Herres-Pawlis' iron(II), guanidine-containing lactide catalysts. 21
Figure 24. (a) Guanidine-phenolate and (b) guanidine-ethenolate ligands. 22
Figure 25. Solid-state structure of ligand **L1**-H. Hydrogen (white), carbon (grey), nitrogen (blue), oxygen (red), sulfur (yellow). For clarity, solvent and hydrogen atoms have been removed, except for the hydrogen bound to nitrogen N1 with its position located on the Fourier difference map. ORTEP drawn at 50% probability. 26
Figure 26. Generic representation of cyclic guanidine's C-N bonds labelled corresponding to equation 3. 27
Figure 27. Generic resonance forms of guanidinium-sulfonates. 28

Figure 28. Solid-state structure of ligand **L4•**$HNEt_3$. The counterion $HNEt_3^+$ has been omitted for clarity. Carbon (grey), nitrogen (blue), oxygen (red), sulfur (yellow). ORTEP drawn at 50% probability. 32
Figure 29. Solid-state structure of Pd(**L1**)(allyl), **(a)** depicts the complex perpendicular to the plane in which each of the ligands coordinates to the metal centre, **(b)** and **(c)** show enantiomers observed in the crystal's unit cell. Palladium (green), carbon (grey), nitrogen (blue), oxygen (red), sulfur (yellow). 35
Figure 30. Different crystal fields formed from repulsion of coordinated ligands (top). Orbital filling for tetrahedral and square-planar fields for a d^8 system (bottom). 36
Figure 31. Variable-temperature ^{1}H-NMR spectra ranging from 300 to 231 K for Pd(**L1**)(allyl), collected on a 300 MHz instrument. Isomers observed due to allylic fluxional behaviour are identified on the spectrum collected at 231 K. 39
Figure 32. Cis and trans isomers of Pd(**L1**)(Me)(MeCN). Isomers have been identified as cis or trans when the coordinating exocyclic nitrogen and acetonitrile moieties are cis or trans to one another. 42
Figure 33. Solid-state structure obtained of Pd(**L1'**)$(MeCN)_2$. Protons are omitted for clarity with the exception of the proton present on N1. Palladium (green), hydrogen (white), carbon (grey), nitrogen (blue), oxygen (red), sulfur (yellow). 44
Figure 34. Generic Illustration of **L1**-H being deprotonated by coordinated base (B) via metal-ligand cooperation. 47
Figure 35. Solid-state structure for Pd(**L1**)$_2$. Hydrogen atoms have been omitted for clarity. Palladium (green), carbon (grey), nitrogen (blue), oxygen (red), sulfur (yellow). 48
Figure 36. Solid-state structure for Pd(**phenolate-1**)$_2$. Hydrogen atoms have been omitted for clarity. Palladium (green), carbon (grey), nitrogen (blue), oxygen (red). 50
Figure 37. Mass spectrometric Data for 10 : 1 norbornene : Pd(**L1**)(Me)(MeCN) oligomerization at different elution times (Left: 2.73 – 2.89 minutes, Right: 4.70 – 4.86 minutes). 53
Figure 38. Single-insertion product upon addition of 2,6-dimethylphenyl isocyanide to Pd(**L1**)(Me)(MeCN) (left) and trimer formed upon addition of 3 equivalents of tert-butyl isocyanide to Pd(**L1**)(Me)(MeCN) (right). 56

List of Schemes

Scheme 1. Ionic polymerization leading to chain-transfer from polyisobutylene to monomer. 3
Scheme 2. Takahashi (top) and Lavoie (bottom) mononuclear palladium(II) based catalysts forming trimeric isocyanide oligomer. 19
Scheme 3. Takahashi's binuclear palladium(II) and platinum(II) catalyst polymerizing isocyanide. 19
Scheme 4. A generic reaction scheme for guanidinium-sulfonate ligand synthesis. 23
Scheme 5. Synthesis routes to coordinate a guanidinium-sulfonate ligand to a series of nickel(II) and palladium(II) precursors....24
Scheme 6. Ligand synthesis methods used to synthesise ligands **L1**-H**, L2**-H, **L3**-H, and **L4**•$HNEt_3$....30
Scheme 7. Pathways for monochelated coordination of **L1** and **L4** to group 10 metal centres...34
Scheme 8. Fluxional behaviour of Pd(**L1**)(allyl). Interconversion of isomers occurs by changing coordination mode of the allyl moiety from η_3 to η_1 where rotations about the C—C single bonds yield either **isomer a** or **isomer b** upon reverting to η_3 coordination. 39
Scheme 9. A proposed mechanism through which Pd(**L1**)(Me)(py) may react intramolecularly in acetonitrile in order to produce Pd(**L1'**)$(MeCN)_2$. L represents either MeCN or Py. 45
Scheme 10. An alternative proposed mechanism for the decomposition of Pd(**L1**)(Me)(MeCN) to Pd(**L1'**)(MeCN)2 following an alternative intramolecular reaction pathway. 46
Scheme 11. Synthesis of bis-chelated nickel, palladium, and zinc-based catalysts. 47
Scheme 12. Migratory Insertion of one equivalent of norbornene into the Pd(**L1**)(Me)(MeCN) catalyst. 52

List of Tables

Table 1. Selected bond lengths and dihedral angles of ligands **L1**-H and **L4**•$HNEt_3$ and calculated ρ values. 28
Table 2. Selected bond lengths and angles in Pd(**L1**)(allyl), Pd(**L1'**)$(MeCN)_2$, Pd(**L1**)$_2$, and Pd(**phenolate-1**)$_2$ 38
Table 3. Results of solvent-free ring-opening polymerizations of *rac*-lactide 58

1. Introduction

1.1 Polyolefins

Polyolefins have many industrial and everyday applications, from safe packaging of materials to automotive parts and architecture.[1] Olefins, hydrocarbons containing one or more non-cumulated carbon-carbon double bond(s), are building blocks for the synthesis of ubiquitous polyolefins (PO), such as polyethylene (PE), polypropylene, and polymethylmethacrylate that comprise over half of the 400 million tonnes of synthetic polymers produced annually around the globe.[2] Polyolefins find widespread industrial applications owing to myriad useful properties, including durability, hydrolysis resilience, and low cost.[2] Polyolefins can also be functionalized to radically affect physical properties such as adhesion, toughness, solubility, chemical resistance etc., greatly broadening their applicability in industry.[3]

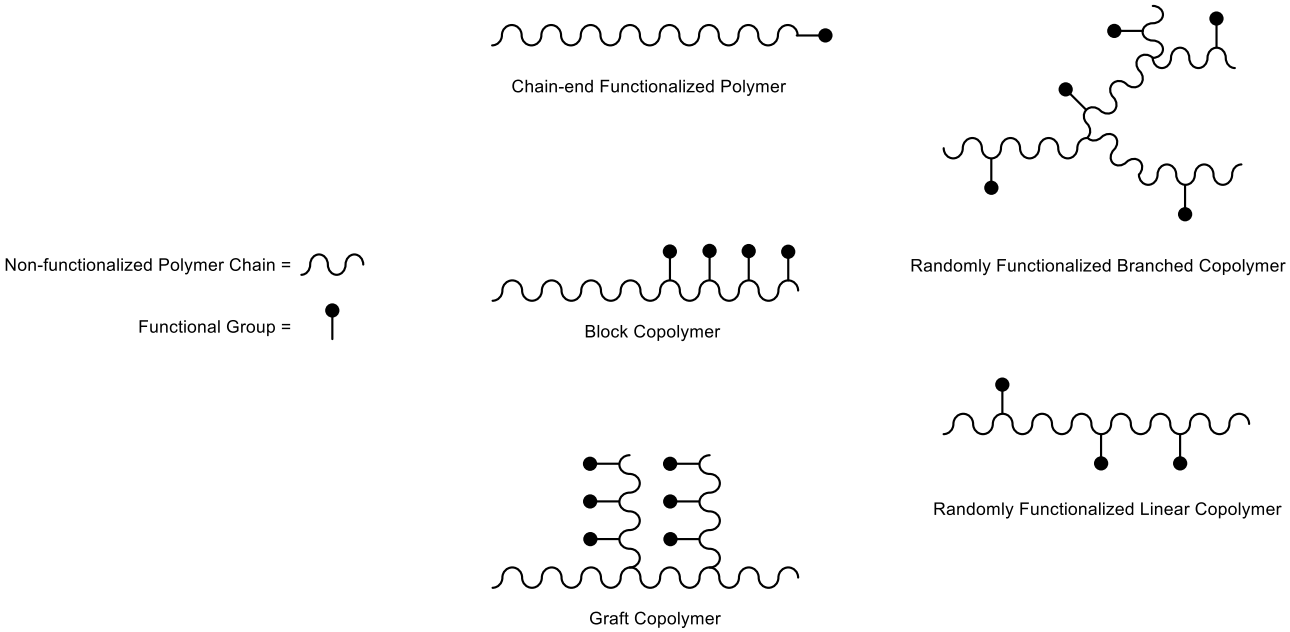

Figure 1. *Copolymers classified by their structure. Adapted from de Bruin B. et al.,* Chem. Soc. Rev. ***2013****,* 42 *(13), 5809–5832.*

Functionalized polyolefins can vary significantly in structure, from chain-end functionalized, block, or graft copolymers, to randomly functionalized linear and branched copolymers (**Figure 1**). Chain-end functionalized copolymers leverage their functionalized end for synthesis of more complex copolymers (like graft copolymers). Like chain-end copolymers, graft and block copolymers incorporate polar functional groups into the structure of the polymer, while retaining many properties of the non-functionalized polymer, such as crystallinity, melting point, and hydrophobicity.[4] Randomly functionalized copolymers owe their altered physical properties to the sporadically dispersed functional groups along the polymer's backbone, which in turn yields a reduction in polymer crystallinity and changing a host of other properties, broadening industrial applicability even further.[4]

Polymer post-functionalization is a common industrial tactic to synthesize randomly functionalized copolymers by retroactively functionalizing an otherwise non-functionalized polymer chain. Harsh conditions (high temperature, unpredictable radical reactions) are typically required to modify the largely unreactive C-H bonds of the non-functionalized polymer, which can yield undesirable side reactions like cross-linking (covalent bonding of multiple points of a polymer chain to one another in a web-like fashion).[4,5,6] Alternative methods involving transition metal C-H bond activation are of interest, though they remain limited by low alkane conversion and turnover numbers.[6] Direct copolymerization circumvents the pitfalls of post-functionalization methods, and can provide additional control over monomer incorporation by tuning the rate of insertion mediated by a chosen catalyst as well as ratios of functionalized and non-functionalized monomer present during copolymerization.[4]

1.1.1 Polyolefin Catalysis Methods

Since the discovery of polyolefins over 100 years ago, many methods for polymerizing olefins have been explored.[7] Radical and ionic methods of polymerization involve utilizing radical or ionic initiators for polymerization.[8]

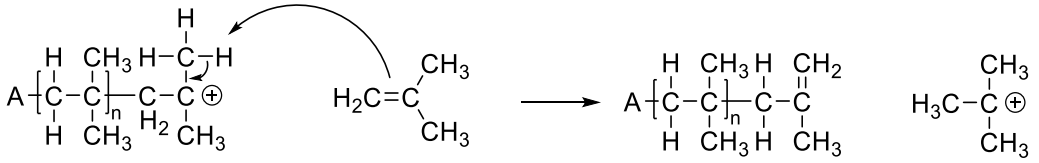

Scheme 1. *Ionic polymerization leading to chain-transfer from polyisobutylene to monomer.*

While radical polymerization methods may be used for the synthesis of many functionalized polymers such as polyacrylates and polystyrenes,[8] both radical and ionic methods tend to encounter issues with chain-transfer, where the propagating chain reacts with another species (another growing chain, or monomer unit for instance), transferring the location of the active site, potentially causing unwanted branching of the polymer (**Scheme 1**).[8]

Other methods of polymerizing olefins, like ring-opening metathesis polymerization (ROMP) and acyclic diene metathesis polymerization (ADMET) utilize transition metal complexes with Fischer carbenes (carbenes strongly bound to a metal center through a metal-carbene double bond) as ligands (**Figure 2**) to initiate and propagate polymerizations.[8,9] ROMP

and ADMET are somewhat limited in applicability due to constraints over monomer selection, as their names imply, ROMP is limited to cyclic olefins and ADMET to acyclic dienes.

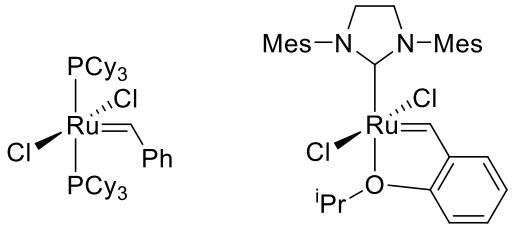

Figure 2. *Grubbs 1st-generation catalyst (left) and Hoveyda-Grubbs 2nd-generation catalyst (right).*[10]

Grubbs catalysts (**Figure 2**) have evolved to yield efficient metathesis capable of copolymerizing with a variety of polar olefins, though limitations of tacticity control, degree of copolymer incorporation, and low molecular weight of copolymers remain an issue.[4, 10]

While ROMP and ADMET can produce copolymers their aforementioned limitations reduce the extent of industrial applicability. The prospect of accessing a large library of copolymers using transition metal-mediated catalytic methods to produce copolymers remains an area of particular interest and challenge. The high activity of early transition-metal catalysts makes them good candidates for olefin polymerization; this high activity conversely limits their effectiveness for copolymerization as polar moieties tend to react with and poison the catalyst. Late transition-metal complexes are of particular interest for copolymerization, though they experience issues with low polar monomer incorporation and β-heteroatom elimination, the latter of which often deactivates a catalyst.[10] Tuning these transition-metal mediated copolymerizations to control the degree of monomer insertion as well as polymer tacticity involves designing and modifying coordinated ligands, as described in section 1.4.

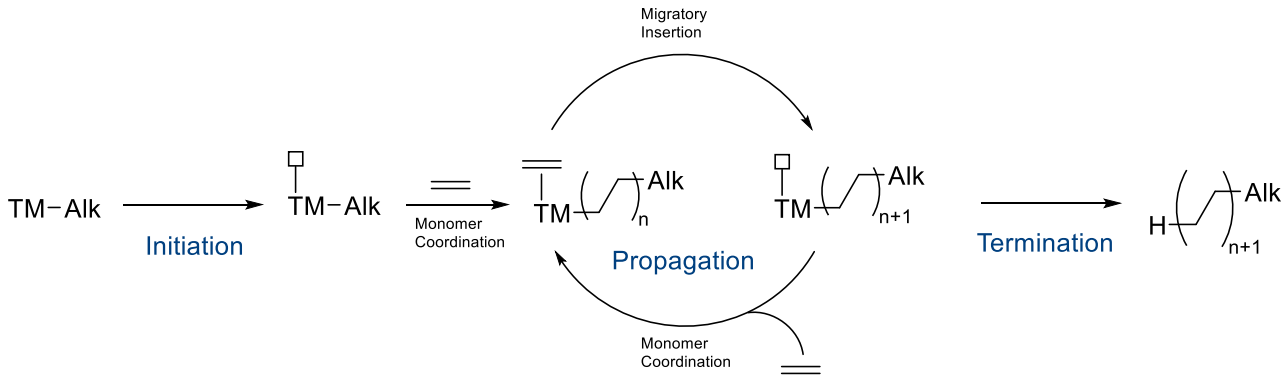

Figure 3. *Coordination-insertion mechanism for ethylene.*

The coordination-insertion mechanism (**Figure 3**) involves the transition metal (TM) catalyst whose open site (pictured as a vacant box) provides a space in which monomer may coordinate, before undergoing migratory insertion into the growing polymer chain, terminated with an alkyl group (Alk). In the initiation step, a vacant spot for coordination of the monomer unit is achieved either through dissociation of a labile ligand, or through addition of an initiator to abstract a ligand from a pre-catalyst, generating the active catalyst. During propagation, the polymer chain continues to grow via coordination of monomer followed by migratory insertion wherein the growing chain migrates to the new monomer unit, extending the polymer. Finally, termination involves the cleavage of the growing chain from the transition metal catalyst, typically through the addition of a terminating agent such as an alcohol.

For migratory insertion to occur, the nucleophilic metal-alkyl bond is proposed to attack the antibonding π* orbital of the coordinating olefin.[11] This leads to breaking of the olefinic double bond and formation of a new carbon-carbon bond. Generally, early transition metals can accept the electron density being donated through η^2 coordination of the olefin, but being electron deficient, cannot significantly back-donate to the olefin's π* orbital. Late transition metals, however, with their occupied non-bonding d-orbitals, back-donate significantly to the olefin's π* orbital, reducing its electrophilicity, leading to higher barriers for migratory insertion. β-hydride

elimination is thus more competitive as insertion barriers increase, which in turn leads to chain walking and increased branching.

1.1.2 Transition Metal Based Polyolefin Catalysis

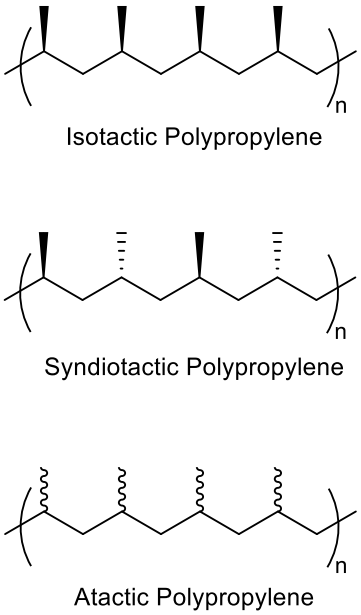

Figure 4. *Tacticity of polypropylene*

In the early 1950s, Karl Ziegler designed the first titanium-based polyethylene catalyst, an ill-defined system prepared by combining titanium tetrachloride with triethyl aluminum. Giulio Natta later utilized these catalysts to prepare stereoregular (isotactic) polypropylene **Figure 4**.[1] These catalysts are generally limited to polymerizing ethylene and propylene. In order to exercise significant control over the physical properties of the material, polar fragments may be incorporated into the structure of the polymer by adding polar monomer into the normal monomer mixture.[3]

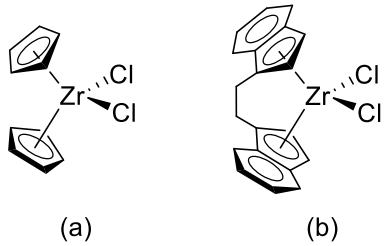

Figure 5*. Kaminsky catalysts, used with an MAO cocatalyst to polymerize olefins. While (a) exercises no polyolefin tacticity, (b) has shown to produce isotactic polypropylene.*

Following the success of the heterogeneous Ziegler-Natta catalyst, attempts to polymerize olefins using transition metal-based catalysts yielded limited results. In 1980, Sinn and Kaminsky were able to apply group 4 metallocenes, such as Cp_2ZrCl_2, activated with a methylalumoxane (MAO) cocatalyst as active catalysts for polymerization of a variety of olefins.[12] These early transition metal containing catalysts are highly oxophilic, increasing their activity for olefin polymerization while at the same time causing significant deactivation of the catalyst in the presence of polar monomers due to binding of the polar fragment to the catalyst.[3] In contrast, later transition metal based catalysts, such as palladium and nickel-based catalysts, have garnered interest due to their relatively low oxophilicity, making them ideal choices for polar monomer incorporation.[3]

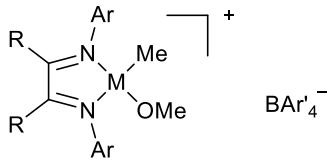

Figure 6. *Brookhart et al.'s diimine containing complex, M = Ni(II) or Pd(II)*

In 1995, Brookhart *et al.* reported bidentate α-diimine ligand based Pd(II) and Ni(II) catalysts (**Figure 6**) that were used to convert ethylene and α-olefins to polymers with molecular weights between 1.8 – 1,600 kg mol^{-1} and 1.2 – 300 branches per 1000 carbons. The polymers had unique microstructures (branched, amorphous polymers or linear, semicrystalline materials), mediated by temperature, ethylene pressure and ligand substituents.[3, 13, 14] These cationic catalysts are able to produce copolymers with functionalized vinyl monomers. However, issues of chain walking, where the site at which insertion occurs changes via β-hydride elimination and isomerization, arose, as this process can yield less desirable amorphous branching polymers.[14]

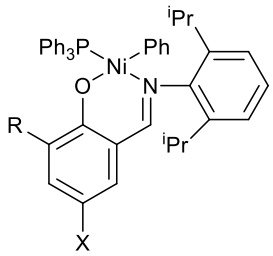

Figure 7. *Grubbs et al.'s neutral salicyldiminato containing complex.*

In 1998, Grubbs *et al.* reported neutral Ni(II) salicylaldiminato complexes for polymerization of ethylene to linear polymers, with molecular weights around 4.0 – 360 kg mol^{-1}, under moderate conditions (7 – 14 atm) with a phosphine scavenger (nickel cyclooctadiene, $Ni(COD)_2$) (**Figure 7**).[15] By modifying the substituents on the phenolate ring, Grubbs *et al.* were able to reduce branching (5 – 55 branches per 1000 carbon units) and increase catalytic activity, additionally providing greater functional group tolerance when compared to the cationic counterparts established by Brookhart *et al.* [13, 14]

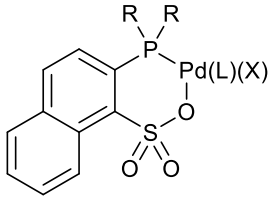

Figure 8. *Nozaki et al.'s phosphine-sulfonate containing complex.*

More recently, Nozaki *et al.* established a series of neutral Ni(II) and Pd(II) complexes incorporating phosphine-sulfonates that have produced highly linear ethylene polymers and linear copolymers with polar monomers (**Figure 8**).[13] While polar monomer incorporation grows more and more facile with each iteration of catalyst discussed above, the underlying issue affecting each of these catalysts remains: low reaction rates and the limited control over the level to which polar monomers are incorporated.

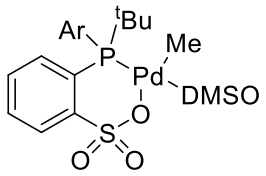

Figure 9. *Xu et al's phosphine-sulfonate containing complex.*

In 2024, Chen and Xu demonstrated high comonomer incorporation (about 20-30%) of norbornene with ethylene. Norbornene is a cyclic olefin discussed in section 1.1.3, (and polar variations thereof) into high molecular weight copolymers (up to 182 kg mol^{-1}),[16] using an analogue to Nozaki's phosphine-sulfonate containing Pd(II) catalyst (**Figure 9**). The relatively low electron donor character of the anionic sulfonate moiety provides increased electrophilicity of the metal centre, increasing catalytic activity while retaining the resistance to poisoning by polar substrates.[17]

1.1.3 Polynorbornene

Norbornene (NB) is a cyclic olefin that when polymerized to polynorbornene (PNB) yields a polymer with a rigid backbone, with industrially advantageous properties like a high decomposition temperature, high refractive index, and chemical and UV resistance. [18] NB can be polymerized through ROMP, radical and ionic polymerization, and coordination insertion polymerization, the latter method being the focus of this work. To remedy issues of brittleness and insolubility, NB is often used to form copolymers with typically nonpolar monomers like ethylene, propylene, or styrene to name a few.[18]

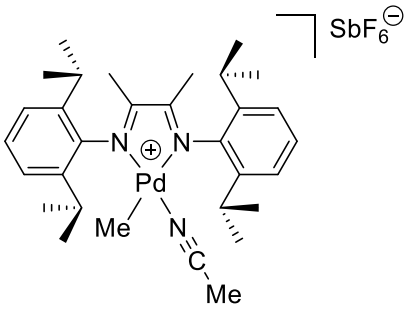

Figure 10. *One of Eisen et al.'s group 10 norbornene copolymerization catalysts.*

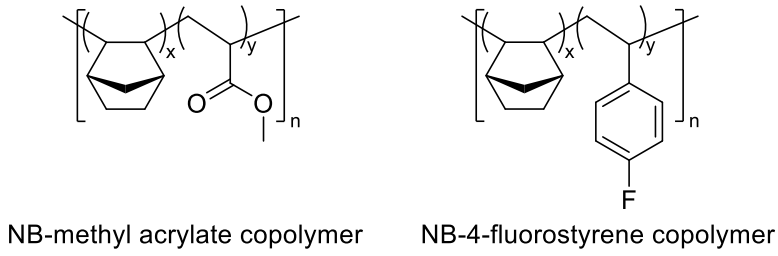

Figure 11. *Copolymers of norbornene (NB) with functionalized monomers.*

Leveraging the unique properties of PNB as a scaffold for polar functional groups through copolymerization of NB with polar monomer is a unique frontier in polymer chemistry.[18] Recent strides in NB copolymers pioneered by Eisen *et al.* have utilized a series of group 10 catalysts (**Figure 10**) to produce functionalized copolymers with a variety of polar moieties (**Figure 11**).

1.2 Polylactide

1.2.1 Polylactide Synthesis Methods

Polylactide (PLA), also known as polylactic acid, is a polymer derived from renewable feedstocks that can be hydrolyzed back into lactic acid under industrial composting conditions,[19] making it much more biodegradable than the aforementioned polyolefins, and thus an ideal remedy for issues of sustainability in polymer chemistry. Additionally, PLA is nontoxic, giving it applications in single-use food packaging and medical equipment. Lactic acid can be polymerized through polycondensation into PLA (**Figure 12**).

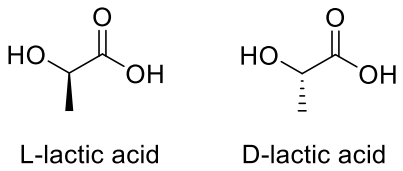

Figure 12. *L and D enantiomers of lactic acid.*

Polycondensation, as a form of step-growth polymerization, entails elimination of water during monomer linkage. Without high levels of monomer conversion, polycondensation results in low molecular weight polymers, making it unfavorable for industrial applications.[20] Instead, PLA is preferentially prepared through ring-opening polymerization (ROP) of the dimeric lactide (LA). ROP is a chain-growth mechanism that, unlike polycondensation, does not require high monomer conversion in order to produce high molecular weight polymers.[21]

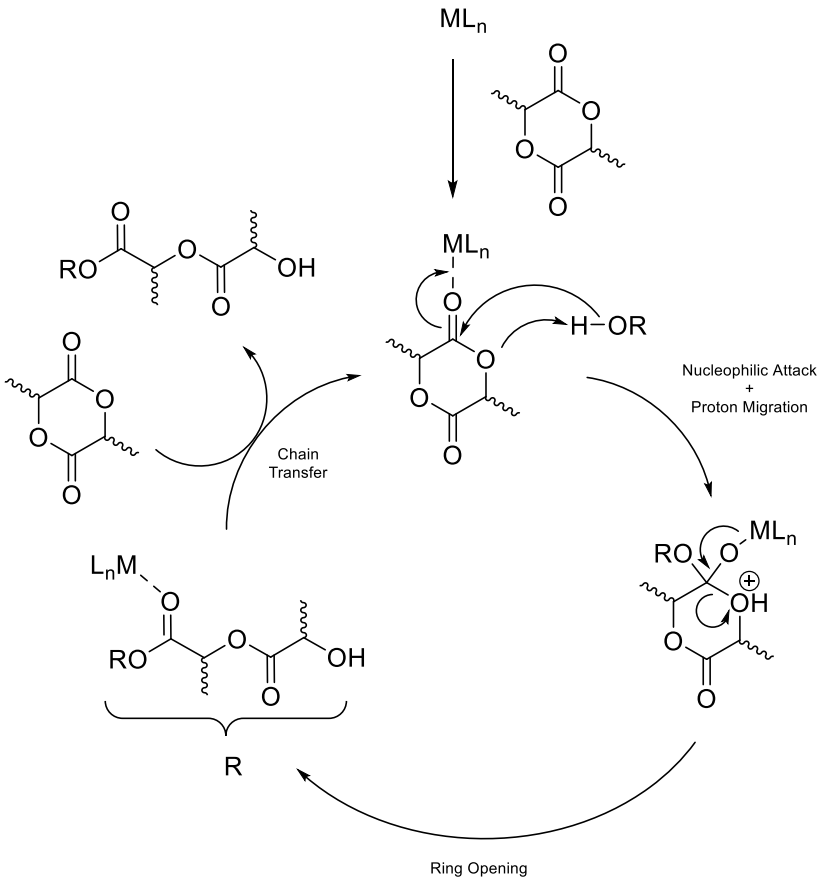

Figure 13. *Activated monomer mechanism for polymerizing lactide reproduced from literature.*

Lewis acidic metals can induce ROP of LA through the activated monomer mechanism (AMM) (**Figure 13**). This mechanism involves coordination of LA to the Lewis acidic metal centre through its carbonyl group, followed by nucleophilic attack about the carbonyl carbon, whose electrophilicity is increased by the coordinating Lewis acid. The external nucleophile (typically an alcohol or water added to the reaction mixture or present as trace contaminant in the LA used) also undergoes proton migration to the endocyclic oxygen. Ring-opening is then induced through cleavage of the endocyclic C—O bond. The ring-opened species then becomes an active nucleophile for further ROP.[22]

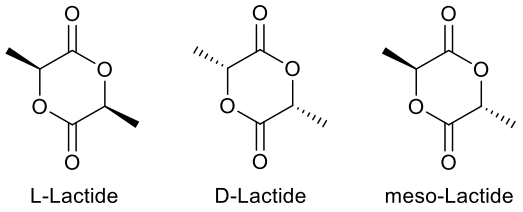

Figure 14. *Stereoisomers of Lactide.*

Due to the presence of two stereogenic centres, lactide exists as L, D, and meso stereoisomers (**Figure 14**) which, when used to produce PLA, affect the microstructure and tacticity of the polymer (**Figure 15**).[19] The tacticity of the polymer, the arrangement of adjacent units in the polymer chain and their respective stereogenic centre (R or S), greatly affects physical properties such as melting point, crystallinity, and toughness.[21] Enantiopure LA produces highly crystalline PLA as all consecutive stereogenic centres have the same relative configuration (isotactic). Racemic lactide (*rac*-LA) is an equal mixture of *L* and *D*-LA isomers and can yield polymers of different tacticities. **Figure 15** displays the effect of the isomer on the polymer tacticities.

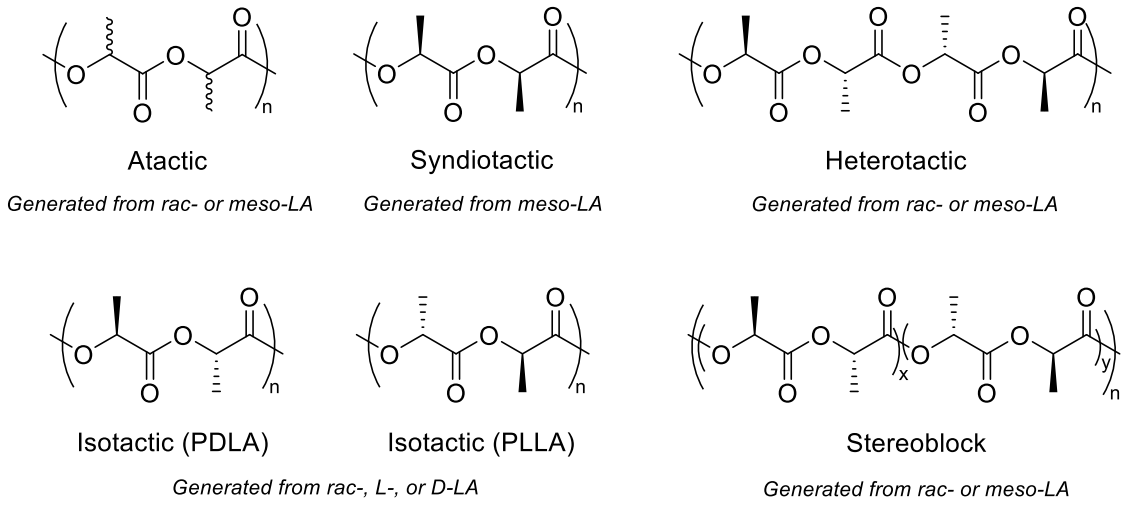

Figure 15. *Tacticity of PLA and the corresponding starting LA stereoisomers.*

When two adjacent stereocentres in the polymer chain are of opposite chirality, the arrangement is referred to as racemic (r), otherwise if the stereocentres are of the same chirality

the arrangement is mesomeric (m). A polymer's tacticity can be probabilistically described via the probability of racemic or mesomeric enchainment, P_r and P_m where $P_r = 1 - P_m$. These metrics describe the probability that two successive stereocentres are related in a racemic or mesomeric fashion, and can be determined through homonuclear decoupled $^1H\{^1H\}$ NMR spectroscopic analysis.[23]

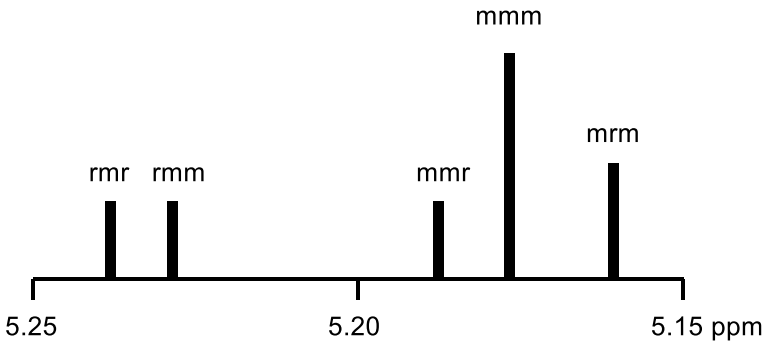

Figure 16. *Representation of a homodecoupled $^1H\{^1H\}$ NMR spectrum (in $CDCl_3$), removing scalar coupling of methyl and methine protons to yield singlets representative of different monomer arrangement patterns.*[22]

Perfectly heterotactic PLA would, for instance, have a P_r of 1 and a P_m of 0. In the homodecoupled NMR experiment, distinct chemical shifts are observed for different patterns of monomer arrangement (**Figure 16**), for instance, a racemic, mesomeric, racemic (rmr) pattern of enchainment has a different characteristic chemical shift than that of a mesomeric, mesomeric, mesomeric (mmm) pattern. In order to determine P_r and P_m values, the following relations have been established:

$$P_r = 2I_1 / (I_1 + I_2) \quad (1)$$

$$P_m = 1 - 2I_1 / (I_1 + I_2) \quad (2)$$

Where I_1 represents the integration between 5.20 to 5.25 ppm (in $CDCl_3$) and represents rmr and rmm arranged units, and I_2 represents the integration between 5.13 to 5.20 ppm (in $CDCl_3$) representing the mmr, mmm, and mrm arranged units.[24]

1.2.2 Polylactide Catalysts

PLA was reportedly first synthesised in 1845 by Théophile-Jules Pelouze through polycondensation of lactic acid.[25] Polycondensation would remain the main method of PLA catalysis for years, until the early 1990's where breakthrough research into PLA production by Cargill Inc. would yield high molecular weight PLA via ROP of L-lactide.

While many metal-based PLA ROP catalysts exist, such as zinc(II) lactate and aluminium isopropoxide, the industrial standard catalyst for lactide polymerization, tin(II) (2-ethylhexanoate), herein after referred to as tin octanoate, $Sn(Oct)_2$ (**Figure 17**), is preferred for its high activity, its ability to produce high molecular weight polymers, and its low cost. It does not however provide tacticity control, and the resultant polymers contain trace tin which limits the application of the resultant PLA in biological settings due to its related toxicity. Additionally, the industrial standard promotes transesterification which, similar to the aforementioned chain-transfer reduces the molecular weights of polymer and can affect its microstructure.[21]

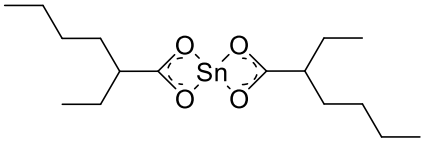

Figure 17. *Tin octanoate industrial standard.*

Alternative catalysts using zinc have been developed by Herres-Pawlis[26] (**Figure 18**) utilizing an imine-phenolate system, yielding high molecular weight polylactic acid. These catalysts have the advantage of zinc being nontoxic, low cost, and highly active for PLA catalysis. However they remain unable to control polymer tacticity.[27]

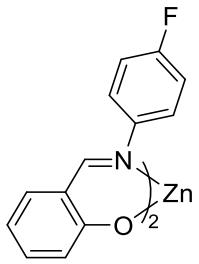

Figure 18. *One of Herres-Pawlis' zinc-based PLA catalysts.*

1.3 Polyisocyanides

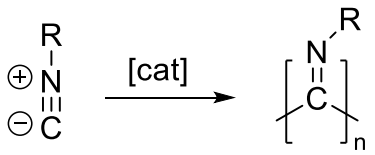

Figure 19. *Preparation of polyisocyanide.*

Polyisocyanides (PICs), made from isocyanide monomer (**Figure 19**), notably adopt a helical conformation in and out of solution as confirmed by Nolte *et al.* in 1974 by resolution of enantiomeric helices of poly(*tert*-butyl isocyanide) through liquid chromatography on a chiral stationary phase.[28,29,30] Isocyanides were first reported in the 1860s, a century later, in 1965, the first catalytic systems for producing polyisocyanides were reported by Millich using an acid-coated glass system, later in the mid 1970s, Nolte would report several Ni(II) salts that were active for PIC catalysis ($NiCl_2 \cdot 6H_2O$ and $Ni(acac)_2$) of a variety of isocyanide monomers to high molecular weights (5000 to 250,000 g/mol).[31]

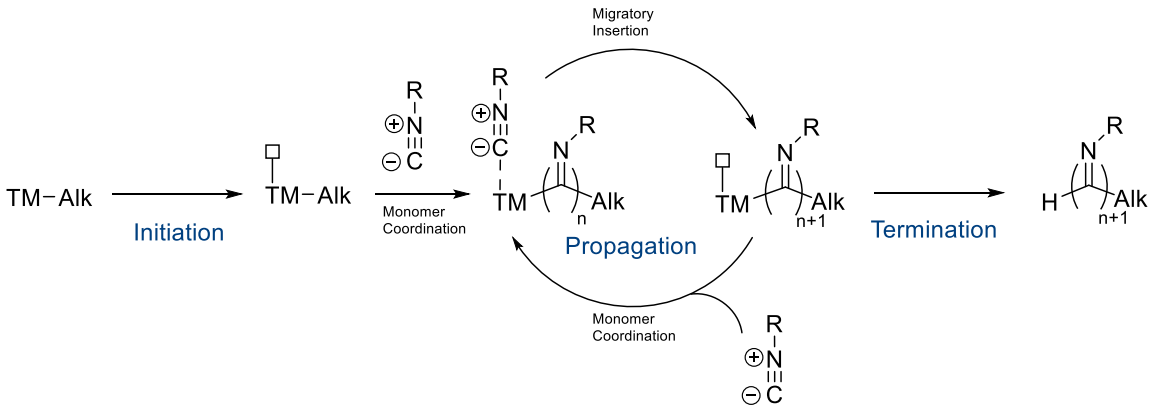

Figure 20. *Generic coordination-insertion mechanism for isocyanide.*

Isocyanide is polymerized into PIC through a coordination insertion mechanism (**Figure 20**), largely like that of the aforementioned olefins. Unlike olefins, isocyanide monomer coordinates in an η^1 fashion to the metal centre before migratory insertion into the position of the

nucleophilic alkyl or growing chain. Polymer cleavage can similarly be performed with a terminating agent like an alcohol.

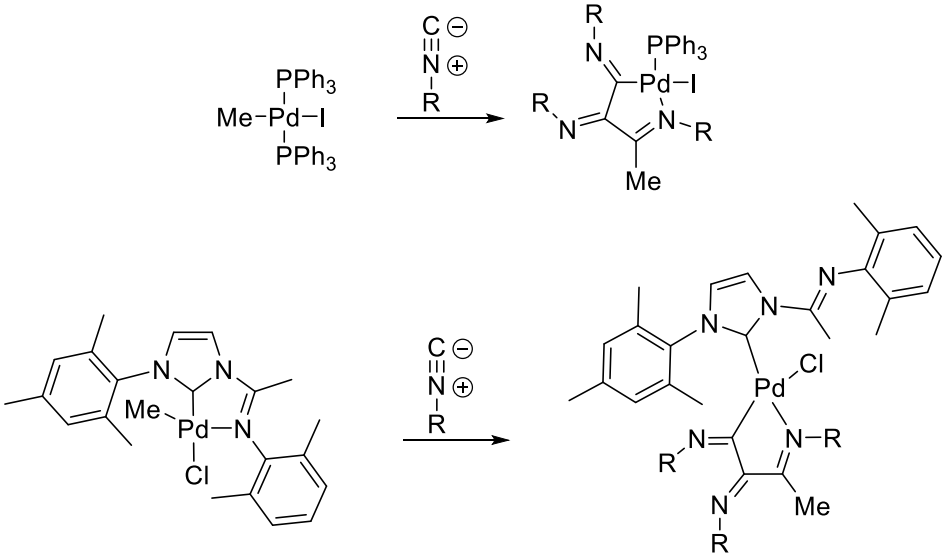

Scheme 2. *Takahashi (top) and Lavoie (bottom) mononuclear palladium(II) based catalysts forming trimeric isocyanide oligomer.*

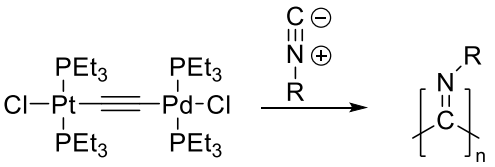

Scheme 3. *Takahashi's binuclear palladium(II) and platinum(II) catalyst polymerizing isocyanide.*

PIC catalysts nowadays continue utilizing late transition metal-based catalysts.[19] Takahashi *et al.* as well as Lavoie *et al.* have reported mononuclear Pd(II) catalysts which favour the production of trimeric oligomers (**Scheme 2.** Takahashi (top) and Lavoie (bottom) mononuclear palladium(II) based catalysts forming trimeric isocyanide oligomer. Takahashi *et al.* has also reported a binuclear Pt(II)-Pd(II) catalyst, connected through an ethylene-1,2-diyl bridging group (**Scheme 3**). While the binuclear catalyst is active for PIC catalysis, it is limited in its applicability, as it has only been successfully demonstrated polymerizing aryl isocyanides.[30]

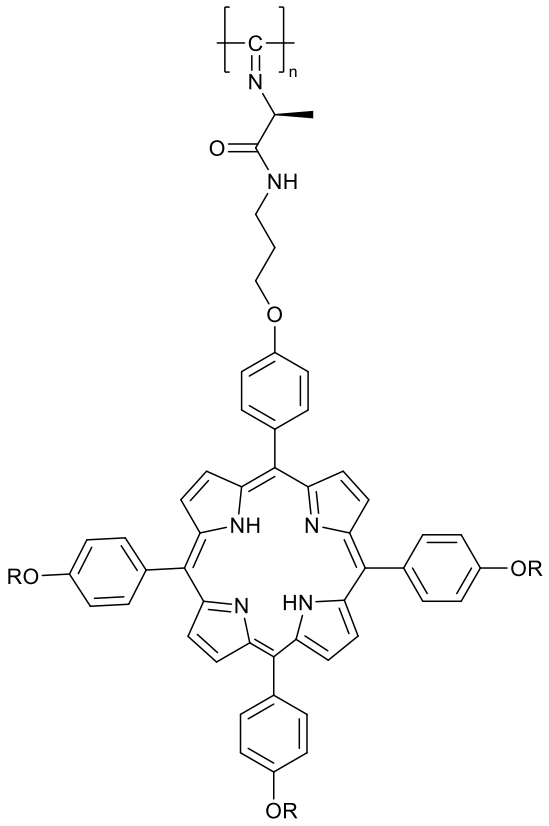

Figure 21. *Porphyrin bearing polyisocyanide.*

Other groups, such as Kitto *et al.* and Amabilino *et al.*[5,33] have continued to expand the library of polyisocyanides to include different substituents affecting the structure and resultant optical properties of the polymer. Polyisocyanides find use in photovoltaics and can act as scaffolds for functional chromophores (**Figure 21**)[29] as well as chiral recognition and enantiomer separation, owing to their helical structure and rigidity. [30]

1.4 Guanidine-Containing Ligands

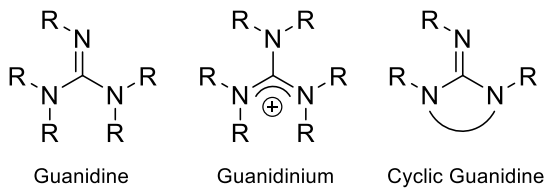

Figure 22. *Generic structures of guanidine and some derivatives.*

Ligand systems designed to produce catalytically active complexes are of incredible industrial importance.[34] Many such systems seek to provide stability and tunability to their catalyst. The unique structure of guanidines allows for delocalization of the electron density across the entire π-system (**Figure 22**), increasing the donor character of the exocyclic nitrogen in coordination, which can in turn help stabilize complexes. The highly modular nature of the guanidine moiety allows for modification of substituents about the endocyclic nitrogens as well as the cyclic guanidine's structure to ultimately modulate the steric and electronic effects of the corresponding ligand. This will then affect the catalytic activity of catalysts incorporating these ligands.

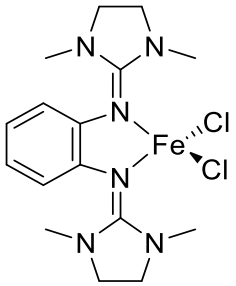

Figure 23. *One of Herres-Pawlis' iron(II), guanidine-containing lactide catalysts.*

Neutral guanidine moieties have seen application in a variety of polymerization studies; they have been applied as neutral donors in catalysis for both olefin and lactide polymerization, leveraging their donor character and modularity to produce a litany of tunable catalysts. Recently, Herres-Pawlis reported a series of bidentate guanidine containing ligands, coordinated to iron(II)

and implemented for L-lactide catalysis (**Figure 23**), which yielded high molecular weight polymers, with M_n as high as 115 kg/mol within 5 hours.[35]

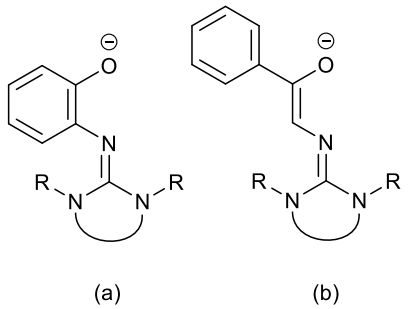

Figure 24. *(a) Guanidine-phenolate and (b) guanidine-ethenolate ligands.*

Systems like the aforementioned Grubbs catalyst (**Figure 7**) as well as Herres-Pawlis' zinc-based PLA catalyst (**Figure 18**) implement similarly bidentate ligands, using neutral donating imine groups with an anionic phenolate moiety to great effect. Extending this structure further, and designing an analogous system to the guanidine-phenolate ligands first reported by Eisen, the Lavoie group has produced a new family of monoanionic donor ligands, the guanidine-ethenolate. Notably, implementing a guanidine functional group in place of an imine leverages their stabilizing ability and high modularity making them attractive as ligands for catalysis [18, 36, 37] The guanidine-ethenolate and guanidine-phenolate ligands were applied for PLA synthesis, following the framework established by Herres-Pawlis *et al.* with their zinc-coordinated phenoxy-imine system and have also shown promise as ligands for olefin polymerization using group 4 metals.[38]

1.5 Scope of Thesis

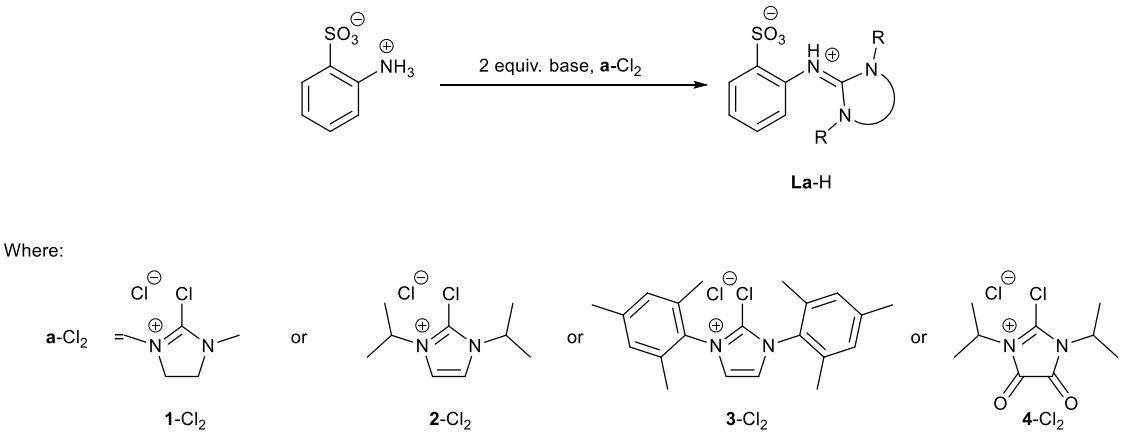

Scheme 4. *A generic reaction scheme for guanidinium-sulfonate ligand synthesis.*

This project aims to develop a series of catalysts for olefin, isocyanide, and lactide polymerization. For these catalysts, a new benzenesulfonate ligand framework that incorporates the aforementioned cyclic guanidines (**Figure 24**) was designed. This system applies similar principles to the phosphine-sulfonate system established by Drent and later iterated upon by Nozaki (**Figure 8**), namely a monoanionic, chelating ligand, whose neutral moiety is strongly coordinating. As was observed with the guanidine-enolate and guanidine-phenolate systems, modification of the ligand structure and substituents allows for steric and electronic control, which in turn, affects catalytic activity and stereoselectivity. Ligand synthesis modifies a previously reported reaction between amino benzenesulfonic acid with a carboxylic acid, using triethyl amine.[39] (**Scheme 4**).

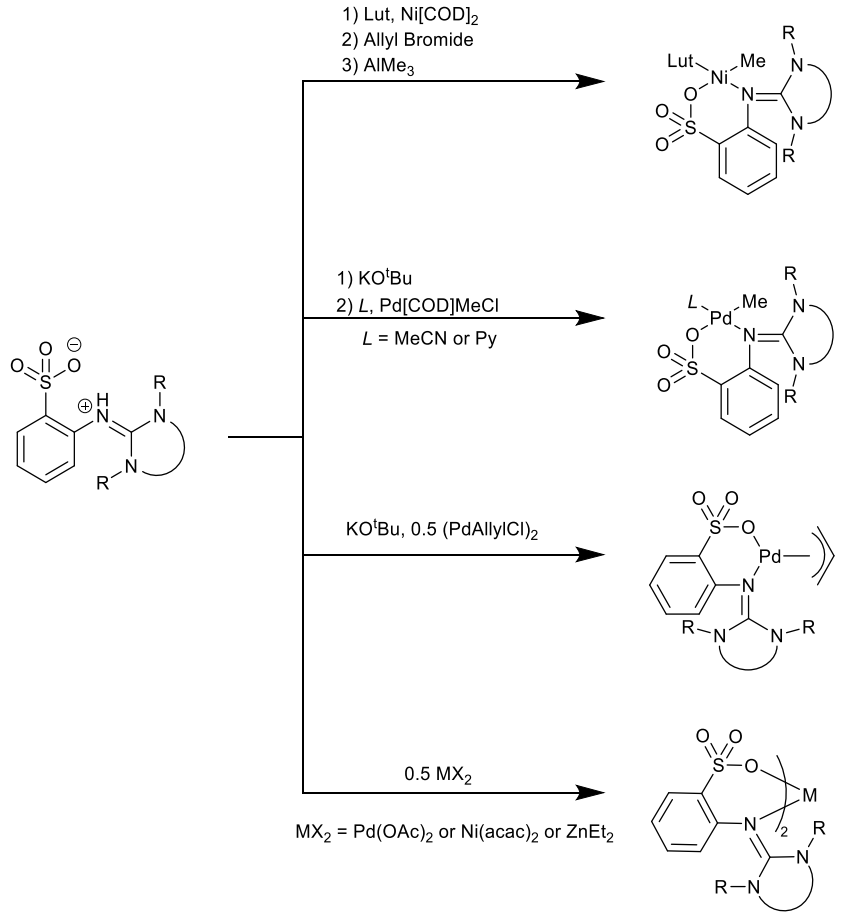

Scheme 5. *Synthesis routes to coordinate a guanidinium-sulfonate ligand to a series of nickel(II) and palladium(II) precursors.*

Properties such as linearity and in the case of polyolefins, the extent of polar monomer incorporation, stand to change when steric and electronics of ligands are modified.[13] For preliminary polyolefin analysis, molecular weights of oligomer were analyzed through mass spectrometry. Additionally concerning polylactide, the guanidine-sulfonate ligand family maintains an analogous structure to that of the Herres-Pawlis' ligand system,[26] as such its coordination to zinc and use in PLA catalysis is also of interest. The effectiveness of these ligands for polymerization as well as the effect of ligand modulation on polymers produced were assessed. Metals to which these ligands were coordinated include palladium(II) and nickel(II). Palladium(II) complexes synthesised were implemented in preliminary studies of olefin, lactide,

and isocyanide polymerization. Additionally, zinc(II) catalysts were developed and tested for the purposes of lactide polymerization.

2. Results and Discussion

2.1 Synthesis of Guanidinium-Sulfonate Ligands

Following the method outlined in **Scheme 4**, **L1**-H was synthesized by reacting aminobenzene sulfonic acid with an excess of triethylamine before addition of the corresponding chloroazolium-chloride salt (**1**-Cl_2, **Scheme 4**). Heat evolved upon addition of **1**-Cl_2. An excess of triethylamine was utilized to mitigate loss of triethylamine via evaporation and following Le Châtelier's principle to drive the reaction to completion. This resulted in increased yields from below 50%, when stoichiometric amounts of triethylamine were used, to as high as 80%. ^{1}H-NMR and proton-decoupled $^{13}C\{^{1}H\}$-NMR spectra were collected (**Figure A1** and **Figure A2**). Aromatic and aliphatic resonances corresponding to the aminobenzene sulfonate and **1**-Cl_2 had drastically shifted, indicating a change in chemical environment, namely, formation of **L1**-H. Furthermore, in ^{1}H-NMR spectra collected, the broad resonance corresponding to the amine group in aminobenzene sulfonic acid which initially had a relative integration of three, after reacting to produce **L1**-H, had instead a relative integration of one. Proton-decoupled $^{13}C\{^{1}H\}$-NMR spectra collected for **L1**-H aligned with the expected nine carbon signals.

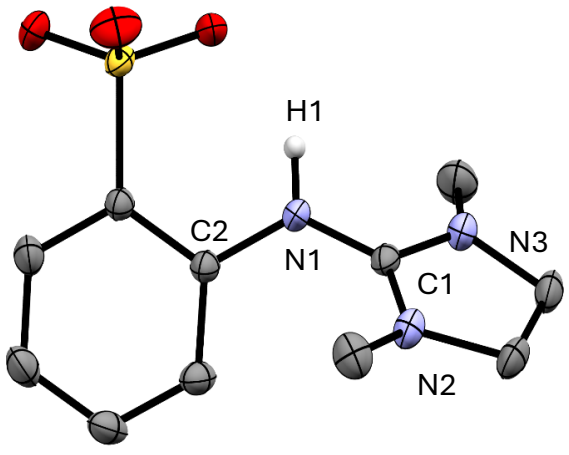

Figure 25. *Solid-state structure of ligand **L1**-H. Hydrogen (white), carbon (grey), nitrogen (blue), oxygen (red), sulfur (yellow). For clarity, solvent and hydrogen atoms have been removed, except for the hydrogen bound to nitrogen N1 with its position located on the Fourier difference map. ORTEP drawn at 50% probability.*

Single crystals of **L1**-H suitable for X-ray diffraction were obtained via vapor diffusion of diethyl ether into a saturated solution of **L1**-H in chloroform to yield the solid-state structure shown in **Figure 25.** The acidic proton H1 is bound to the exocyclic nitrogen N1 (located via the Fourier difference map), confirming a zwitterionic structure. It is for this reason that the protonated ligands are hereinafter referred to as guanidinium-sulfonates.

Density functional theory (DFT) calculations were performed on **L1**-H, using Gaussian 16 on SHARCNET computational resources. Geometry optimizations and vibrational frequency calculations were performed in the gas phase at the B3LYP level of theory with the LANL2DZ basis set. This approach was applied to this and all other calculations herein. Separate optimizations were performed placing the acidic proton on either the exocyclic nitrogen N1 or the sulfonate oxygen. In both cases, the final single point energy was essentially identical (0.0079 kJ/mol difference) with the acidic proton on N1 regardless of the initial structure, providing further evidence that the proton's placement in **Figure 25** is accurate.

$$\rho = \frac{2a}{b+c} \tag{3}$$

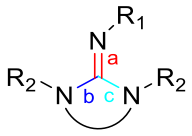

Figure 26. *Generic representation of cyclic guanidine's C-N bonds labelled corresponding to equation 3.*

Table 1. *Selected bond lengths and dihedral angles of ligands* ***L1****-H and* ***L4****•HNEt₃ and calculated ρ values.*

	L1-H	**L4**•$HNEt_3$
Dihedral Angles (°)		
N2–C1–N1–C2	39.9 (2)	6.2 (2)
Bond Lengths (Å)		
N1–C1 (a)	1.3549 (15)	1.2588 (23)
N2–C1 (b)	1.3308 (17)	1.4143 (22)
N3–C1 (c)	1.3241 (17)	1.4063 (23)
ρ	1.021	0.893

Carbon–nitrogen bond lengths showed an exocyclic N1–C1 bond longer than that of N2–C1 and N3–C1 (**Table 1**). The structural factor, ρ, represents the degree to which a double bond's electron density is delocalized, where a value of 1 indicates uniform charge distribution within the guanidine. The value of ρ is determined using **Equation 3**,[40,38] wherein 'a', 'b' and 'c' are the bond length for N1–C1, N2–C1 and N3–C1, respectively.

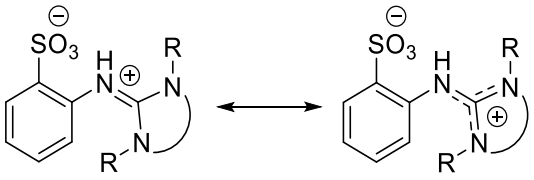

Figure 27. *Generic resonance forms of guanidinium-sulfonates.*

A lower ρ value indicates little delocalization of electron density from the formal double bond. The calculated value of ρ for **L1**-H is greater than 1, which indicates delocalization of the electron density throughout endocyclic portion of the guanidine functional group, as is depicted in **Figure 27** (right). Furthermore, the dihedral angle between N2–C1–N1–C2 was 39.9 ± 0.2° (**Table**

1). Were the C1–N1 bond a localized double bond, this angle would typically be either 0° or 180° as the rigid double bond would restrict rotation causing adjacent atoms to remain in either *cis* or *trans* conformations.[41] It should be noted that some formal double bonds can "pyramidalize" causing them to stray from either of these dihedral angles, though this is typically observed in systems exhibiting ring strain, which is not the case about this N1–C1 bond. The large deviation of this dihedral angle from these theoretical angles provides further evidence that the electron density has been delocalized over the guanidine functional group and that the N1 and C1 atoms' orbitals are not sp^2 hybridized and thus their bond is not a double bond.

$$s = e^{(\frac{R_o - R}{b})} \quad (4)$$

Equation 4, the bond valence sum method, can be utilized to determine the bond valence, *s*, which is the number of electron pairs used to form a bond, using the experimentally determined bond length in Å, *R*, the theoretical single bond length in Å, R_o, which is obtained from a variety of reference crystal structures and varies depending on bonding atoms, and a corresponding fitting parameter, *b*. This equation was used to determine that the N1–C1 bond had a bond valence of 1.26 (with R_o being 1.44 Å, and *b* being 0.37). This bond valence being approximated as the bond order implies that the N1–C1 bond has some double bond character.[42,43]

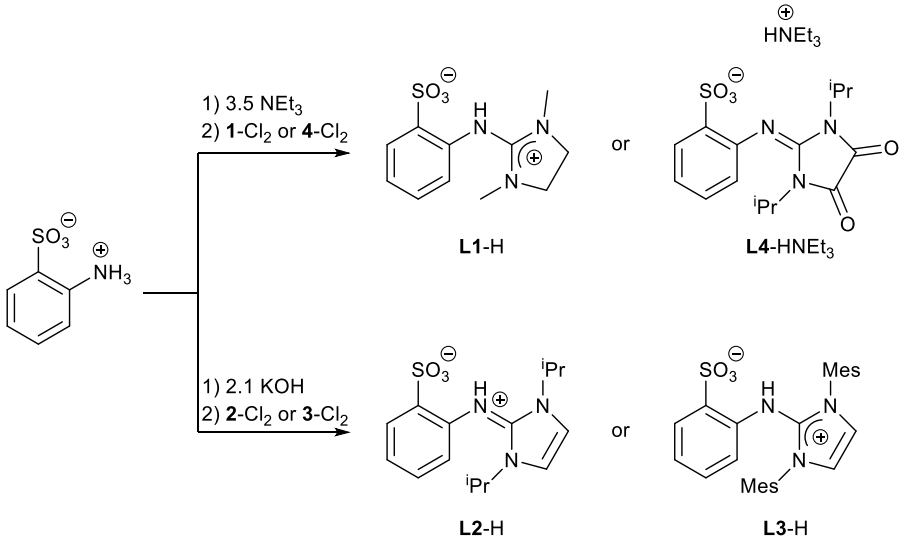

Scheme 6. Ligand synthesis methods used to synthesise ligands **L1**-H**, L2**-H, **L3**-H, and **L4**•$HNEt_3$.

When triethylamine was used in the synthesis of ligands **L2**-H and **L3**-H (**Scheme 6**), ^{1}H-NMR spectroscopy data indicated that the reactions were unsuccessful. In both cases, while chemical shifts of the chloroazolium chloride salts had changed, resonances attributed to the salts integrated to half of their expected values relative to those of the benzene sulfonate, making it unlikely that the desired products were formed. Ligands **L2**-H and **L3**-H were instead synthesised using two equivalents of the stronger base, potassium hydroxide. Notably, KOH was also tested as the base for the synthesis of **L1**-H, with **L1**-H being the minor product, the major product being the cyclic urea of the chloroazolium chloride salt presumably formed when **1** reacted with water present in the reaction mixture. The presence of **L1**-H was confirmed via comparison to the spectrum of **L1**-H prepared with NEt_3 (**Figure A1**). As water was likely causing the formation of the cyclic ureas, synthesis of **L2**-H and **L3**-H was performed in a glovebox, under an argon atmosphere. ^{1}H-NMR spectra of **L2**-H and **L3**-H were consistent with the desired products in both cases (**Figure A3** and **Figure A5**, respectively). In the case of **L2**-H, two sets of resonances were observed for both the methyl and methine protons of the isopropyl substituents as well as the unsaturated backbone. The magnetically-inequivalent protons suggest that rotation about the

$C{=}N_{exocyclic}$ bond might be restricted by increased double bond character about the exocyclic nitrogen–carbon bond rather than electrons being delocalized about the endocyclic nitrogens, as was the case for **L1**-H. These magnetically-inequivalent protons were not observed in either **L1**-H or **L4**•$HNEt_3$. **L3**-H also did not to exhibit the magnetically-inequivalent protons that would indicate restricted rotation in the ^{1}H-NMR spectrum, indicating free rotation about the exocyclic nitrogen-carbon bond, and thus delocalization of the electron density about the endocyclic nitrogens, as was the case with **L1**-H. When attempting to synthesize **L4**-H using an excess of triethylamine, **L4**•$HNEt_3$ was instead produced, indicating that the extra equivalent of NEt_3 was able to deprotonate **L4**-H. The ^{1}H-NMR spectrum supported the proposed structure being **L4**•$HNEt_3$ (**Figure A7**). This result provided further indication that ligands **L2**-H and **L3**-H, both of which had unsaturated backbones, were unable to be synthesised using triethylamine as both **L1**-H and **L4**•$HNEt_3$ were able to be synthesised in this fashion, with ^{1}H-NMR spectra (as well as XRD data) corroborating this result.

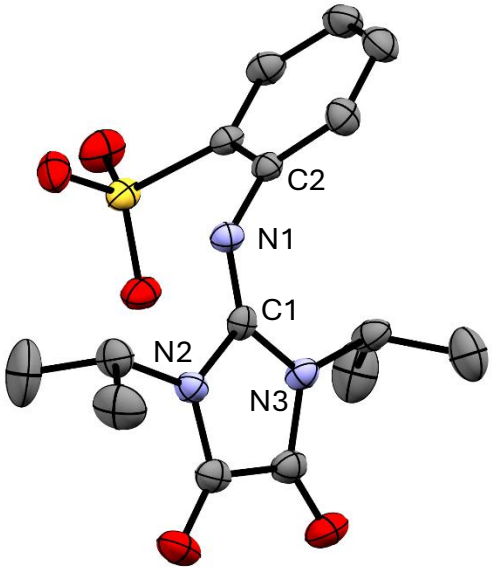

Figure 28. *Solid-state structure of ligand* ***L4•****HNEt₃. The counterion* $HNEt_3^+$ *has been omitted for clarity. Carbon (grey), nitrogen (blue), oxygen (red), sulfur (yellow). ORTEP drawn at 50% probability.*

The solid-state structure of **L4**•$HNEt_3$ (**Figure 28**) confirmed that the excess triethylamine had deprotonated **L4**-H forming anionic $\mathbf{L4}^-$ with $HNEt_3^+$ as the counteranion. While stoichiometric ratios were kept the same for the syntheses of **L1**-H and **L4**-H, only the latter was deprotonated by the excess triethylamine, indicating a difference in basicity among ligands. $\mathbf{L1}^-$ is thus more basic than triethylamine (pK_b around 3.25) [44] while $\mathbf{L4}^-$ is less basic. The difference in basicity is due to the electron-withdrawing acyl groups in $\mathbf{L4}^-$, reducing the basicity of the guanidine.[45]

Selected bond lengths in **L4**•$HNEt_3$ are summarized in **Table 1**. Notably, from the solid state structure of **L4**•$HNEt_3$, the exocyclic nitrogen-carbon bond length is much shorter than that of the endocyclic nitrogens to the central carbon, indicating that the double bond character is mostly about the exocyclic nitrogen-carbon bond, as is reflected in **Scheme 6**. The ρ value of **L4**•$HNEt_3$ (0.893) when compared to that of **L1**-H (1.021) indicates significantly lower

delocalization of electron density about the endocyclic nitrogens in **L4•**$HNEt_3$, which in turn further explains its lower basicity. A dihedral angle of 6.2 ± 0.2° was the planes generated containing atoms N2–C1–N1–C2 respectively (**Table 1**). This angle's proximity to the expected 0° provides further evidence of a stronger N1=C1 double bond character with little electron delocalization along the C1–N2 and C1–N3 bonds.

2.2 Transition Metal Complexes of Guanidinium–Sulfonate Ligands

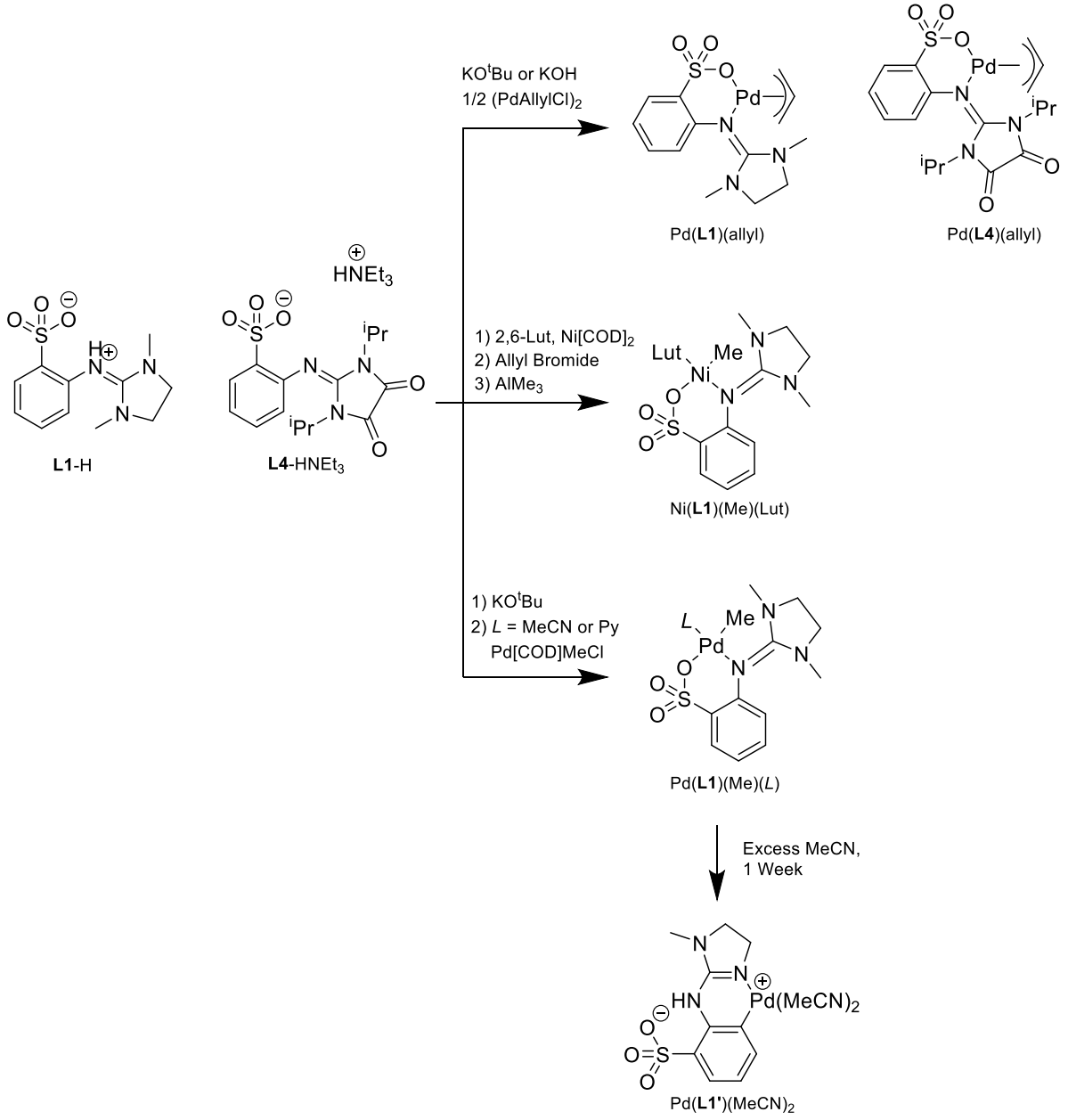

Scheme 7. Pathways for monochelated coordination of **L1** and **L4** to group 10 metal centres.

As discussed in Section 1.1.2 Transition Metal Based Polyolefin Catalysis, the relatively low oxophilicity of group 10 metal containing complexes has garnered recent interest for use in copolymerization of functionalized olefins. The guanidine-sulfonate system builds on previous work with monoanionic, guanidine containing ligands established by the Lavoie group (Section

1.4 Guanidine-Containing Ligands and mirrors other successful ligands applied for olefin copolymerization, like Xu *et al.*'s phosphine-sulfonate system.[39] Active complexes for olefin polymerization require an open site for η^2 olefin coordination, which can be achieved by using labile L-type ligands such as the ones used in this work namely, acetonitrile, lutidine, and pyridine. A metal-coordinated alkyl or hydride nucleophile is also required to undergo migratory insertion. It is for these reasons that a series of group 10 complexes containing monochelated ligands **L1**$^-$ and **L4**$^-$ were synthesised (**Scheme 7**).

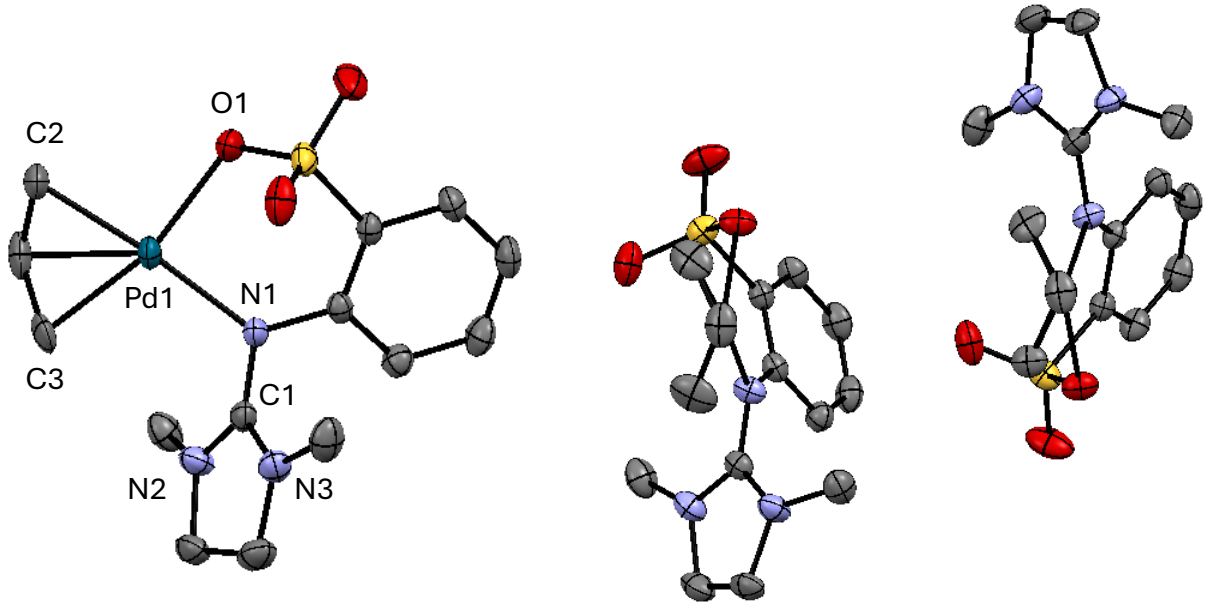

Figure 29. *Solid-state structure of Pd(**L1**)(allyl), **(a)** depicts the complex perpendicular to the plane in which each of the ligands coordinates to the metal centre, **(b)** and **(c)** show enantiomers observed in the crystal's unit cell. Palladium (green), carbon (grey), nitrogen (blue), oxygen (red), sulfur (yellow).*

When **L1**-H was stirred in the presence of $[Pd(allyl)Cl]_2$ and potassium *tert*-butoxide, the resulting yellow coloured product was identified as being Pd(**L1**)(allyl). This was first confirmed through ^{1}H-NMR analysis (**Figure A9**). Resonances attributed to coordinated **L1**$^-$ in the aromatic region were well resolved, while in the alkyl region, two overlapping resonances were observed

between 3.0 and 2.5 ppm. With a relative integration of 8.27 in this region being attributed to the six methyl protons of **L1**$^-$ and the two protons from the coordinated allyl. Three resonances with relative integrations in a 1:2:2 ratio, were assigned to the coordinated allyl ligand, the central proton integrating to one and the terminal protons integrating to four in total (one of the two resonances corresponding to the overlapping peaks between 3.0 and 2.5 ppm).[46]

$$\tau_4 = \left|\frac{360-(\alpha+\beta)}{141°}\right| \quad (5)$$

The τ_4 parameter is a metric that describes the level to which a four-coordinate complex can be considered square planar or tetrahedral,[47] Wherein α and β are the two largest angles made between ligands about the metal centre. A τ_4 value of 1 indicates a tetrahedral geometry while a value of 0 indicates a square planar one.

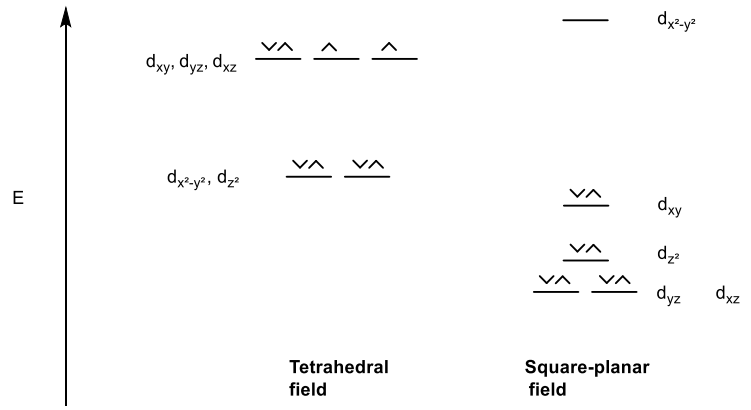

Figure 30. *Different crystal fields formed from repulsion of coordinated ligands (top). Orbital filling for tetrahedral and square-planar fields for a d^8 system (bottom).*

While allyl coordinates to the palladium metal centre in an η^3 fashion, it remains an LX type ligand formally, making Pd(**L1**)(allyl) an ML_2X_2 type complex. As is the case with many palladium(II) complexes, Pd(**L1**)(allyl) adopts a distorted square-planar geometry with a τ_4 value of 0.1592 (**Table 2**), determined using the largest angles made from each of the terminal allylic carbons' C-Pd bonds to ligand **L1**$^-$.[48] The reason for which this and other palladium complexes

adopt this geometry can be explained by a crystal field splitting diagram (**Figure 30**).[49] Typically square-planar complexes have a large crystal field splitting energy difference, caused by the repulsion from coordinated ligands, simplified to point charges around the metal centre.[50] This in turn promotes the pairing of free electrons, as opposed to tetrahedral complexes whose degenerate orbitals facilitate the presence of unpaired electrons. 4d Transition metal complexes tend to have a much higher crystal field splitting than 3d transition metal complexes owing to their larger, more diffuse orbitals interacting more strongly with surrounding ligands. For d^8 transition metals, such as Pd(II) and Ni(II), this difference in electron repulsion explains their general tendency towards diamagnetism and paramagnetism respectively, as the 3d Ni(II) tends to form high spin tetrahedral complexes, whose unpaired electrons cause paramagnetism. 4d Pd(II) complexes however, tend to be square planar, leading to low spin diamagnetic species. Certain Ni(II) complexes with strong-field ligands (whose strong σ-donor or π-acceptor character increase splitting) such as $Ni[(CN)_4]^{2-}$ are square planar, adopting a low spin conformation, making them diamagnetic.

Table 2. *Selected bond lengths and angles in Pd(**L1**)(allyl), Pd(**L1'**)(MeCN)$_2$, Pd(**L1**)$_2$, and Pd(**phenolate-1**)$_2$.*

	Pd(**L1**)(allyl)[a,b]	Pd(**L1'**)(MeCN)$_2$	Pd(**L1**)$_2$	Pd(**phenolate-1**)$_2$
Bond Angles (°)				
α (x-Pd-y)	195.20 (9) (N1-Pd-C2)	183.90 (8) (N2-Pd-N5)	181.56 (9) (N1-Pd-N4)	180.00 (10) (N1-Pd-N1)
β (z-Pd-w)	187.24 (8) (O1-Pd-C3)	181.61 (9) (C2-Pd-N4)	182.86 (7) (O1-Pd-O2)	180.00 (13) (O1-Pd-O1)
τ_4	0.159	0.0391	0.0314	0.0000
Bond Lengths (Å)				
N1-Pd	2.1205 (23)	—	2.0380 (29)	2.0353 (28)
N2-Pd	—	1.9820 (19)	—	—
O1-Pd	2.1304 (20)	—	2.0091 (26)	1.9943 (26)
C2-Pd	—	1.9856 (21)	—	—
N1-C1 (a)	1.3542 (36)	1.3436 (28)	1.3610 (33)	1.3354 (41)
N2-C1 (b)	1.3405 (37)	1.3041 (30)	1.3244 (34)	1.3426 (44)
N3-C1 (c)	1.3306 (37)	1.3647 (27)	1.3329 (34)	1.3542 (46)
ρ	1.014	1.007	1.024	0.990

[a]Bond lengths are averages from both independent molecules in the unit cell.[b]Terminal allylic carbons were used to determine bond angles.

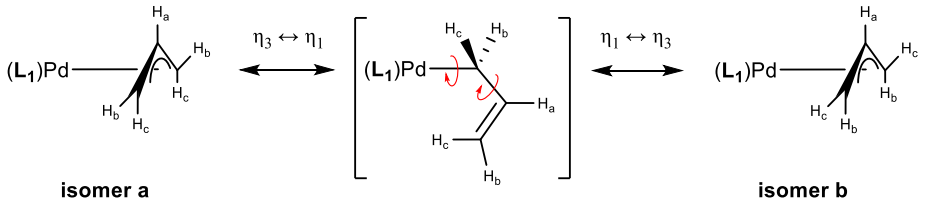

Scheme 8. *Fluxional behaviour of Pd(**L1**)(allyl). Interconversion of isomers occurs by changing coordination mode of the allyl moiety from η_3 to η_1 where rotations about the C—C single bonds yield either **isomer a** or **isomer b** upon reverting to η_3 coordination.*

Broadness observed in the ^{1}H-NMR spectrum is caused by fluxional behavior of the η^3-coordinated allyl ligand, which can rapidly interconvert between conformations in solution as is depicted in **Scheme 8**.[46, 51] In order to confirm that the broadening observed in the ^{1}H-NMR spectrum was caused by fluxional behaviour of the allyl moiety, a variable-temperature (VT) NMR experiment was performed.[52]

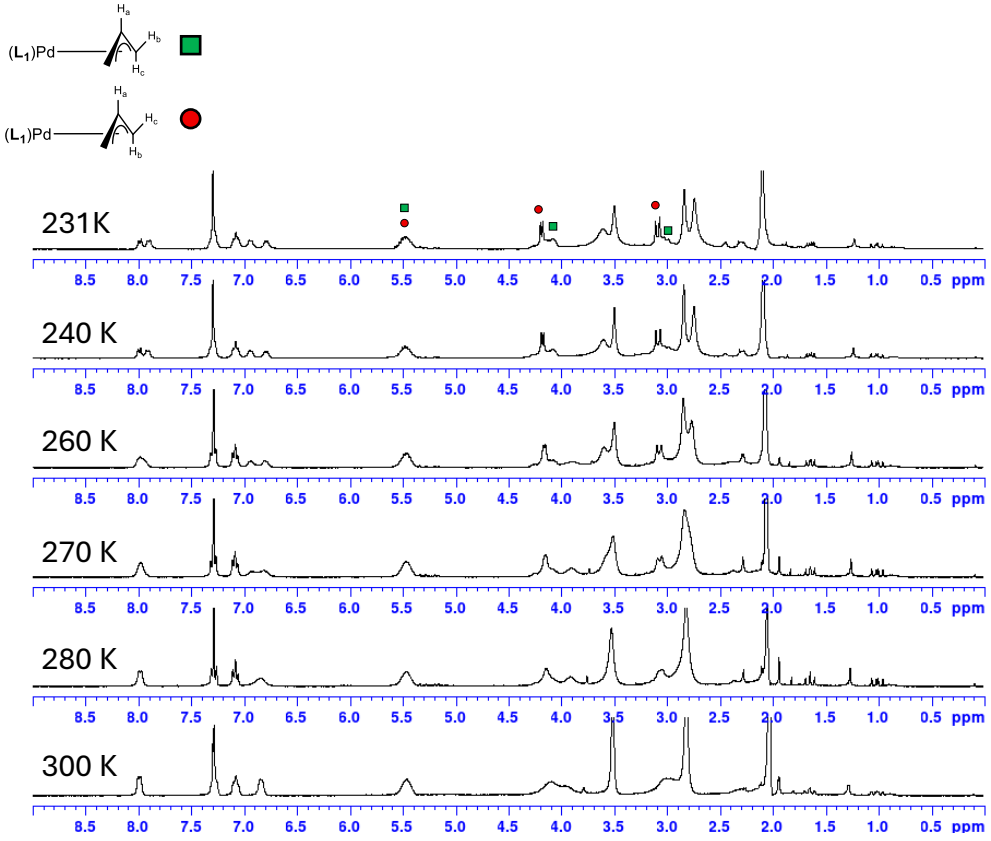

Figure 31. *Variable-temperature ^{1}H-NMR spectra ranging from 300 to 231 K for Pd(**L1**)(allyl), collected on a 300 MHz instrument. Isomers observed due to allylic fluxional behaviour are identified on the spectrum collected at 231 K.*

$$\Delta G^{\ddagger} = RT_c ln\left(\frac{k_B T_c \sqrt{2}}{\pi h|\upsilon_A - \upsilon_B|}\right) \quad (6)$$

$$\Delta G^{\ddagger} = (8.314 Jmol^{-1}K^{-1})(280K) ln\left(\frac{(1.381 \cdot 10^{-23} m^2 kg \cdot s^{-2}K^{-1})(280K)\sqrt{2}}{\pi(6.626 \cdot 10^{-34} m^2 kg \cdot s^{-1})|30\ s^{-1}|}\right)$$

$$\Delta G^{\ddagger} = 58.60\ kJ/mol$$

Coalescence of the resonances for the allylic protons at about 4.2 and 3.1 ppm in the ^{1}H-NMR spectra (**Figure 31**) was observed at 280 K. At temperatures below the coalescence point, the peaks at 4.2 and 3.1 ppm each began to resolve into distinct peaks. Notably, while each peak was initially a broad singlet, they began to resolve into doublets at lower temperatures which was initially concluded to be a consequence of fluxional behaviour, however, integrations of these peaks relative to an aromatic resonance, normalized to 1, were approximately 1:1, indicating that these resolved peaks were likely a consequence of J-coupling. New peaks were observed, as the sample temperature dropped, slightly upfield of both distal allylic resonances. When the better resolved peaks at 4.2 and 4.1 ppm were integrated, their sum was about 2:1 relative to the aromatic resonance previously used, indicating that these resonances were the consequence of fluxional behaviour.

The temperature at which the peaks were best resolved (231 K) was then used to determine the Gibbs free energy of the fluxional behaviour using the Eyring equation (**Equation 6**).[53] In the Eyring equation, Tc is the coalescence temperature (280 K), υ_A and υ_B are the chemical shifts of the resolved resonances at 231 K, k_B is the Boltzmann constant, h is Planck's constant, R is the ideal gas constant, and $\Delta G^{\ddagger}$ represents the activation energy barrier for the fluxional behaviour, which was determined to be 58.60 kJ/mol. Jalón *et al.* published similar results for related methallyl palladium(II) complexes (2[Pd(η^3-C_4H_7)(3,5-Me_2bpzm)PF_6, 64.01 – 64.48 kJ/mol).[52]

Pd(**L4**)(allyl) was synthesized in a similar fashion to Pd(**L1**)(allyl), by reacting $[Pd(allyl)(Cl)]_2$ with **L4**•$HNEt_3$ using potassium hydroxide in methanol instead of potassium *tert*-butoxide. Unlike **L1**-H, **L4**•$HNEt_3$ was able to be stripped of its acidic proton by potassium hydroxide in methanol. The complex was characterized through ^{1}H-NMR spectroscopy (**Figure A11**) wherein changes in chemical shifts were observed for both the allylic protons and in the ligand itself. Pd(**L4**)(allyl), unlike its counterpart Pd(**L1**)(allyl), did not display fluxional behaviour of the allyl moiety at room temperature. This indicates a larger activation energy barrier for the fluxional behaviour compared to that of Pd(**L1**)(allyl), possibly induced by steric interactions with the isopropyl groups in **L4**$^-$.[54]

Ni(**L1**)(Me)(Lut) was synthesized by reacting nickel bis(1,5-cyclooctadiene) (COD) with 2,6-lutidine and **L1**-H, followed by addition of allyl bromide, and finally methylation via trimethylaluminum (**Scheme 7**). Broad resonances were observed in the ^{1}H-NMR spectrum of Ni(**L1**)(Me)(Lut) (**Figure A13**), possibly due to paramagnetism of the resultant complex, not observed in the diamagnetic nickel precursor.[55] As illustrated in **Figure 30**, nickel(II) complexes are typically paramagnetic due to a tendency to form tetrahedral complexes whose lowest energy state has two unpaired electrons. The geometry of this nickel complex, along with the loss of COD in the ^{1}H-NMR spectrum suggest a change in the chemical environment of the complex. The relative integrations of the aromatic and alkyl protons and the change in chemical shifts are consistent with coordination of **L1**$^-$ to Ni.

Two complexes, Pd(**L1**)(Me)(MeCN) and Pd(**L1**)(Me)(py) were produced for olefin and isocyanide polymerization. These complexes were selected for preliminary polymerizations due to their ease of synthesis, relatively high yields (60-80%), and diamagnetic character, making characterization by NMR analysis facile. They each also contain a metal-alkyl bond and labile

ligand (MeCN and py), crucial for the coordination-insertion mechanism. The complexes were prepared by stirring **L1**-H with chloro(1,5-cyclooctadiene)methylpalladium(II) and potassium *tert*-butoxide, in the presence of either acetonitrile or pyridine as coordinating solvent. In both cases, the solution went from green to yellow and a white, NMR-silent precipitate formed. This precipitate was likely potassium chloride, indicating a reaction had taken place. Both complexes were isolated as yellow oils after filtration followed by removal of volatile compounds under reduced pressure. The structure of complexes Pd(**L1**)(Me)(MeCN) and Pd(**L1**)(Me)(py) is supported by ^{1}H-NMR spectroscopic data (**Figure A14** and **Figure A16** respectively). While Pd(**L1**)(Me)(py) is soluble in a variety of organic solvents, Pd(**L1**)(Me)(MeCN), due to its more polar character, is soluble only in coordinating, solvents like MeCN and THF.

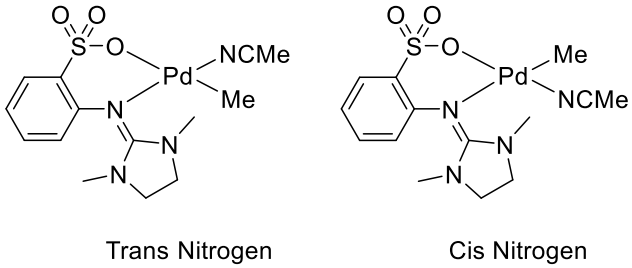

Figure 32. *Cis and trans isomers of Pd(**L1**)(Me)(MeCN). Isomers have been identified as cis or trans when the coordinating exocyclic nitrogen and acetonitrile moieties are cis or trans to one another.*

Pd(**L1**)(Me)(MeCN) exists as two diastereomers depicted in **Figure 32**. This doubled the number of resonances observed in the ^{1}H-NMR, though relative integrations remained consistent with the expected structures. The two diastereomers were present in a 1:1.8 ratio, determined using the resonances assigned to the methyl and methine protons.

DFT calculations (B3LYP/LanL2DZ) were performed to determine the relative energies of each of the two diastereomers, a common level of theory for organometallic molecules.[56,57] It should be noted that these calculations were performed in the gas phase. Solvent systems are likely to have an impact on the stability of these isomers to varying degrees, the polar solvent (MeCN)

in which the NMR spectrum was collected for instance, may affect the relative stabilities and thus abundance of the two isomers observed.[58] The calculated single point energy difference between the two isomers was 1.3 kJ/mol at 298 K. The *trans* isomer, having a lower absolute energy, likely being the more abundant of the two isomers observed in solution at room temperature. The lower energy of the *trans* isomer may be due to trans influence: generally, X type (anionic) ligands can weaken the bonds of *trans* coordinating ligands, in this case, making *trans* coordination of the two X type ligands favourable and the *cis* conformation less stable as weakly coordinating L type (neutral donor) ligands are further repelled by the more strongly σ-donating X type ligands, destabilizing the complex.[59]

$$\frac{N2}{N1} = e^{-\Delta G/RT} \tag{7}$$

Equation 7 was used to calculate expected ratios of each isomer (N1 and N2) present using the calculated Gibbs free energy difference, ΔG (in kJ/mol), at T = 298 K. This yields a ratio of about 1:1.67 which mirrors the experimental 1:1.8 ratio, further indicating that the additional resonances observed in the ^{1}H-NMR spectrum were caused by the presence of two isomers. Diastereomerism was not observed in the case of Pd(**L1**)(Me)(py), likely due to the larger pyridine hindering the formation of one of the two diastereomers, unlike the acetonitrile bearing Pd(**L1**)(Me)(MeCN).

DFT calculations performed on the *cis* and *trans* diastereomers of Pd(**L1**)(Me)(py) estimates an energy difference of 27.9 kJ/mol. This energy difference translates into a ratio of 1 : 80 000, for the *cis* and *trans* diastereomers respectively, at room temperature. This was consistent with the experimental results where only one isomer was observed. It is likely that the trans isomer, due to its relatively low energy, is the isomer observed at room temperature.

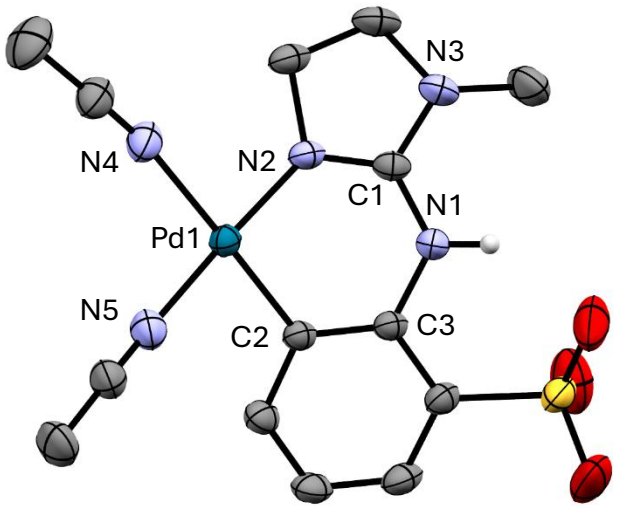

Figure 33. *Solid-state structure obtained of Pd(**L1'**)(MeCN)₂. Protons are omitted for clarity with the exception of the proton present on N1. Palladium (green), hydrogen (white), carbon (grey), nitrogen (blue), oxygen (red), sulfur (yellow).*

When a pure sample of Pd(**L1**)(Me)(MeCN) was left in solution in acetonitrile for a week, a majority of the complex decomposed yielding a black powder, presumably palladium(0), with a few red crystals. A solid-state structure of the crystals was obtained and is displayed in **Figure 33**. Due to the small yield of the decomposition product, an NMR spectrum could not be recorded. Interestingly, an endocyclic nitrogen lost a methyl group and the phenyl ring underwent C–H activation. The modified version of **L1**$^{-}$, hereinafter referred to as **L1'**$^{2-}$, was coordinating through an endocyclic nitrogen and a new carbon-palladium bond had formed.

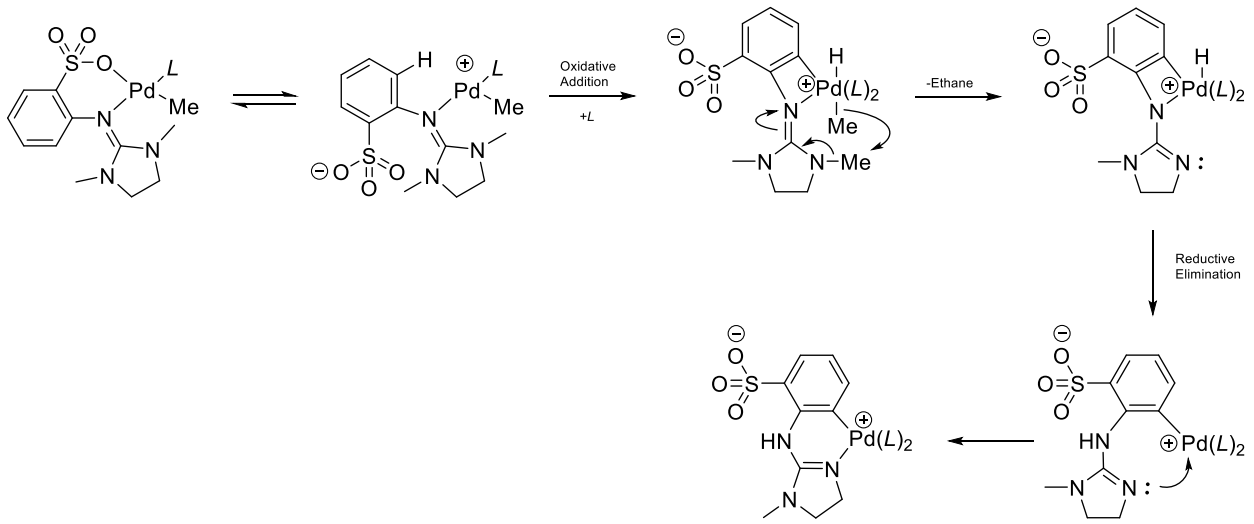

Scheme 9. *A proposed mechanism through which Pd(**L1**)(Me)(py) may react intramolecularly in acetonitrile in order to produce Pd(**L1'**)(MeCN)$_2$. L represents either MeCN or Py.*

A mechanism for this result is proposed in **Scheme 9**. The mechanism begins with the reversible breaking of the coordination bond between the sulfonate moiety and the metal centre. The sulfonate moiety is more likely to dissociate than the exocyclic nitrogen from the guanidine due to its relatively low basicity (substantiated by the zwitterionic solid-state structure, **Figure 25**). This bond cleavage provides rotational freedom about the $N_{exocyclic}$–C_{phenyl} bond, allowing for the C–H bond *meta* to the sulfonate to be oriented towards the now cationic metal centre. Oxidative addition of the C–H moiety to the palladium(II) centre brings its oxidation state to palladium(IV), while forming a transient azametallacyclobutane. Two methyl groups were lost in the decomposition of Pd(**L1**)(Me)(*L*) to Pd(**L1'**)(*L*)$_2$ (the sum of the atoms lost in the decomposition being equivalent to that of ethane, C_2H_6). Ethane gas is presumed to have been released when the nucleophilic methyl group attacked one of the endocyclic nitrogen's methyl groups, pushing electron density from the formal double bond to the exocyclic nitrogen. Reductive elimination, likely favoured due to strain in the metallacycle, yields an $N_{exocyclic}$–H bond. The endocyclic nitrogen, no longer bearing a methyl group and driven by the chelate effect, then coordinates to the metal centre to yield Pd(**L1'**)(MeCN)$_2$.

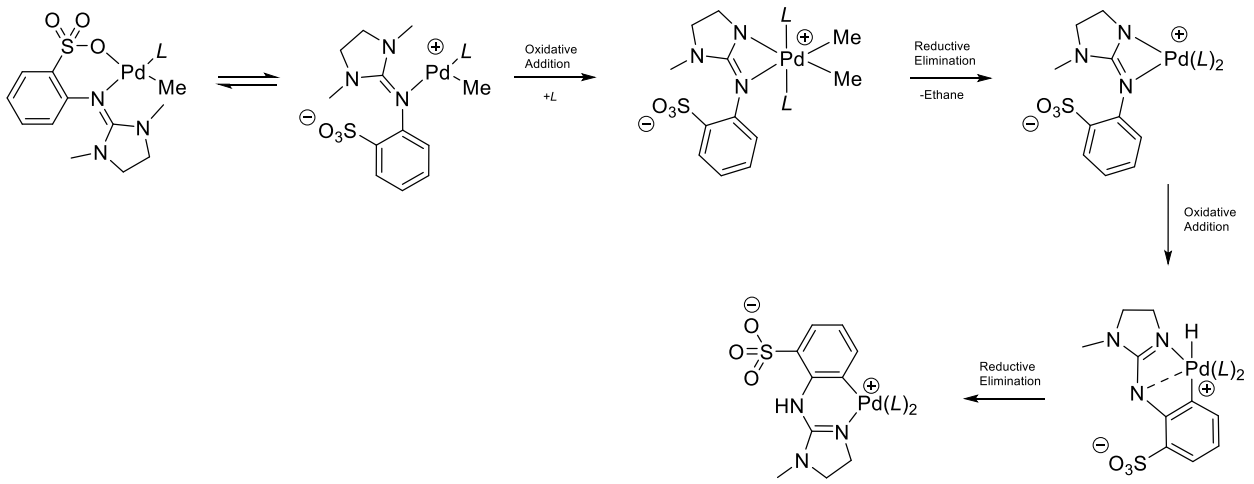

***Scheme 10**. An alternative proposed mechanism for the decomposition of Pd(**L1**)(Me)(MeCN) to Pd(**L1'**)(MeCN)2 following an alternative intramolecular reaction pathway.*

An alternative plausible pathway for the decomposition product Pd(**L1'**)$(MeCN)_2$ is represented in **Scheme 10**. This mechanism begins similarly with the hemilabile sulfonate dissociating from the metal centre. The mechanisms diverge as oxidative addition is instead undergone through the $N_{endocyclic}$–C_{methyl} bond to the palladium(II) centre. The bis-methylated palladium(IV) species then undergoes reductive elimination to release ethane gas. The next step, similar to **Scheme 9**, involves oxidative addition of the C–H moiety to the palladium(II) metal centre, before subsequent reductive elimination to yield Pd(**L1'**)$(MeCN)_2$.

From the solid-state structure of Pd(**L1'**)$(MeCN)_2$ (**Table 2**), the N2–C1 bond has the most double bond character (**Table 2**). In this complex, **L1'$^{2-}$** acts as an LX type ligand (as did **L1**$^{-}$), coordinating in a unique fashion compared to the other complexes presented (see **Figure 35** and **Figure 36** below). Pd(**L1'**)$(MeCN)_2$ is a zwitterionic species, with a cationic palladium metal centre (PdL_3X) charge-balanced with the distal anionic sulfonate. The cationic palladium metal may be stabilized by the strong donor character of the guanidine group in **L1'$^{2-}$**, while the SO_3^- group hydrogen bonds with N1–H, providing additional rigidity and stability to the ligand system.[60]

Compared to the solid-state structure of Pd(**L1**)(allyl), Pd(**L1'**)$(MeCN)_2$ had notably shorter metal–ligand bonds. The zwitterionic nature of this complex likely contributes to the shorter bond lengths observed, as the palladium(II) metal centre is not proximal to the anionic sulfonate moiety, which in turn more strongly attracts the σ-donating ligands.[61]

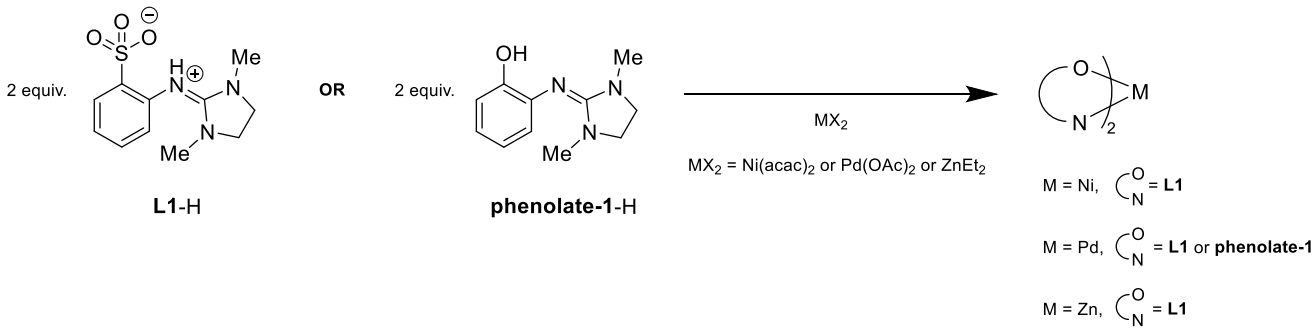

L1-H **phenolate-1**-H

Scheme 11. *Synthesis of bis-chelated nickel, palladium, and zinc-based catalysts.*

Coordination of two equivalents of ligand **L1**$^-$ to nickel, palladium and zinc was successfully achieved. These complexes emulate the previously discussed lactide polymerization catalysts pioneered by Herres-Pawlis (**Figure 18**), the zinc bearing complexes being of particular interest for its biological inertness, making trace inclusions safer for biological applications. In all cases, a basic metal precursor was used to deprotonate **L1**-H in the absence of any additional base (**Scheme 11**).

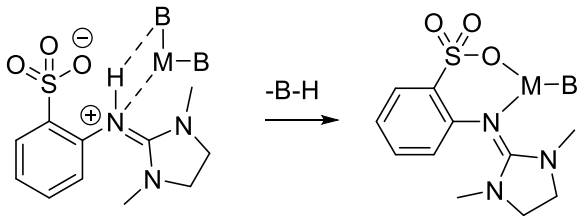

Figure 34. *Generic Illustration of **L1**-H being deprotonated by coordinated base (B) via metal-ligand cooperation.*

The basicity of **L1**$^-$ has been found to be greater than that of triethylamine (pK_b = 3.25, section 2.1), while a free acetate anion's pK_b is around 9.24.[62] The ability of this relatively weak base to deprotonate **L1**-H may be explained by metal-ligand cooperation (MLC) (**Figure 34**),

where the cationic metal centre further polarizes the weak base, to allow for deprotonation of **L1**-H.[63]

Similar to Ni(**L1**)(Me)(Lut), Ni(**L1**)$_2$ also displayed paramagnetic character. While the collected ^{1}H-NMR spectrum of Ni(**L1**)$_2$ was broad due to the formation of a paramagnetic complex (**Figure A17**), chemical shifts of coordinated **L1**$^-$ changed and no resonances appeared to belong to coordinated acetylacetonate nor its conjugate acid, indicating that free acetylacetone was likely lost when volatiles were removed from the mixture before NMR analysis, and that **L1**$^-$ was successfully able to coordinate in its place.

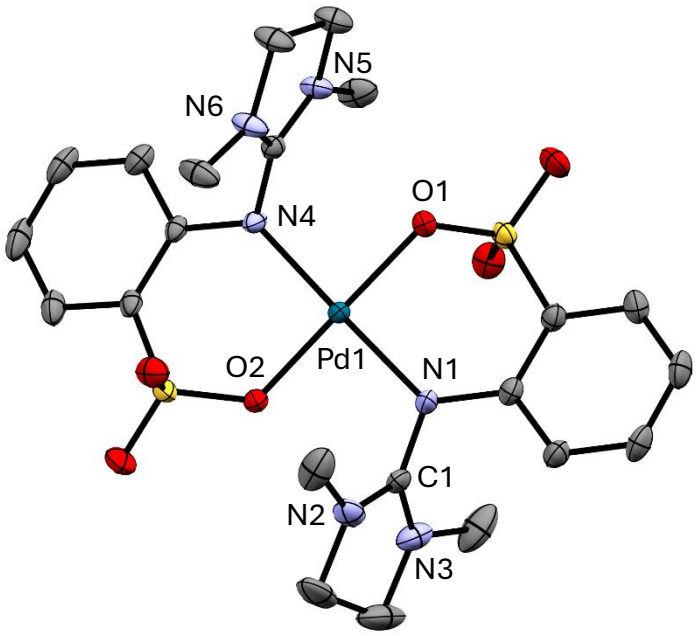

***Figure 35**. Solid-state structure for Pd(**L1**)$_2$. Hydrogen atoms have been omitted for clarity. Palladium (green), carbon (grey), nitrogen (blue), oxygen (red), sulfur (yellow).*

While Ni(**L1**)$_2$ was paramagnetic, the palladium homologue Pd(**L1**)$_2$ is not, owing entirely to a difference in the structures' geometries. As stated above (**Figure 30**) nickel(II) tends to form tetrahedral complexes, which, owing to their unpaired electrons, are paramagnetic. This is not the case for four-coordinate palladium(II) complexes like Pd(**L1**)$_2$, whose solid-state structure (**Figure**

35) elucidates its square-planar geometry. Like the solid-state structure obtained for Pd(**L1**)(allyl), in Pd(**L1**)$_2$, **L1**$^-$ coordinated to the metal centre in a bidentate fashion, through the anionic sulfonate and neutral exocyclic nitrogen. The ρ value in Pd(**L1**)$_2$ is nearly identical to that of **L1**-H, implying that the highly delocalized electron density of the exocyclic nitrogen's double bond is maintained between **L1**-H and Pd(**L1**)$_2$. The ^{1}H-NMR spectrum collected of the diamagnetic Pd(**L1**)$_2$ is consistent with its structure (**Figure A19**). Notably, aromatic peaks were observed moving upfield, indicating a reduction in deshielding effects, while resonances corresponding to alkyl groups were observed moving downfield, indicating deshielding.

Coordination of **L1**$^-$ to zinc was performed using diethyl zinc as a precursor. The product, Zn(**L1**)$_2$, was characterized by ^{1}H-NMR spectroscopy and showed a similar pattern to that of the nickel and palladium complexes, namely a change in chemical shift and loss of the precursor ligand's conjugate acid, in this case ethane, produced after deprotonation and subsequent coordination of **L1**-H (**Figure A21**). The zinc and palladium bis-chelates were then used for PLA catalysis (see section 2.3.3).

Following the synthesis method employed for Pd(**L1**)$_2$, an analogous system was explored and coordinated to palladium(II) to form a 5-membered chelate. The analogous guanidine–phenolate **phenolate-1**$^-$ (named as such due to its similarity to ligand **L1**$^-$) has previously been reported by Eisen.[18]

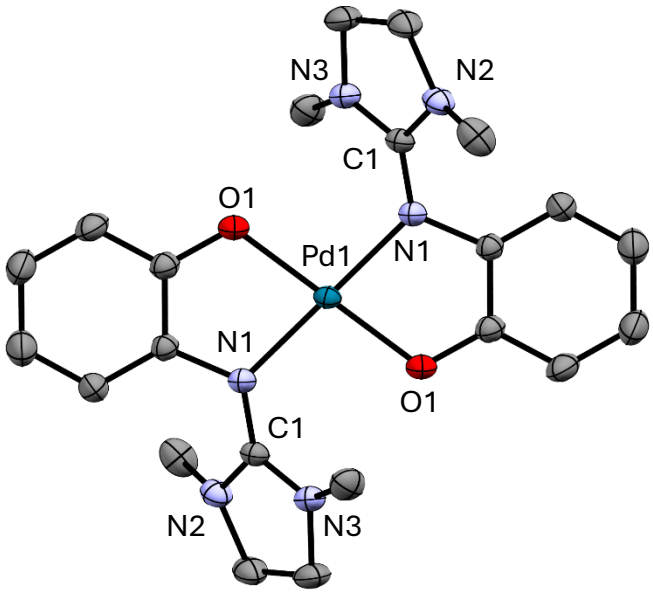

Figure 36. *Solid-state structure for Pd(**phenolate-1**)$_2$. Hydrogen atoms have been omitted for clarity. Palladium (green), carbon (grey), nitrogen (blue), oxygen (red).*

A solid-state structure for Pd(**phenolate-1**)$_2$ was obtained (**Figure 36**), confirming a square-planar geometry, as was the case for each of the solid-state structures of palladium(II) complexes obtained. Comparing the structures of Pd(**L1**)$_2$ and Pd(**phenolate-1**)$_2$, several similarities are apparent. For both complexes, ligands oriented with anionic moieties trans to one another, with similar internuclear distances between chelating ligands to the metal centre. The slight distortion in the geometry of the square-planar Pd(**L1**)$_2$ when compared to Pd(**phenolate-1**)$_2$ (confirmed by their τ_4 values, **Table 2**) may speak to the relative stabilities of 5 and 6-membered metallocycles more generally. 5-membered palladacycles in particular tend to be more thermodynamically stable than their 6-membered counterparts, which often distort to alleviate ring strain.[64] This is largely due to the relatively smaller bite angle of 5-membered chelates, which more closely matches the 90º ideal coordination geometry of square-planar palladium(II) complexes.[65] These complexes' relative thermodynamic stabilities are supported by attempts to recrystallize both complexes: after being left on the benchtop in DCM for multiple days, Pd(**phenolate-1**)$_2$

remained unchanged, while Pd(**L1**)$_2$ decomposed into palladium(0) and **L1**-H when left in the same environment as confirmed by ^{1}H-NMR spectroscopy. The ρ value determined for Pd(**phenolate-1**)$_2$ is similar to that of Pd(**L1**)$_2$ and **L1**-H, indicating that the electron density of the guanidine in moiety's double bond in the coordinated **phenolate-1** is similarly delocalized about the endocyclic nitrogens.

Section 2.3 Polymerization Studies

Section 2.3.1 Olefin Polymerization

Pd(**L1**)(Me)(MeCN) was tested for preliminary olefin polymerization studies. This complex was designed to have a few helpful features for coordination-insertion style olefin polymerization. The aforementioned late transition metal's balance between oxophilicity and activity, and the guanidine-sulfonate's high donor character and chelating nature further stabilizing the complex, are leveraged to produce a suitable catalyst for olefin polymerization and potential copolymerization. Beyond these features, the labile acetonitrile is able to freely dissociate from the palladium(II) metal centre, leaving an open site for η^2 coordination of an olefin, whereupon the nucleophilic methyl group attacks the double bond, leading to its migratory insertion, freeing another open site for coordination and subsequent insertion of another monomer unit. The growing polymer chain then becomes the active nucleophile.[66]

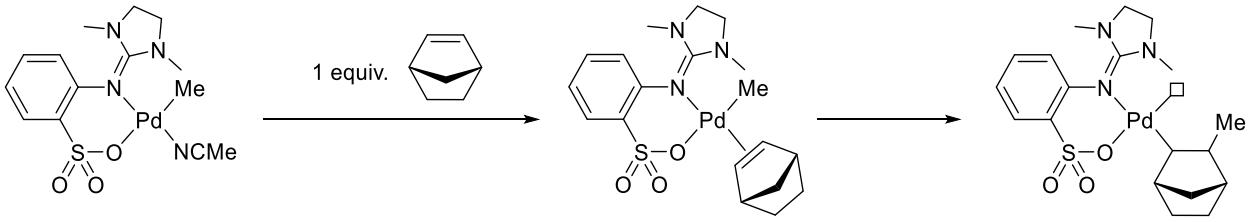

Scheme 12. *Migratory Insertion of one equivalent of norbornene into the Pd(**L1**)(Me)(MeCN) catalyst.*

Norbornene (NB) was selected for preliminary olefin insertion reactions. While being solid under ambient conditions, its boiling point is low enough to remove under reduced pressure facilitating removal of unreacted monomer for NMR analysis. Pd(**L1**)(Me)(MeCN) was dissolved in MeCN-d_3 along with 1 equivalent of norbornene. The proposed product, Pd(**L1**)(MeCN)(C_8H_{13}), is pictured in **Scheme 12**. In the ^{1}H-NMR spectrum of the crude product collected 30 minutes after addition of norbornene (**Figure A25**) the olefinic resonance of norbornene (observed at 6.0 ppm in MeCN-d_3) is not observed. Resonances corresponding to

palladium-coordinated **L1**$^-$ had shifted. Resonances in the alkyl region attributed to coordinated C_8H_{13} when integrated represented 14 protons in total. The resonances attributed to both isomers of Pd(**L1**)(Me)(MeCN) were no longer seen upon addition of norbornene, which may suggest that the bulkier ligand causes one conformation to be energetically favoured, similar to the case of Pd(**L1**)(Me)(py) which also had no visible isomers (**Figure A16**). The proposed complex, Pd(**L1**)(MeCN)(C_8H_{13}), indicated that the catalyst can undergo coordination-insertion, providing evidence toward olefin polymerization activity.

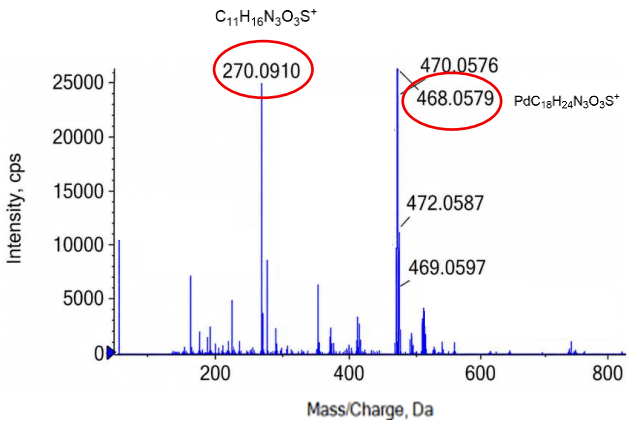

Figure 37. *Mass spectrometric Data for 10 : 1 norbornene : Pd(**L1**)(Me)(MeCN).*

Another experiment was conducted in a 10:1 stoichiometric ratio to confirm the capability of Pd(**L1**)(Me)(MeCN) to polymerize NB. The experiment was similarly conducted in MeCN-d_3 in an NMR tube at 60 °C. The experiment was monitored by ^{1}H-NMR spectroscopy. After 2 hours, little reaction had occurred, though some broadening of the resonances in the ^{1}H-NMR spectrum were observed, as well as loss of diastereomerism characteristic of Pd(**L1**)(Me)(MeCN). After 14 hours, precipitate had formed in the NMR tube. The ^{1}H-NMR spectrum collected in $CDCl_3$ after 14 hours and removal of volatiles (**Figure A26**) no olefinic resonances were observed, though broad resonances in the alkyl region attributed to norbornene were present, indicating conversion

of norborbornene to oligonorbornene. The relative ratios of resonances attributed to PNB and coordinated **L1**$^-$ (identified by comparison to literature NMR spectra of PNB)[18] was 9:1. This indicates activity towards NB polymerization. However, the limitation of Pd(**L1**)(Me)(MeCN) requiring coordinating solvent in order to dissolve may be contributing to low activity as dissociation of acetonitrile to permit coordination of norbornene is an integral part of the coordination-insertion pathway. Mass spectrometric data indicated the presence of coordinated, singly inserted norbornene, after cleavage of a methyl moiety ($PdC_{18}H_{24}N_3O_3S$: m/z 468.0579 (actual) vs 468.0573 (theoretical)) **Figure 37** (left). The relative intensities of peaks observed between m/z values of 468 and 474 align with theoretically calculated values determined from the isotopic abundance of atoms present in $PdC_{18}H_{24}N_3O_3S$. No m/z peaks were observed corresponding to oligonorbornene (free or coordinated). It is possible that some smaller free oligonorbornene species were lost during the removal of volatiles before sample analysis. In the acquired mass spectra, high amounts of dissociation of **L1**$^-$ were observed (m/z of 270.0910 (actual) vs 270.0907 (theoretical) representing protonated **L1**-H remaining after cleavage). This was likely to have occurred in the methanol solution used during elution of sample for mass spectrometric analysis, as no decomposition of the complex was indicated in the prior NMR spectrum collected (**Figure A26**).

Another catalyst designed for NB polymerization, Pd(**L1**)(Me)(py), was tested to be compared to the performance of Pd(**L1**)(Me)(MeCN). Due to its higher solubility in non-coordinating solvents, the reaction was able to be performed in $CDCl_3$. This was done to avoid interference from coordinating solvent competing with NB to bind to the catalyst's open site. A 20:1 NB:catalyst stoichiometric ratio was used and the experiment was conducted in an NMR tube, at 60 °C. ^{1}H-NMR analysis showed little oligomerization occurring after over 100 hours of mixing

time (indicated by the relatively large olefinic resonance of norbornene still present) (**Figure A27**). It is likely that pyridine, being more strongly coordinating than acetonitrile, was less prone to dissociate from the catalyst to provide an active site for norbornene coordination, limiting the rate of the reaction significantly.

In comparison to the works of Eisen et al., the activity and stability of these catalysts is severely limited.[18] Eisen's guanidine-phenolate systems display high activity for norbornene polymerization ($\sim 10^6$ g mol^{-1} h^{-1}) and good thermal stability up to 100 ºC. As was the case for Pd(**phenolate-1**)$_2$ and Pd(**L1**)$_2$ it is likely that the phenolate complexes are generally more thermally stable, allowing for them to be heated to higher temperatures for polymerization. One key difference that may be adopted to improve the performance of future guanidine-sulfonate based catalysts involves the implementation of a cocatalyst. In each case, with largely similar Pd(L_2X_2) type catalysts, a cocatalyst was used as an initiator to strip a neutral donor from the complex, producing an active site. For instance, cocatalysts like methylaluminumoxane, MAO were used to strip PPh_3 from their guanidine-phenolate containing palladium(II) species, forming their active Pd(II) catalyst. It is probable, in the case of Pd(**L1**)(Me)(MeCN) and Pd(**L1**)(Me)(py), that competition with the coordinating MeCN and py in the reaction mixtures greatly reduced the activity of their corresponding complexes. This conclusion is supported by the relatively higher activity of Pd(**L1**)(Me)(MeCN) when compared to that of Pd(**L1**)(Me)(py), whose more strongly coordinating pyridine ligand would be less likely to dissociate such that η^2 coordination of the olefin may occur.

Section 2.3.2 Isocyanide Polymerization

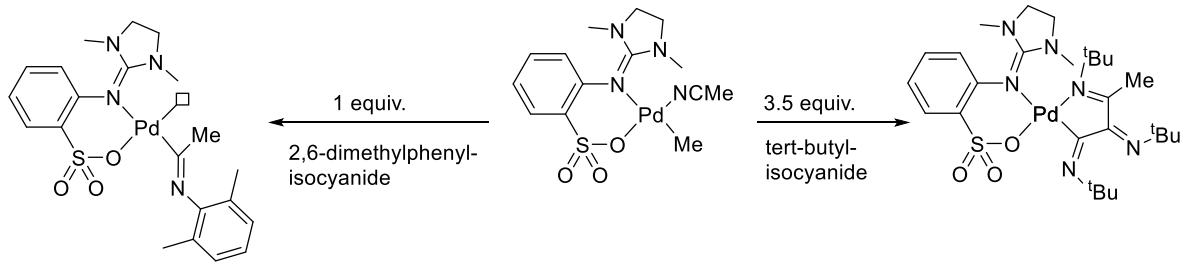

Figure 38. *Single-insertion product upon addition of 2,6-dimethylphenyl isocyanide to Pd(**L1**)(Me)(MeCN) (left) and trimer formed upon addition of 3 equivalents of tert-butyl isocyanide to Pd(**L1**)(Me)(MeCN) (right).*

Following promising results from norbornene polymerization using Pd(**L1**)(Me)(MeCN), a 1:1 isocyanide:catalyst experiment was performed using 2,6-dimethylphenyl isocyanide (DMIC) at 20 ºC in MeCN-d_3. The presence of the single insertion product, Pd(**L1**)(MeCN)($C_{10}H_{14}N$) (**Figure 38**), was confirmed by NMR spectroscopy. After removing volatiles and collecting a ^{1}H-NMR spectrum (**Figure A29**), integrations aligned with the presence of an inserted isocyanide. The spectrum, for instance, displayed a new peak about 2.38 ppm, attributed to the 6 benzylic protons. Additionally, a total of 7 aromatic protons were counted, which can be attributed to the aromatic protons of coordinated **L1**$^-$ and (2,6-dimethylphenyl)N=CMe insertion product. Finally, as was the case for Pd(**L1**)(MeCN)(C_8H_{13}) (the single insertion product from addition of norbornene to Pd(**L1**)(Me)(MeCN)), diastereomerism observed by NMR in the pure catalyst was no longer observed upon insertion of DMIC.

Compound Pd(**L1**)(Me)(MeCN) was next dissolved in protio-MeCN along with 3.5 equivalents of tert-butyl isocyanide. The proposed product, Pd(**L1**)(MeCN)($C_{16}H_{30}N_3$), is pictured in **Figure 38**, this product contains a 5-membered metallocycle coordinating in an LX fashion, similar to that of **L1**$^-$. After removal of volatiles, the product appeared physically similar to the catalyst precursor (yellow oil), though its solubility in chloroform was much higher than that of Pd(**L1**)(Me)(MeCN). In the ^{1}H-NMR spectrum collected in $CDCl_3$ (**Figure A28**), the resonance

of pure tert-butyl isocyanide (1.46 ppm in $CDCl_3$) was not present. The resonance corresponding to the coordinated tert-butyl isocyanide trimer instead appears between 1.62 – 1.52 ppm and is much broader. When integrated relative to the aromatic resonance attributed to coordinated **L1**$^-$ at 8.1 ppm, this signal corresponds to 33 protons compared to the expected 30 protons of the methylated trimer. Similar to the single insertion product illustrated in **Figure 38**, the diastereomerism observed in Pd(**L1**)(Me)(MeCN) is no longer visible in the ^{1}H-NMR spectrum. Addition of more tert-butyl isocyanide to the reaction mixture and heating to 60 °C yielded no change in the ^{1}H-NMR spectrum after removal of volatiles. This suggests that the chelating trimer would not further react to produce the tetramer (or larger oligomer). Similar observations were reported by Takahashi *et al.* and Lavoie *et al.* with Pd(II) catalysts unable to produce higher than trimeric oligomers of isocyanides (see section 1.3).[30,32]

Section 2.3.3 Lactide Polymerization

Lactide polymerization was attempted with bis-chelated complexes Zn(**L1**)$_2$ and Pd(**L1**)$_2$, following the work done by Herres-Pawlis with their analogous zinc system,[40] using unpurified *rac*-lactide to test the catalytic performance in the presence of impurities. As was discussed in section 1.2.1, the presence of alcohol and water impurities in the lactide used is essential as an initiator for ring-opening.[22] Tin octoate was used as the benchmark catalyst. Analyses were performed using chain end analysis of ^{1}H-NMR spectra to determine the in addition to 2D DOSY experiments to determine the number average and weight average molecular weights respectively, as well as the dispersity, Đ (**Table 3**).

Table 3. Results of solvent-free ring-opening polymerizations of *rac*-lactide

	k_{obs} (s^{-1}) [a]	P_r	M_w (Da) [b]	M_n (Da) [c]	Đ [d]
Zn(**L1**)$_2$	1.04 x 10^{-4}	0.73	2100	1500	1.42
Pd(**L1**)$_2$	1.49 x 10^{-5}				
Sn(Oct)$_2$	1.42 x 10^{-3}	0.51	3500	2000	1.72

*[a] Each polymerization was performed at 130 ± 3°C, solvent-free, in an inert atmosphere of nitrogen at a 1:100 catalyst to lactide molar ratio. Note: the observed rate of polymerization (k_{obs}) obtained for Pd(**L1**)$_2$ was obtained after 25% conversion, due to decomposition of the catalyst, while that of Sn(oct)$_2$ and Zn(**L1**)$_2$ was obtained after about 80% conversion.[b] Determined by DOSY NMR in C_6D_6. [c] Determined by end-group analysis. [d] Đ = M_w / M_n.*

The k_{obs} of Sn(Oct)$_2$ is roughly an order of magnitude higher than that of Zn(**L1**)$_2$ which itself is nearly an order of magnitude higher than that of Pd(**L1**)$_2$. Palladium(0) was observed forming when Pd(**L1**)$_2$ was used for polymerization, indicating decomposition of the catalyst during polymerization.

The average molecular weights for tin octoate were higher than those of Zn(**L1**)$_2$. However, it should be noted that the dispersity, Đ, is higher for tin octoate than the zinc complex, indicating less variation in molecular weights when using Zn(**L1**)$_2$. Reliable molecular weight data could not

be obtained for Pd(**L1**)$_2$ due to decomposition of the catalyst during the polymerization. This was determined as black, insoluble solid (palladium(0)) was observed forming in the polymerization vessel. Theoretical molecular weights for polymers produced can be calculated using the following formula:

$$MW_T = \frac{n_{monomer}}{n_{initiator}}\ x\ (percent\ conversion)\ x\ MW_{monomer} + MW_{end\ groups} \quad (8)$$

Where MW_T is the theoretical molecular weight of the polymer, $n_{monomer}$ and $n_{initiator}$ are the moles of monomer and initiator (assumed to be the catalyst), whose ratio in 100:1 for the polymerizations performed, *percent conversion*, which is assumed to be 80%, $MW_{monomer}$ and $MW_{end\ groups}$ are the molecular weight of the monomer and end groups respectively. For Zn(**L1**)$_2$, theoretical molecular weights of polymer can be calculated using **Equation 8** as being around 5900 g/mol. The discrepancy between theoretical and actual molecular weights (1500 g/mol, **Table 3**) is likely due to chain-transfer and transesterification, both of which tend to reduce polymer molecular weights and occur in the presence of alcohol, a likely contaminant in the unpurified lactide used.[8,21]

To determine the probability of heterotactic enchainment P_r,[22] homodecoupled ^{1}H-NMR experiments were performed. Tin octoate has a P_r of 0.51, indicating no tacticity control, while the Zn(**L1**)$_2$ catalyst has a marked improvement in polymer heterotacticity, with a P_r of 0.73. This result shows a notable increase in tacticity control when compared to other zinc based catalysts produced by the Lavoie group which had not exceeded a P_r of 0.62.[37] Stereocontrol can be achieved by chain-end control, where the stereochemistry of the preceding unit in the growing polymer chain affects the next inserted unit, or by enantiomorphic site control, where the chirality of the catalyst governs the stereochemistry of the resultant polymer.[67,68] It is likely that the heterotactic bias observed when using Zn(**L1**)$_2$ as a catalyst is primarily a consequence of chain-end control, as no persistent chiral centre or notable asymmetry is present in the catalyst, which would be

required to achieve a significant heterotactic bias via enantiomorphic site control. It should be noted that the relatively high temperature of the polymerization (130 °C) as well as the presence of alcohol used to initiate the reaction may have had adverse effects on the tacticity observed as these factors increase side reactions like chain-transfer and transesterification, which in turn affects polymer tacticity.[8,21]

3. Conclusions

A new family of ligand, the guanidine-sulfonate, was established. Four new monoanionic guanidine containing ligands were synthesised. Modifying the functional groups about the endocyclic nitrogen moieties as well as the backbone of the heterocycle had profound impacts on the coordination chemistry and general reactivity of the ligands. Two solid-state structures of the novel ligand system were obtained and compared, notable differences in electron density about each ligand's guanidine moiety yielded differences in basicity and reactivity between ligands. This novel class of ligands, the guanidine-sulfonate, builds on its predecessors the guanidine-phenolate and guanidine-ethenolate to provide a scaffold for ligand modification and activity studies.

Successful coordination of ligands **L1**$^{-}$ and **L4**$^{-}$ to group 10 metals was confirmed by NMR spectroscopy and single-crystal X-ray diffraction. Two novel palladium(II) complexes containing **L1**$^{-}$ and one containing a guanidine-phenolate analogue were characterized via XRD. A zwitterionic palladium(II) species containing a modified version of ligand **L1**$^{-}$ (**L1'**$^{2-}$) was also observed by XRD. All obtained complexes had square-planar (or distorted square-planar) geometry.

Complexes Pd(**L1**)(Me)(MeCN) and Pd(**L1**)(Me)(py) were implemented for norbornene polymerization. Both complexes were active for single insertion of norbornene, with Pd(**L1**)(Me)(MeCN) being the more active of the two. Pd(**L1**)(Me)(MeCN) also displayed ability to undergo coordination-insertion with isocyanides, whereupon a chelating trimer was observed forming. Studies of zinc(II) and palladium(II) bis-chelated complexes containing **L1**$^{-}$ showed activity for ROP of lactide. Zn(**L1**)$_2$ showed significantly more heterotactic bias than the industrial

standard (Pr of 0.73 vs 0.51 for $Sn(Oct)_2$) with a rate of polymerization nearly within an order of magnitude.

Future work implementing the guanidine-sulfonate ligand system may benefit from modification of the aromatic ring system as this has been shown to affect similar systems' polymerization results significantly, such as the phenoxy-imine systems' significant increase in activity upon addition of a tert-butyl group to the benzene ring.[69] Cyclic alkyl(amino)imines are in many ways analogous to cyclic guanidines, notably replacing one of their π-donor endocyclic nitrogen groups with an alkyl group, making the imine a stronger σ-donor and better π-acceptor.[70] Cyclic alkyl(amino)imine-sulfonate ligands may relieve issues of decomposition observed at moderate temperatures in guanidine-sulfonate complexes and may make the catalyst more robust against poisoning by polar moieties.

4. Experimental

General Considerations

Unless stated otherwise, all reactions were performed under inert atmosphere in a nitrogen filled glovebox. 1,3-Diisopropyl-1H-imidazol-3-ium bromide was synthesised according to literature procedure.[15] All reagents were purchased from Sigma-Aldrich or Strem Chemicals and used as received. Deuterated solvents $CDCl_3$, C_6D_6, and CD_3CN were purchased from Sigma-Aldrich. C_6D_6 was vacuum distilled over sodium and benzophenone, $CDCl_3$ and CD_3CN were dried over calcium hydride. All deuterated solvents were degassed by freeze-pump-thaw cycles and vacuum transferred to dry ampules containing molecular sieves. Unless otherwise stated, ^{1}H-NMR spectra were referenced to residual protio solvent resonances (δ 7.26 ppm for $CDCl_3$, 7.15 ppm for C_6D_6, 5.32 ppm for CD_2Cl_2, 1.94 ppm for CD_3CN, 3.43 and 3.66 ppm for MeOD-d_4 and 4.67 ppm for D_2O). All glassware was dried in an oven overnight prior to use. All NMR spectra were collected using either Bruker UltraShield 600, Bruker 400, or Bruker 300 MHz spectrometers. Unless otherwise stated, all NMR spectra were collected at room temperature. Mass spectrometry data was collected using York University's ZenoToF7600 and Waters M-class systems.

General Procedures for Polymerizing Norbornene

All polymerizations were prepared in a dry, nitrogen filled MBraun glovebox. NMR tubes were prepared, charged with norbornene and catalyst in a 10:1 or 20:1 stoichiometric ratio and capped with NMR tube caps. NMR tubes were heated to 60 ºC in either $CDCl_3$ or MeCN-d_3. ^{1}H-NMR analysis was implemented to compare oligonorbornene species to reported values Li *et al.*[18]

General Procedures for Polymerizing Isocyanide

All polymerizations were prepared in a dry, nitrogen filled Mbraun glovebox. Vials, charged with isocyanide monomer and catalyst in a 3.5 : 1 stoichiometric ratio and capped. Reactions were performed in protio-MeCN heated to 60 ºC. After removal of volatiles, ^{1}H-NMR analysis was performed in $CDCl_3$.

General Procedure for Polymerizing *rac*-Lactide

All polymerizations were performed unpurified *rac*-lactide. In a dry, nitrogen filled MBraun glovebox, a flask, charged with *rac*-lactide and catalyst in a 100:1 ratio, was capped with a rubber septa. The flask was placed in an oil bath, stirring at 130 ± 3°C, aliquots were taken every 5 minutes once the lactide had fully melted. After an hour elapsed, aliquots were taken every 30 minutes, aliquots were taken every hour after 2 hours had elapsed. Collecting a ^{1}H-NMR spectrum of each aliquot, to determine percent conversion of lactide to polylactide allows for analysis of k_{obs}. DOSY experiments were performed in C_6D_6, spectra were acquired following conditions reported by Sosnowski.[13]

Methods for Analysis of PLA

To determine the k_{obs}, aliquots were taken periodically during polymerization and ^{1}H-NMR was taken in $CDCl_3$. Integrations of peaks observed from the polymer itself were compared to those of the remaining monomer to determine the percent conversion. Graphs were then created, plotting $\ln\left(\frac{1}{1-conversion}\right)$ as a function of time (s). The slope of the line of best fit of the corresponding graph is k_{obs}. The diffusion coefficient, D, was determined via DOSY NMR and was in turn used to calculate the M_w using the following equation: $D = K'M_w^{-\nu}$, where K' and $-\nu$ are constants determined by Sosnowski.[13] M_n, number average molecular weight, was calculated using end chain analysis.

Crystal Structure Determination

Diffraction data for ligands and complexes was collected on a Bruker APEX-II CCD diffractometer with a Mo Kα (λ = 0.71073 Å) radiation source. Crystals were mounted under a stream of N_2 and kept at 173K during data collection. Structures were solved in Olex2-v1.5 using direct methods and refined with ShelXL refinement package using least-squares minimization.

Density Functional Theory Calculations

DFT calculations were performed using Gaussian 16 on SHARCNET computational resources. Geometry optimizations and vibrational frequency calculations were performed in the gas phase at the B3LYP level of theory with the LANL2DZ basis set.

Synthesis of Ligands

Compound L1-H. In open atmosphere, orthanilic acid (0.10 g, 0.58 mmol, 1.0 equiv.) and triethylamine (0.20 mL, 1.4 mmol, 2.5 equiv.) were dissolved in 15 mL DCM. In a vial, 2-chloro-1,3-dimethylimidazolinium chloride (0.13 g, 0.75 mmol 1.3 equiv.) was dissolved in 2 mL of DCM; this was added dropwise to the sulfonic aniline containing flask while stirring. The solution was allowed to mix for 24 hours before filtering and washing the solids with 20 mL of DCM. Volatiles were then removed under vacuum to yield a white solid (0.040 g, 0.15 mmol, 30%) ^{1}H-NMR (400 MHz, $CDCl_3$): δ 9.95 (s, 1H, NH), 8.02-8.01 (dd, J = 7.68, 1.2 Hz, 1H, Ar-CH), 7.33-7.29 (dt, J = 7.52, 1.20 Hz, 1H, Ar-CH), 7.24-7.20 (t, J = 7.84 Hz, 1H, Ar-CH), 7.04-7.02 (d, J = 7.80 Hz, 1H, Ar-CH), 3.78 (s, 4H, CH_2), 2.86 (s, 6H, CH_3). $^{13}C\{^{1}H\}$ NMR (75.5 MHz, CD_3CN) 156.6, 137.2, 133.2, 130.2, 127.5, 124.4, 120.8. Anal. Calc. for $C_{11}H_{15}N_3O_3S$ (%): C, 49.06; H, 5.61; N, 15.60. Found (%): C, 47.68; H, 5.07; N, 14.7.

Compound L2-H. In open atmosphere, KOH (0.031 g, 0.55 mmol, 2.1 equiv.) and orthanilic acid (0.045 g, 0.26 mmol, 1.0 equiv.) and 2-chloro-1,3-diisopropylimidazolinium chloride (0.058 g, 0.27 mmol, 1.0 equiv.) were stirred in 5 mL MeCN and 1 mL H_2O. After 1 hour of stirring, the mixture was filtered before removing volatiles, and washing the solids with hexanes yielding a yellow oily solid (0.065 g, 0.20 mmol, 77%). ^{1}H-NMR (400 MHz, $CDCl_3$): δ 7.62 (s, 2H, CH), 7.60-7.58 (d, J = 8.12 Hz, 1H, Ar-CH), 7.07 (s, 1H, Ar-CH), 6.64-6.62 (d, J = 7.48 Hz, 1H, Ar-CH), 6.56 (s, 1H, Ar-CH), 5.16 (s, 1H, NH), 4.77-4.67 (sept, J = 6.72 Hz, 2H, ^{i}Pr-CH), 1.53-1.51 (d, J = 6.72 Hz, 12H, ^{i}Pr-CH_3). $^{13}C\{^{1}H\}$ NMR (75.5 MHz, CD_3CN) 144.3, 136.1, 130.4, 130.1, 128.0, 121.3, 119.2, 116.5, 116.4, 53.1, 23.0, 21.9. Anal. Calc. for $C_{15}H_{21}N_3O_3S$ (%): C, 55.71; H, 6.55; N, 12.99. Found (%): C, 55.45; H, 6.29; N, 13.26.

Compound L3-H. In open atmosphere, KOH (0.012 g, 0.22 mmol, 2.2 equiv.) and orthanilic acid (0.019 g, 0.11 mmol, 1.1 equiv.) and 2-Chloro-1,3-mesitylimidazolinium chloride (0.037 g, 0.099 mmol, 1.0 equiv.) were stirred in 5 mL MeCN and 1 mL H_2O. After 1 hour of stirring, the mixture was filtered before removing volatiles and washing the solids with hexanes yielding a yellow oily solid (0.043 g, 0.084 mmol, 84%). ^{1}H-NMR (400 MHz, $CDCl_3$) δ 8.40 (s, 2H, CH), 7.67 (d, J = 8.1 Hz, 1H, Ar-CH), 7.08 (s, 4H, Ar_{mes}-CH), 7.00 (m, 1H, Ar-CH), 6.55 (m, 2H, Ar-CH), 2.39 (s, 6H, Ar_{mes}-CH_3), 2.07 (s, 12H, Ar_{mes}-CH_3). $^{13}C\{^{1}H\}$ NMR (75.5 MHz, $CDCl_3$) δ 144.3, 142.4,

134.3, 130.2, 130.1, 129.9, 129.2, 128.1, 127.8, 116.3, 116.2, 21.2, 17.3. Anal. Calc. for $C_{27}H_{29}N_3O_3S$ (%): C, 68.22; H, 5.87; N, 9.09. Found (%): C, 68.19; H, 6.15; N, 8.84.

Compound L4•$HNEt_3$**.** In open atmosphere, orthanilic acid (0.014 g, 0.081 mmol, 1.0 equiv.) and triethylamine (0.10 mL, 0.72 mmol, 9.0 equiv.) were dissolved in 15 mL DCM. In a vial, 2-chloro-1,3-dimethylimidazolinium chloride (0.0.20 g, 0.079 mmol 1.0 equiv.) was dissolved in 2 mL of DCM; this was added dropwise to the sulfonic aniline containing flask while stirring. The solution was allowed to mix for 24 hours before filtering and washing solids with 20 mL of DCM, volatiles were then removed under vacuum to yield a white solid (0.029 g, 0.068 mmol, 0.84 equiv.). ^{1}H-NMR (400 MHz, $CDCl_3$) δ 10.62 (s, 1H, NH), 7.94 (d, *J* = 6.9 Hz, 1H, Ar-CH), 7.33 (t, *J* = 7.6 Hz, 1H, Ar-CH), 7.07 (t, *J* = 7.6 Hz, 1H, Ar-CH), 6.83 (d, *J* = 7.8 Hz, 1H, Ar-CH), 4.25 (s, 2H, ^{i}Pr-CH), 3.17 (q, *J* = 7.3 Hz, 6H, N-C*H*$_2$CH$_3$), 1.42 (d, *J* = 7.8 HZ, 6H, ^{i}Pr-CH$_3$), 1.40 (m, 15H, N-CH$_2$C*H*$_3$, iPr-CH$_3$). ^{13}C{^{1}H} NMR (75.5 MHz, $CDCl_3$) δ 157.5, 142.6, 136.5, 133.9, 130.6, 127.9, 122.7, 119.6, 46.5, 46.2, 19.3, 19.1, 8.6. Anal. Calc. for $C_{21}H_{34}N_4O_5S$ (%): C, 55.48; H, 7.53; N, 12.32. Found (%): C, 55.57; H, 7.47; N, 11.96.

Synthesis of Complexes

Pd(L1)(allyl). In open atmosphere, in a vial, a mixture of allylpalladium chloride dimer (0.015 g, 0.041 mmol, 0.5 equiv.), **L1**-H (0.022 g, 0.082 mmol, 1.0 equiv.), and KO^{t}Bu (0.010 g, 0.090 mmol, 1.1 equiv.) was prepared in MeCN and allowed to stir for 1 hour. After an hour of stirring, the mixture was filtered and volatiles were removed under vacuum to yield a pale-yellow oil (0.027 g, 0.065 mmol, 81%). ^{1}H-NMR (400 MHz, $CDCl_3$) δ 7.88 (s, 1H, Ar-CH), 7.19 (s, 1H, Ar-CH), 6.92 (s, 1H, Ar-CH), 6.72 (s, 1H, Ar-CH), 5.41 (s, 1H, allyl-CH), 3.88 (s, 2H, allyl-CH_2), 3.39 (s, 4H, CH_2), 2.89 (s, 2H, allyl-CH_2), 2.74 (s, 6H, CH_3). ^{13}C{^{1}H} NMR (75.5 MHz, $CDCl_3$) δ 145.7, 137.1, 130.8, 128.3, 123.9, 122.3, 111.6, 62.9, 59.9, 53.5, 48.6, 35.3, 31.2. Anal. Calc. for $C_{13}H_{17}N_3O_3PdS$ (%): C, 40.44; H, 4.61; N, 10.11. Found (%): C, 40.69; H, 4.61; N, 9.83.

Pd(L4)(allyl). In open atmosphere, in a vial, a mixture of **4•**$HNEt_3$ (0.037 g, 0.082 mmol, 1 equiv.) and KOH (0.007 g, 0.14 mmol, 1.8 equiv.) was prepared in methanol and allowed to stir for 1 hour. Volatiles were then removed under vacuum before redissolving in DCM and adding allylpalladium chloride dimer (0.015 g, 0.041 mmol, 0.5 equiv.). The mixture was allowed to stir for 1 hour. The

mixture was then filtered and volatiles were removed under vacuum to yield a pale-yellow oil (0.034 g, 0.068 mmol, 83%). ^{1}H-NMR (400 MHz, MeOD-d_4) δ 7.93 (d, J = 7.8, 1H, Ar-CH), 7.43 (t, J = 7.7, 1H, Ar-CH), 7.14 (t, J = 7.32, 1H, Ar-CH), 6.96 (d, J = 7.84, 1H, Ar-CH), 5.58 (sep, J = 6.6 Hz, 1H, allyl-CH), 4.26 (s, 2H, ^{i}Pr-CH), 4.04 (d, J = 6.68, 2H, allyl-CH_2), 3.03 (d, J = 12.08 Hz, 2H, allyl-CH_2), 1.45 (dd, J = 31.8, 6.72, 12H). ^{13}C{^{1}H} NMR (75.5 MHz, MeOD-d_4) δ 158.0, 142.8, 136.5, 130.6, 127.6, 122.4, 119.6, 111.3, 18.6, 18.1, 18.0. Anal. Calc. for $C_{18}H_{23}N_3O_5PdS$ (%): C, 43.25; H, 4.64; N, 8.41. Found (%): C, 43.53; H, 4.88; N, 8.19.

Ni(L1)(Me)(Lut). In a vial, a mixture of 1,5-lutidine (0.05 mL, 0.45 mmol, 4.7 equiv.) and **L1**-H in DCM was allowed to stir for 24 hours before addition to a separate vial in which nickel bis(1,5-cyclooctadiene) (26.4 mg, 0.097 mmol, 1.0 equiv.) had been dissolved in DCM. After 24 hours of stirring, allyl bromide (0.05 mL, 0.6 mmol, 6.0 equiv.) was added. The mixture was allowed to stir another 48 hours before addition of trimethyl aluminum (0.05 mL, 0.1 mmol, 1.0 equiv.) and allowing to stir an additional 12 hours before extracting with ether, yielding a red solid (15 mg, 0.033 mmol, 34%). ^{1}H-NMR (400 MHz, C_6D_6): δ 7.16-7.14 (d, J = 6.4 Hz, 1H, Ar-CH), 7.13-7.10 (d, J = 8.5 Hz, 1H, Ar-CH), 6.72-6.68 (t, J = 7.52 Hz, 1H, Ar-CH), 6.40-6.38 (d, J = 7.6 Hz, 1H, Ar-CH), 4.03 (s, 3H, CH_3), 2.33 (s, 3H, CH_3), 2.21 (s, 2H, CH_2).

Pd(L1)(Me)(MeCN). In a vial, a mixture of chloro(1,5-cyclooctadiene)methylpalladium (0.020 g, 0.075 mmol, 1.0 equiv.), **L1**-H (0.021 g, 0.078 mmol, 1.0 equiv.), and KO^{t}Bu (0.0090 g, 0.075 mmol, 1.0 equiv.) was prepared in MeCN and allowed to stir for 1 hour. After an hour of stirring, the mixture was filtered and volatiles were removed under vacuum to yield a yellow solid (0.029 g, 0.066 mmol, 84%). ^{1}H-NMR (400 MHz, CD_3CN) major isomer (64%) δ 7.80 (m, 2H, Ar-CH overlapping isomers), 7.34 (m, 2H, Ar-CH overlapping isomers), 7.15 (m, 1H, Ar-$CH_{(minor)}$), 7.07 (m, 1H, Ar-$CH_{(major)}$), 6.96 (m, 2H, Ar-CH overlapping isomers), 3.59 (s, 4H, $CH_{2(major)}$), 3.40 (s, 3H, $CH_{2(minor)}$), 3.03 (s, 4H, $CH_{3(minor)}$), 2.78 (s, 6H, $CH_{3(major)}$), 1.99 (s, 1H, $CH_3CN_{(minor)}$), 1.29 (s, 2H, $CH_{3(major)}$), 0.78 (s, 2H, $CH_{3(minor)}$). ^{13}C{^{1}H} NMR (75.5 MHz, $CDCl_3$) δ 130.9, 130.2, 127.6, 127.0, 125.2, 123.2, 122.6, 122.2, 78.2, 48.9, 48.6, 35.7, 34.4, 29.4, -7.7. Anal. Calc. for $C_{14}H_{20}N_4O_3PdS$ (%): C, 39.03; H, 4.68; N, 13.00. Found (%): C, 39.11; H, 4.41; N, 12.89.

Pd(L1)(Me)(py). In a vial, a mixture of chloro(1,5-cyclooctadiene)methylpalladium (0.020 g, 0.077 mmol, 1.0 equiv.) and pyridine (0.012 mL, 0.15 mmol, 2.0 equiv.) was allowed to stir for 30 minutes in 5 mL DCM before addition of a mixture of **1**-H (0.023 g, 0.085 mmol, 1.1 equiv.), and KO^{t}Bu (0.010 g, 0.09 mmol, 1.2 equiv.) in 3 mL DCM. The mixture was allowed to stir for 1 hour before filtering and removing volatiles under vacuum to yield a yellow solid (0.025 g, 0.053 mmol, 69%). ^{1}H-NMR (400 MHz, $CDCl_3$) δ 8.87 (m, 2H, py-CH), 8.08 (d, *J* = 6.1 Hz, 1H, py-CH), 7.76 (m, 2H, Ar-CH, overlap with pyridine), 7.33 (m, 2H, py-CH), 7.19 (t, *J* = 7.9 Hz, 1H, Ar-CH), 6.98 (d, *J* = 7.9 Hz, 1H, Ar-CH), 3.42 (s, 4H, CH_2), 3.17 (s, 6H, CH_3), 0.81 (s, 3H, Pd-CH_3). Anal. Calc. for $C_{17}H_{22}N_4O_3PdS$ (%): C, 43.64; H, 4.52; N, 11.98. Found (%): C, 43.9; H, 4.26; N, 12.11.

Ni(L1)$_2$. In open atmosphere, in a round bottom flask, nickel bis(acetylacetonate) (25 mg, 0.10 mmol, 1.0 equiv.) was dissolved in 5 mL of MeOH along with **L1**-H (50 mg, 0.19 mmol, 1.9 equiv.). The mixture was allowed to stir for 12 hours before removing volatiles under vacuum, yielding a light green solid (30 mg, 0.050 mmol, 50%). ^{1}H-NMR (400 MHz, $CDCl_3$): *δ* 7.90-7.84 (m, 1H, Ar-CH), 7.49-7.37 (m, 1H, Ar-CH), 7.35-7.18 (m, 2H, Ar-CH), 3.66 (m, 4H, CH_2), 2.76 (m, 6H, CH_3). ^{13}C{^{1}H} NMR (75.5 MHz, D_2O) δ 132.7, 128.0, 127.5, 126.8, 48.7, 33.4. Anal. Calc. for $C_{22}H_{28}N_6O_6PdS_2$ (%): C, 44.39; H, 4.74; N, 14.12. Found (%): C, 44.43; H, 4.56; N, 14.38.

Pd(L1)$_2$. In open atmosphere, in a round bottom flask, palladium acetate (22 mg, 0.098 mmol, 1.0 equiv.) was dissolved in 5 mL of MeOH along with **L1**-H (61 mg, 0.23 mmol, 2.3 equiv.). The mixture was allowed to stir for 1 hour before filtering, washing with MeOH (5 mL) and acetone (5 mL) and extracting with chloroform. Volatiles were removed yielding a dark orange solid (20 mg, 0.030 mmol, 30%). ^{1}H-NMR (400 MHz, $CDCl_3$): *δ* 7.73-7.71 (dd, *J* = 7.8, 1.6 Hz, 1H, Ar-CH), 7.11-7.10 (dt, *J* = 7.3, 1.6 Hz, 1H, Ar-CH), 6.74-6.70 (dt, *J* = 7.5, 0.76 Hz, 1H, Ar-CH), 6.26-6.24 (d, *J* = 7.9 Hz, 1H, Ar-CH), 3.87 (s, 4H, CH_2), 3.23 (s, 6H, CH_3). ^{13}C{^{1}H} NMR (75.5 MHz, $CDCl_3$) δ 166.2, 146.3, 131.7, 128.27, 127.16, 117.2, 116.2, 117.2, 116.2, 117.23, 116.20, 46.9,

33.6. Anal. Calc. for $C_{22}H_{28}N_6O_6PdS_2$ (%): C, 41.09; H, 4.39; N, 13.07. Found (%): C, 41.22; H, 4.60; N, 13.13.

Zn(L1)$_2$. In a vial, **L1**-H (30 mg, 0.11 mmol, 2.2 equiv.) was dissolved in 3 mL DCM. To this solution, a solution of 1M diethylzinc in pentanes (0.05 mL, 0.05 mmol, 1.0 equiv.) was added dropwise while stirring. After allowing to stir for 2 hours, the mixture was decanted, washed with pentanes and volatiles were removed under vacuum to yield a white solid (45 mg, 0.075 mmol, 68%). ^{1}H-NMR (400 MHz, CD_3CN): δ 7.88-7.86 (dd, J = 7.8, 1.6 Hz, 1H, Ar-CH), 7.45-7.40 (dt, J = 8.1, 1.8 Hz, 1H, Ar-CH), 7.17-7.13 (dd, J = 7.6, 1.1 Hz, 1H, Ar-CH), 7.00-6.98 (dd, J = 8.1, 1.0 Hz, 1H, Ar-CH), 3.61 (s, 4H, CH_2), 2.67 (s, 6H, CH_3). ^{13}C{^{1}H} NMR (75.5 MHz, D_2O) δ 156.1, 136.8, 132.7, 132.5, 128.0, 127.4, 126.7, 48.6, 33.4. Anal. Calc. for $C_{22}H_{28}N_6O_6S_2Zn$ (%): C, 43.89; H, 4.69; N, 13.96. Found (%): C, 43.61; H, 4.37; N, 14.30.

Pd(phenolate-1)$_2$. In open atmosphere, in a round bottom flask, palladium acetate (30 mg, 0.13 mmol, 1.0 equiv.) was dissolved in 5 mL of MeOH along with **phenolate-1**-H (57 mg, 0.28 mmol, 2.1 equiv.). The mixture was allowed to stir for 1 hour before filtering, washing with MeOH (5 mL) and acetone (5 mL) and extracting with chloroform. Volatiles were removed yielding a deep purple solid (45 mg, 0.087 mmol, 65%). ^{1}H-NMR (400 MHz, $CDCl_3$): δ 7.73-7.71 (dd, J = 7.8, 1.6 Hz, 1H, Ar-CH), 7.11-7.10 (dt, J = 7.3, 1.6 Hz, 1H, Ar-CH), 6.74-6.70 (dt, J = 7.5, 0.76 Hz, 1H, Ar-CH), 6.26-6.24 (d, J = 7.9 Hz, 1H, Ar-CH), 3.87 (s, 4H, CH_2), 3.23 (s, 6H, CH_3). ^{13}C{^{1}H} NMR (75.5 MHz, D_2O) δ 164.6, 164.3, 142.0, 120.6, 117.2, 115.3, 113.6, 48.0, 36.1. Anal. Calc. for $C_{22}H_{28}N_6O_6S_2Zn$ (%): C, 51.32; H, 5.48; N, 16.32. Found (%): C, 51.44; H, 5.70; N, 16.12.

5. References

(1) Stürzel, M.; Mihan, S.; Mülhaupt, R. From Multisite Polymerization Catalysis to Sustainable Materials and All-Polyolefin Composites. *Chem. Rev.* **2016**, *116* (3), 1398–1433. https://doi.org/10.1021/acs.chemrev.5b00310.

(2) *Plastics - the Fast Facts*. plastics europe. https://plasticseurope.org/knowledge-hub/plastics-the-fast-facts-2024/ (accessed 2025-10-29).

(3) Johnson, L. K.; Mecking, S.; Brookhart, M. Copolymerization of Ethylene and Propylene with Functionalized Vinyl Monomers by Palladium(II) Catalysts. *J. Am. Chem. Soc.* **1996**, *118* (1), 267–268. https://doi.org/10.1021/ja953247i.

(4) Franssen, N. M. G.; Reek, J. N. H.; de Bruin, B. Synthesis of Functional 'Polyolefins': State of the Art and Remaining Challenges. *Chem. Soc. Rev.* **2013**, *42* (13), 5809–5832. https://doi.org/10.1039/C3CS60032G.

(5) Kitto, H. J.; Schwartz, E.; Nijemeisland, M.; Koepf, M.; Cornelissen, J. J. L. M.; Rowan, A. E.; Nolte, R. J. M. Post-Modification of Helical Dipeptido Polyisocyanides Using the 'Click' Reaction. *J. Mater. Chem.* **2008**, *18* (46), 5615–5624. https://doi.org/10.1039/B811002F.

(6) Boaen, N. K.; Hillmyer, M. A. Post-Polymerization Functionalization of Polyolefins. *Chem. Soc. Rev.* **2005**, *34* (3), 267–275. https://doi.org/10.1039/B311405H.

(7) *Raw Material*. pespine. https://www.pespipe.com/en-us/Technical-Resources/Raw-Material (accessed 2025-10-29).

(8) Michalovic, M.; Brust, G.; Parrish, D.; DePara Springsteen, P.; Grassino, S.; Mathias, L. *the Macrogalleria*. the Macrogalleria. https://pslc.ws/macrog/maindir.htm.

(9) Patra, S. G.; Das, N. K. Recent Advancement on the Mechanism of Olefin Metathesis by Grubbs Catalysts: A Computational Perspective. *Polyhedron* **2021**, *200*, 115096. https://doi.org/10.1016/j.poly.2021.115096.

(10) Schrodi, Y.; Pederson, R. Evolution and Applications of Second-Generation Ruthenium Olefin Metathesis Catalysts. *Aldrichimica Acta* **2007**, *40*, 45–52.

(11) Fernandez, M. H6-Arene Tethered Ruthenium (II) Complexes and Half-Metallocene Dithiocarbamate Ruthenium (IV) Complex for Olefin Polymerization: Experimental, Mechanistic, and DFT Studies. Dissertation, University of California, Irvine, 2014.

(12) Resconi, L.; Cavallo, L.; Fait, A.; Piemontesi, F. Selectivity in Propene Polymerization with Metallocene Catalysts. *Chem. Rev.* **2000**, *100* (4), 1253–1346. https://doi.org/10.1021/cr9804691.

(13) Noda, S.; Nakamura, A.; Kochi, T.; Chung, L. W.; Morokuma, K.; Nozaki, K. Mechanistic Studies on the Formation of Linear Polyethylene Chain Catalyzed by Palladium Phosphine−Sulfonate Complexes: Experiment and Theoretical Studies. *J. Am. Chem. Soc.* **2009**, *131* (39), 14088–14100. https://doi.org/10.1021/ja9047398.

(14) Johnson, L. K.; Killian, C. M.; Brookhart, M. New Pd(II)- and Ni(II)-Based Catalysts for Polymerization of Ethylene and .Alpha.-Olefins. *J. Am. Chem. Soc.* **1995**, *117* (23), 6414–6415. https://doi.org/10.1021/ja00128a054.

(15) Wang, C.; Friedrich, S.; Younkin, T. R.; Li, R. T.; Grubbs, R. H.; Bansleben, D. A.; Day, M. W. Neutral Nickel(II)-Based Catalysts for Ethylene Polymerization. *Organometallics* **1998**, *17* (15), 3149–3151. https://doi.org/10.1021/om980176y.

(16) Liu, Y.; Cong, R.; Pan, Y.; Chen, M.; Xu, M. Efficient Copolymerization of Ethylene with Norbornene Mediated by Phosphine-Sulfonate Palladium Catalysts. *Eur. Polym. J.* **2024**, *203*, 112674. https://doi.org/10.1016/j.eurpolymj.2023.112674.

(17) Berkefeld, A.; Mecking, S. Coordination Copolymerization of Polar Vinyl Monomers H2C=CHX. *Angew. Chem.* **2008**, *47*.
(18) Li, M.; Fang, Y.; Cai, Z.; Eisen, M. S. Nickel- and Palladium-Catalyzed Copolymerizations of Norbornene with Polar α-Olefins. *ChemCatChem* **2024**, *16* (17), e202301731. https://doi.org/10.1002/cctc.202301731.
(19) Künkel, A.; Becker, J.; Börger, L.; Hamprecht, J.; Koltzenburg, S.; Loos, R.; Schick, M. B.; Schlegel, K.; Sinkel, C.; Skupin, G.; Yamamoto, M. Polymers, Biodegradable. In *Ullmann's Encyclopedia of Industrial Chemistry*; 2016; pp 1–29. https://doi.org/10.1002/14356007.n21_n01.pub2.
(20) Gupta, A. P.; Kumar, V. New Emerging Trends in Synthetic Biodegradable Polymers – Polylactide: A Critique. *Eur. Polym. J.* **2007**, *43* (10), 4053–4074. https://doi.org/10.1016/j.eurpolymj.2007.06.045.
(21) Tschan, M. J.-L.; Gauvin, R. M.; Thomas, C. M. Controlling Polymer Stereochemistry in Ring-Opening Polymerization: A Decade of Advances Shaping the Future of Biodegradable Polyesters. *Chem. Soc. Rev.* **2021**, *50* (24), 13587–13608. https://doi.org/10.1039/D1CS00356A.
(22) Khan, B. Neutral Bidendate Guanidine-Based Zinc Complexes for the Ring Opening Polymerization of Lactide, York University, **2022**.
(23) Ovitt, T. M.; Coates, G. W. Stereochemistry of Lactide Polymerization with Chiral Catalysts: New Opportunities for Stereocontrol Using Polymer Exchange Mechanisms. *J. Am. Chem. Soc.* **2002**, *124* (7), 1316–1326. https://doi.org/10.1021/ja012052+.
(24) Singha Roy, S.; Sarkar, S.; Chakraborty, D. Determination of Polylactide Microstructure by Homonuclear Decoupled 1H NMR Spectroscopy. *Chem. Rec.* **2021**, *21* (8), 1968–1984. https://doi.org/10.1002/tcr.202100073.
(25) Masutani, K.; Kimura, Y. PLA Synthesis. From the Monomer to the Polymer. In *Poly(lactic acid) Science and Technology: Processing, Properties, Additives and Applications*; Royal Society of Chemistry, Jiménez, A., Peltzer, M., Ruseckaite, R., Eds.; The Royal Society of Chemistry, 2014; p 0. https://doi.org/10.1039/9781782624806-00001.
(26) Fuchs, M.; Schmitz, S.; Schäfer, P. M.; Secker, T.; Metz, A.; Ksiazkiewicz, A. N.; Pich, A.; Kögerler, P.; Monakhov, K. Y.; Herres-Pawlis, S. Mononuclear Zinc(II) Schiff Base Complexes as Catalysts for the Ring-Opening Polymerization of Lactide. *Eur. Polym. J. 122*, 109302. https://doi.org/10.1016/j.eurpolymj.2020.109302.
(27) Ke, J.; Conen, N.; Latz, F.; Neumann, J. N.; Fuchs, M.; Hoffmann, A.; Jupke, A.; Herres-Pawlis, S. Unleashing the Power of Non-Toxic Zn-Guanidine Catalysts for Sustainable Lactide Polymerization through Smart Modeling. *Faraday Discuss.* **2025**. https://doi.org/10.1039/D5FD00062A.
(28) Yashima, E.; Maeda, K.; Iida, H.; Furusho, Y.; Nagai, K. Helical Polymers: Synthesis, Structures, and Functions. *Chem. Rev.* **2009**, *109* (11), 6102–6211. https://doi.org/10.1021/cr900162q.
(29) Nolte, R. J. M.; Van Beijnen, A. J. M.; Drenth, W. Chirality in Polyisocyanides. *J. Am. Chem. Soc.* **1974**, *96* (18), 5932–5933. https://doi.org/10.1021/ja00825a038.
(30) Liu, N.; Zhou, L.; Wu, Z.-Q. Alkyne-Palladium(II)-Catalyzed Living Polymerization of Isocyanides: An Exploration of Diverse Structures and Functions. *Acc. Chem. Res.* **2021**, *54* (20), 3953–3967. https://doi.org/10.1021/acs.accounts.1c00489.
(31) Nolte, R. J. M. Helical Poly(Isocyanides). *Chem. Soc. Rev.* **1994**, *23* (1), 11–19. https://doi.org/10.1039/CS9942300011.

(32) Badaj, A. C.; Lavoie, G. G. Reactivity Study of Imino-N-Heterocyclic Carbene Palladium(II) Methyl Complexes. *Organometallics* **2013**, *32* (16), 4577–4590. https://doi.org/10.1021/om400533d.
(33) Amabilino, D. B.; Serrano, J.-L.; Sierra, T.; Veciana, J. Long-Range Effects of Chirality in Aromatic Poly(Isocyanide)s. *J. Polym. Sci. Part Polym. Chem.* **2006**, *44* (10), 3161–3174. https://doi.org/10.1002/pola.21366.
(34) Coles, M. P. Application of Neutral Amidines and Guanidines in Coordination Chemistry. *Dalton Trans.* **2006**, No. 8, 985–1001. https://doi.org/10.1039/B515490A.
(35) Conrads, C.; Burkart, L.; Soerensen, S.; Noichl, S.; Kara, Y.; Heck, J.; Hoffmann, A.; Herres-Pawlis, S. Understanding Structure–Activity Relationships: Iron(Ii) Complexes of "Legacy Guanidines" as Catalysts for the Synthesis of Polylactide. *Catal. Sci. Technol.* **2023**, *13* (20), 6006–6021. https://doi.org/10.1039/D3CY01117H.
(36) Larocque, T.; Dastgir, S.; Lavoie, G. Coordination and Reactivity Study of Titanium and Zirconium Complexes of the First Imidazol-2-Imine Ethenolate Ligand. *Organometallics* **2013**, *32*, 4314–4320. https://doi.org/10.1021/om4004708.
(37) Flores-Romero, V.; LeBlanc, J.; Lavoie, G. G. Zinc Complexes of Guanidine– and Amidine–Phenolate Ligands for the Ring-Opening Polymerization of Lactide. *Inorganics* **2025**, *13* (8), 265. https://doi.org/10.3390/inorganics13080265.
(38) Flores-Romero, V.; LeBlanc, J.; Chen, Z.; Lavoie, G. G. Ti and Zr Complexes Bearing Guanidine-Phenolate Ligands: Coordination Chemistry and Polymerization Studies. *RSC Adv.* **2024**, *14* (35), 25889–25899. https://doi.org/10.1039/D4RA05146G.
(39) Xu, Y.; Qi, N.; Wen, H.; Zhang, G.; Wang, Y.; Cui, H. Synthesis and Evaluation of Benzenesulfonic Acid Derivatives as Human Neutrophil Elastase (hNE) Inhibitors. *Med. Chem. Res.* **2021**, *30*, 387–398. https://doi.org/10.1007/s00044-020-02684-4.
(40) Stanek, J.; Rösener, T.; Metz, A.; Mannsperger, J.; Hoffmann, A.; Herres-Pawlis, S. Guanidine Metal Complexes for Bioinorganic Chemistry and Polymerisation Catalysis; 2015. https://doi.org/10.1007/7081_2015_173.
(41) Vázquez, S.; Camps, P. Chemistry of Pyramidalized Alkenes. *Tetrahedron* **2005**, *61* (22), 5147–5208. https://doi.org/10.1016/j.tet.2005.03.055.
(42) David Brown, I. Bond Valence Parameters, 2020. https://www.iucr.org/resources/data/datasets/bond-valence-parameters.
(43) David Brown, I. *The Chemical Bond in Inorganic Chemistry*; II; 2002; Vol. 1.
(44) *Triethylamine*. pubchem. https://pubchem.ncbi.nlm.nih.gov/compound/Triethylamine.
(45) Chataigner, I.; Panel, C.; Gérard, H.; Piettre, S. R. Sulfonyl vs. Carbonyl Group: Which Is the More Electron-Withdrawing? *Chem. Commun.* **2007**, No. 31, 3288–3290. https://doi.org/10.1039/B705034H.
(46) Toniolo, L.; Boschi, T.; Deganello, G. Synthesis, Characterization and Fluxional Behaviour of Allylic Palladium(II) Carboxylate and N,N′- Diarylformamidido Complexes. *J. Organomet. Chem.* **1975**, *93* (3), 405–414. https://doi.org/10.1016/S0022-328X(00)94013-0.
(47) Yang, L.; Powell, D. R.; Houser, R. P. Structural Variation in Copper(i) Complexes with Pyridylmethylamide Ligands: Structural Analysis with a New Four-Coordinate Geometry Index, T4. *Dalton Trans.* **2007**, No. 9, 955–964. https://doi.org/10.1039/B617136B.
(48) Tsutsumi, K.; Itagaki, K.; Nomura, K. Synthesis and Structural Analysis of Palladium(II) Complexes Containing Neutral or Anionic C2-Symmetric Bis(Oxazoline) Ligands: Effects of Substituents in the 5-Position. *ACS Omega* **2017**, *2* (7), 3886–3900. https://doi.org/10.1021/acsomega.7b00457.

(49) Hamad Gomez, S.; Hernández, N.; Aziz, A.; Ruiz-Salvador, A. R.; Calero, S.; Grau-Crespo, R. Electronic Structure of Porphyrin-Based Metal-Organic Frameworks and Their Suitability for Solar Fuel Production Photocatalysis. *J. Mater. Chem. A* **2015**, *3*, 23458–23465. https://doi.org/10.1039/C5TA06982C.
(50) Kaizaki, S. Ligand Field Theory. In *Instrumental Analysis of Coordination Compounds: Volume 1*; Oshio, H., Newton, G. N., Eds.; Royal Society of Chemistry, 2024; Vol. 4, p 0. https://doi.org/10.1039/9781837674978-00001.
(51) Ryan, D. E.; Cardin, D. J.; Hartl, F. H3-Allyl Carbonyl Complexes of Group 6 Metals: Structural Aspects, Isomerism, Dynamic Behaviour and Reactivity. *Coord. Chem. Rev.* **2017**, *335*, 103–149. https://doi.org/10.1016/j.ccr.2016.12.018.
(52) Jalón, F. A.; Manzano, B. R.; Otero, A.; Rodrúez-Péz, M. C. Synthesis and Fluxional Behaviour of Allylpalladium Complexes with Poly (Pyrazol-1-Yl)Methane Ligands. *J. Organomet. Chem.* **1995**, *494* (1), 179–185. https://doi.org/10.1016/0022-328X(94)05393-P.
(53) Krishnan, V. Molecular Thermodynamics Using Nuclear Magnetic Resonance (NMR) Spectroscopy. *Invent. Basel* **2019**, *4* (1), 13. https://doi.org/10.3390/inventions4010013.
(54) Howarth, C. Enyl and Dienyl Complexes of Molybdenum, 1995.
(55) Bridgeman, A. J. On the Origin of Paramagnetism in Planar Nickel(Ii) Complexes. *Dalton Trans.* **2008**, No. 15, 1989–1992. https://doi.org/10.1039/B717767D.
(56) Solmaz, U.; Arslan, H. Spectral, Crystallographic, Theoretical, and Catalytic Activity Studies of the PdII Complexes in Different Coordination Modes of Benzoylthiourea Ligand. *J. Mol. Struct.* **2022**, *1269*, 133839. https://doi.org/10.1016/j.molstruc.2022.133839.
(57) Ahmed, M.; Malhotra, S.; Yadav, O.; Yadav, M.; Saini, C.; Sharma, N.; Gupta, M.; Mohapatra, R.; Ansari, A. DFT and TDDFT Exploration on Electronic Transitions and Bonding Aspect of DPA and PTDC Ligated Transition Metal Complexes. *J. Mol. Model.* **2024**, *30*, 122. https://doi.org/10.1007/s00894-024-05912-5.
(58) El-Demerdash, S. H.; Halim, S. A.; El-Nahas, A. M.; El-Meligy, A. B. A Density Functional Theory Study of the Molecular Structure, Reactivity, and Spectroscopic Properties of 2-(2-Mercaptophenyl)-1-Azaazulene Tautomers and Rotamers. *Sci. Rep.* **2023**, *13* (1), 15626. https://doi.org/10.1038/s41598-023-42450-1.
(59) Pinter, B.; Van Speybroeck, V.; Waroquier, M.; Geerlings, P.; De Proft, F. Trans Effect and Trans Influence: Importance of Metal Mediated Ligand–Ligand Repulsion. *Phys. Chem. Chem. Phys.* **2013**, *15* (40), 17354–17365. https://doi.org/10.1039/C3CP52383G.
(60) BHADRA, M.; Lee, J.; Cowley, R.; Kim, S.; Siegler, M.; Solomon, E.; Karlin, K. Intramolecular Hydrogen Bonding Enhances Stability and Reactivity of Mononuclear Cupric Superoxide Complexes. *J. Am. Chem. Soc.* **2018**, *140*. https://doi.org/10.1021/jacs.8b04671.
(61) Whangbo, M.-H.; Wolfe, S.; Bernardi, F. A Correlation between Bond Length and Ionic Application to the Ylide-Ylene Problem. *Caadian J. Chem.* **1975**, *53*, 3040.
(62) PubChem Compound Summary for CID 176, Acetic Acid, 2004. https://pubchem.ncbi.nlm.nih.gov/compound/Acetic-Acid.
(63) Khusnutdinova, J. R.; Milstein, D. Metal–Ligand Cooperation. *Angew. Chem. Int. Ed.* **2015**, *54* (42), 12236–12273. https://doi.org/10.1002/anie.201503873.
(64) Zhou, P. S.; Sanders, K. M.; Guzei, I. A.; Musaev, D. G.; Stahl, S. S. Divergent Kinetic/Thermodynamic Selectivity in Palladium(II)-Mediated C–H Activation to Form 5- and 6-Membered Palladacycles. *J. Am. Chem. Soc.* **2025**, *147* (30), 26091–26096. https://doi.org/10.1021/jacs.5c02735.

(65) Bonnette, A.; Mague, J. T.; Chandrasekaran, P. Crystal Structure of a Palladium(II) Complex Containing the Wide Bite-Angle Bis-(Selenium) Ligand, Cis-[(tBuNH)(Se)P(μ-NtBu)2P(Se)(NHtBu)]. *Acta Crystallogr. Sect. E Crystallogr. Commun.* **2018**, *74*, 180–183. https://doi.org/10.1107/S2056989018000841.
(66) Chianese, A. R.; Lee, S. J.; Gagné, M. R. Electrophilic Activation of Alkenes by Platinum(II): So Much More Than a Slow Version of Palladium(II). *Angew. Chem. Int. Ed.* **2007**, *46* (22), 4042–4059. https://doi.org/10.1002/anie.200603954.
(67) Thomas, C. M. Stereocontrolled Ring-Opening Polymerization of Cyclic Esters: Synthesis of New Polyester Microstructures. *Chem. Soc. Rev.* **2010**, *39* (1), 165–173. https://doi.org/10.1039/B810065A.
(68) Peterson, A.; Hador, R.; Pink, M.; Popowski, Y.; Kol, M.; Tolman, W. B. Defining Stereochemistry in the Polymerization of Lactide by Aluminum Catalysts: Insights into the Dual-Stereocontrol Mechanism. *J. Am. Chem. Soc.* **2022**, *144* (43), 20047–20055. https://doi.org/10.1021/jacs.2c09073.
(69) Makio, H.; Terao, H.; Iwashita, A.; Fujita, T. FI Catalysts for Olefin Polymerization—A Comprehensive Treatment. *Chem. Rev.* **2011**, *111* (3), 2363–2449. https://doi.org/10.1021/cr100294r.
(70) Huynh, S.; Arrowsmith, M.; Meier, L.; Dietz, M.; Härterich, M.; Michel, M.; Gärtner, A.; Braunschweig, H. Cyclic Alkyl(Amino)Iminates (CAAIs) as Strong 2σ,4π-Electron Donor Ligands for the Stabilisation of Boranes and Diboranes(4): A Synthetic and Computational Study. *Dalton Trans.* **2023**, *52* (12), 3869–3876. https://doi.org/10.1039/D3DT00298E.

Appendix

Figure A1. ^{1}H-NMR spectrum of **L1**-H (400 MHz, $CDCl_3$).*Note, the signal at 1.62 ppm is H_2O solvent impurity. 78
Figure A2. $^{13}C\{^{1}H\}$ NMR spectrum of **L1**-H (75.5 MHz, CD_3CN). 79
Figure A3. ^{1}H-NMR spectrum of **L2**-H (400 MHz, $CDCl_3$).*Note, the signals at 4.42 and 1.29 ppm are 1,3-diisopropylimidazolin-2-one 80
Figure A4. $^{13}C\{^{1}H\}$ NMR spectrum of **L2**-H (75.5 MHz, $CDCl_3$)..... 81
Figure A5. ^{1}H-NMR spectrum of **L3**-H (400 MHz, $CDCl_3$). 82
Figure A6. $^{13}C\{^{1}H\}$ NMR spectrum of **L3**-H (75.5MHz, $CDCl_3$)..... 83
Figure A7. ^{1}H-NMR spectrum of **L4**•$HNEt_3$ (400 MHz, $CDCl_3$). 84
Figure A8. $^{13}C\{^{1}H\}$ NMR spectrum of **L4**•$HNEt_3$ (75.5MHz, $CDCl_3$)..... 85
Figure A9. ^{1}H-NMR spectrum of Pd(**L1**)(allyl) (400 MHz, $CDCl_3$). *Note the resonance at 5.30 ppm is DCM. **Note the resonance at 1.27 ppm is HO^{t}Bu. 86
Figure A10. $^{13}C\{^{1}H\}$ NMR spectrum of Pd(**L1**)(allyl) (75.5MHz, $CDCl_3$)..... 87
Figure A11. ^{1}H-NMR spectrum of Pd(**L4**)(allyl) (400 MHz, CD_3OD). 88
Figure A12. $^{13}C\{^{1}H\}$ NMR spectrum of Pd(**L4**)(allyl) (75.5 MHz, CD_3OD). 89
Figure A13. ^{1}H-NMR spectrum of Ni(**L1**)MeLut (400 MHz, C_6D_6)..... 90
Figure A14. ^{1}H-NMR spectrum of Pd(**L1**)(Me)(MeCN) (400 MHz, CD_3CN). *Note, the signal at 7.60 ppm is $CHCl_3$. 91
Figure A15. $^{13}C\{^{1}H\}$ NMR spectrum of Pd(**L1**)(Me)(MeCN) (75.5 MHz, CD_3CN). 92
Figure A16. ^{1}H-NMR spectrum of Pd(**L1**)(Me)(py) (400 MHz, $CDCl_3$). Note, the signals at 8.55, 7.76, and 7.22 ppm are remnant pyridine, the signal at 1.57 ppm is H_2O solvent impurity.93
Figure A17. *^{1}H-NMR spectrum of Ni(**L1**)$_2$ (400 MHz, MeOD-d_4). *Note, the signal at 4.90 ppm is H_2O.* 94
Figure A18. $^{13}C\{^{1}H\}$ NMR spectrum of Ni(**L1**)$_2$ (75.5 MHz, D_2O)..... 95
Figure A19. ^{1}H-NMR spectrum of Pd(**L1**)$_2$ (400 MHz, $CDCl_3$). *Note, the signal at 1.56 ppm is H_2O solvent impurity. 96
Figure A20. $^{13}C\{^{1}H\}$ NMR spectrum of Pd(**L1**)$_2$ (75.5 MHz, $CDCl_3$). 97
Figure A21. ^{1}H-NMR spectrum of Zn(**L1**)$_2$ (400 MHz, D_2O). 98
Figure A22. $^{13}C\{^{1}H\}$ NMR spectrum of Zn(**L1**)$_2$ (75.5 MHz, D_2O). 99
Figure A23. ^{1}H-NMR spectrum of Pd(**phenolate-1**)$_2$. *Note, signal at 5.3 ppm is DCM. **Note, signal at 2.19 ppm is acetone, *** Note, signal at 1.6 ppm is water. 100
Figure A 24. $^{13}C\{^{1}H\}$ NMR spectrum of Pd(**phenolate-1**)$_2$ (75.5 MHz, $CDCl_3$). *Note, signals at 206.9 and 30.9 ppm are from acetone. 101
Figure A25. ^{1}H-NMR spectrum of Pd(**L1**)(MeCN)(C_8 H $_{13}$) (400 MHz, CD_3CN)..... 102
Figure A26. ^{1}H-NMR spectrum of mixture of 10:1 norbornene:Pd(**L1**)(Me)(MeCN) (400 MHz, $CDCl_3$). *Note, signal at 2.16 ppm attributed to acetone. 103

Figure A27. ^{1}H-NMR spectrum of mixture of 20:1 norbornene:Pd(**L1**)(Me)(py) (400 MHz, $CDCl_3$)..... 104
Figure A28. ^{1}H-NMR spectrum of Pd(**L1**)(MeCN)($C_{16}H_{30}N_3$) (400 MHz, $CDCl_3$). 105
Figure A29. ^{1}H-NMR spectrum of Pd(**L1**)(MeCN)($C_{10}H_{12}N$) (400 MHz, CD_3CN)..... 106

Table A1. Crystal data and structure refinement for **L1**-H..... 107
Table A2. Fractional Atomic Coordinates ($\times 10^4$) and Equivalent Isotropic Displacement Parameters ($Å^2 \times 10^3$) for **L1**-H. U_{eq} is defined as 1/3 of the trace of the orthogonalised U_{IJ} tensor. 107
Table A3. Crystal data and structure refinement for **L4**•$HNEt_3$..... 108
Table A4. Fractional Atomic Coordinates ($\times 10^4$) and Equivalent Isotropic Displacement Parameters ($Å^2 \times 10^3$) for **L4**•$HNEt_3$. U_{eq} is defined as 1/3 of the trace of the orthogonalised U_{IJ} tensor..... 109
Table A5. Crystal data and structure refinement for Pd(**L1**)(Allyl)..... 110
Table A6. Fractional Atomic Coordinates ($\times 10^4$) and Equivalent Isotropic Displacement Parameters ($Å^2 \times 10^3$) for Pd(**L1**)(allyl). U_{eq} is defined as 1/3 of the trace of the orthogonalised U_{IJ} tensor..... 111
Table A7. Crystal data and structure refinement for Pd(**L1**)$_2$ 112
Table A8. Fractional Atomic Coordinates ($\times 10^4$) and Equivalent Isotropic Displacement Parameters ($Å^2 \times 10^3$) for Pd(**L1**)$_2$. U_{eq} is defined as 1/3 of the trace of the orthogonalised U_{IJ} tensor..... 113
Table A9. Crystal data and structure refinement for Pd(**L1'**)$(MeCN)_2$ 114
Table A10. Fractional Atomic Coordinates ($\times 10^4$) and Equivalent Isotropic Displacement Parameters ($Å^2 \times 10^3$) for Pd(**L1'**)$(MeCN)_2$. U_{eq} is defined as 1/3 of the trace of the orthogonalised U_{IJ} tensor. 114
Table A11. Crystal data and structure refinement for Pd(**phenolate-1**)$_2$..... 115
Table A12. Fractional Atomic Coordinates ($\times 10^4$) and Equivalent Isotropic Displacement Parameters ($Å^2 \times 10^3$) for Pd(**phenolate-1**)$_2$. U_{eq} is defined as 1/3 of the trace of the orthogonalised U_{IJ} tensor. 116

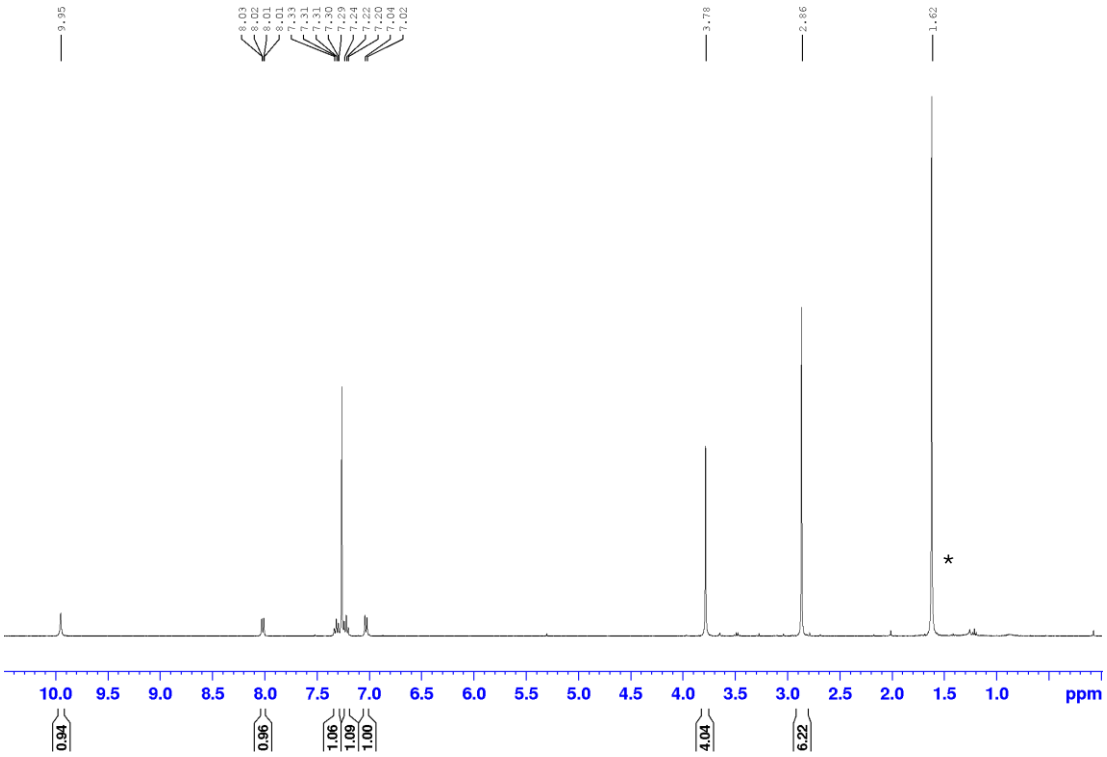

Figure A1. *^{1}H-NMR spectrum of* ***L1-****H (400 MHz, $CDCl_3$).*Note, the signal at 1.62 ppm is H_2O solvent impurity.*

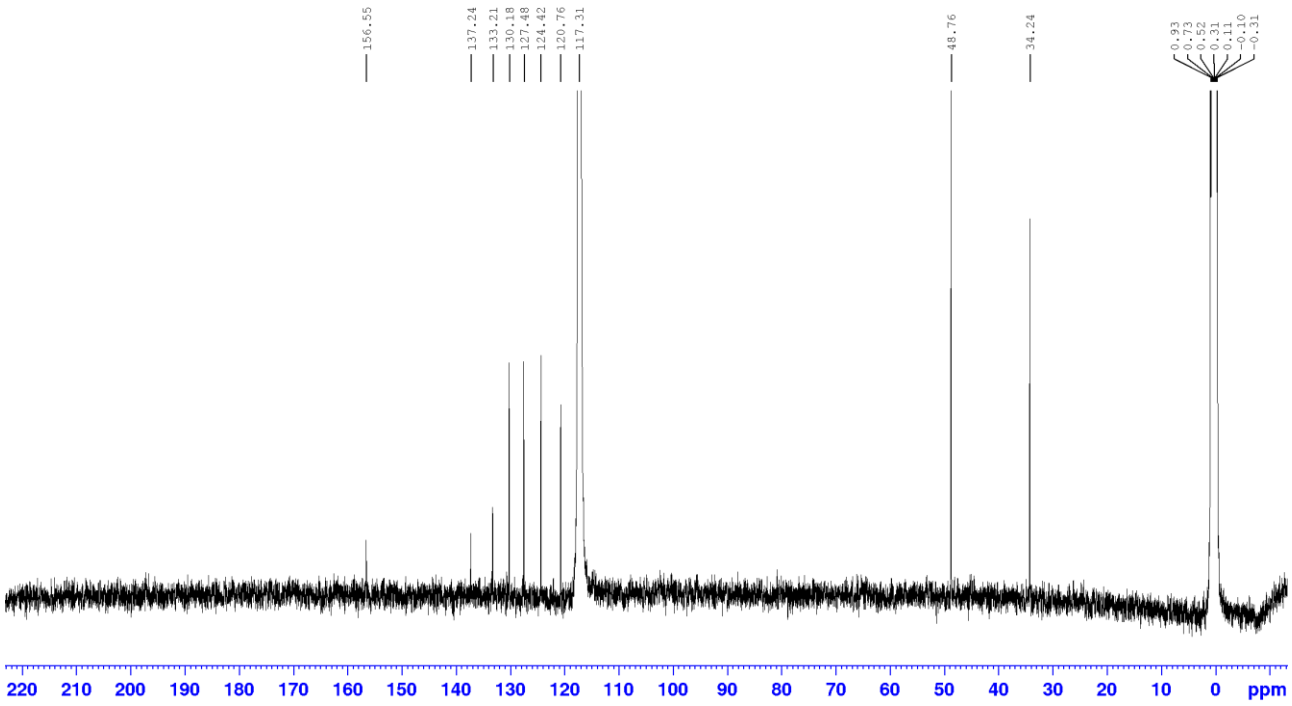

Figure A2. *$^{13}C\{^{1}H\}$ NMR spectrum of* ***L1-****H (75.5 MHz, CD_3CN).*

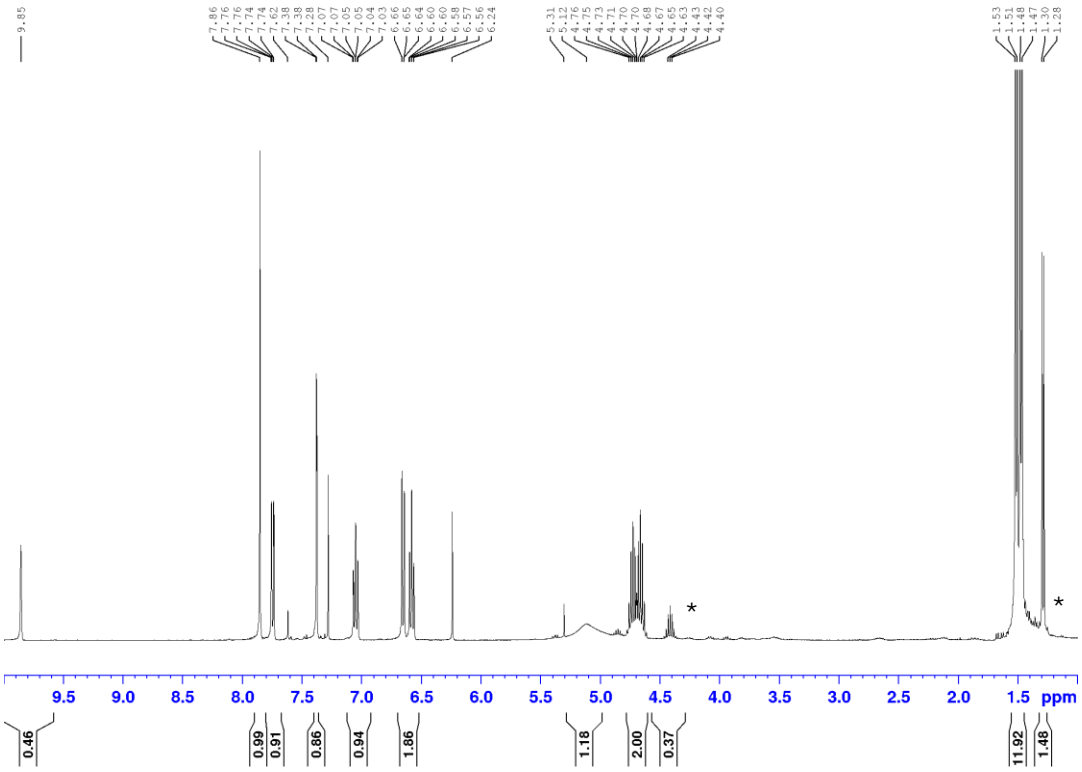

Figure A3. *^{1}H-NMR spectrum of **L2**-H (400 MHz, $CDCl_3$).*Note, the signals at 4.42 and 1.29 ppm are 1,3-diisopropylimidazolin-2-one*

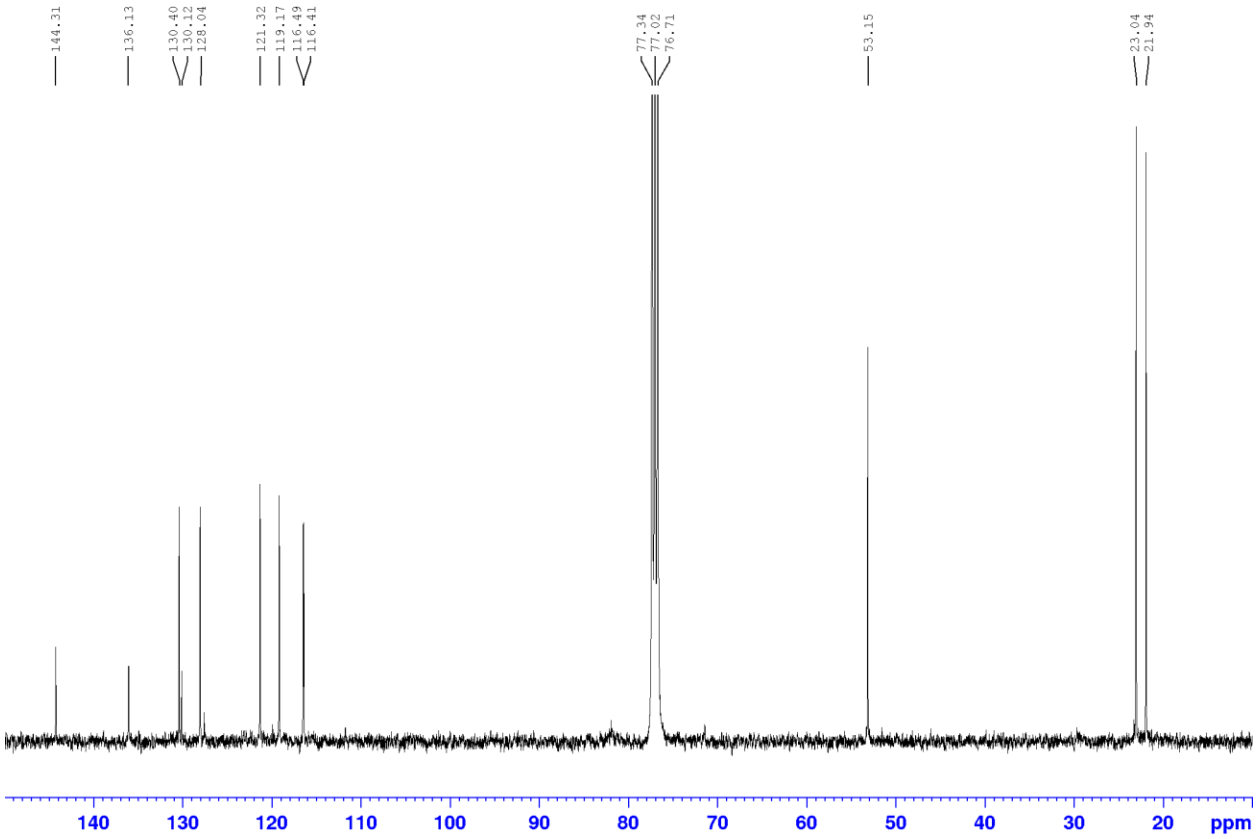

Figure A4. *$^{13}C\{^{1}H\}$ NMR spectrum of* ***L2-H*** *(75.5 MHz, $CDCl_3$).*

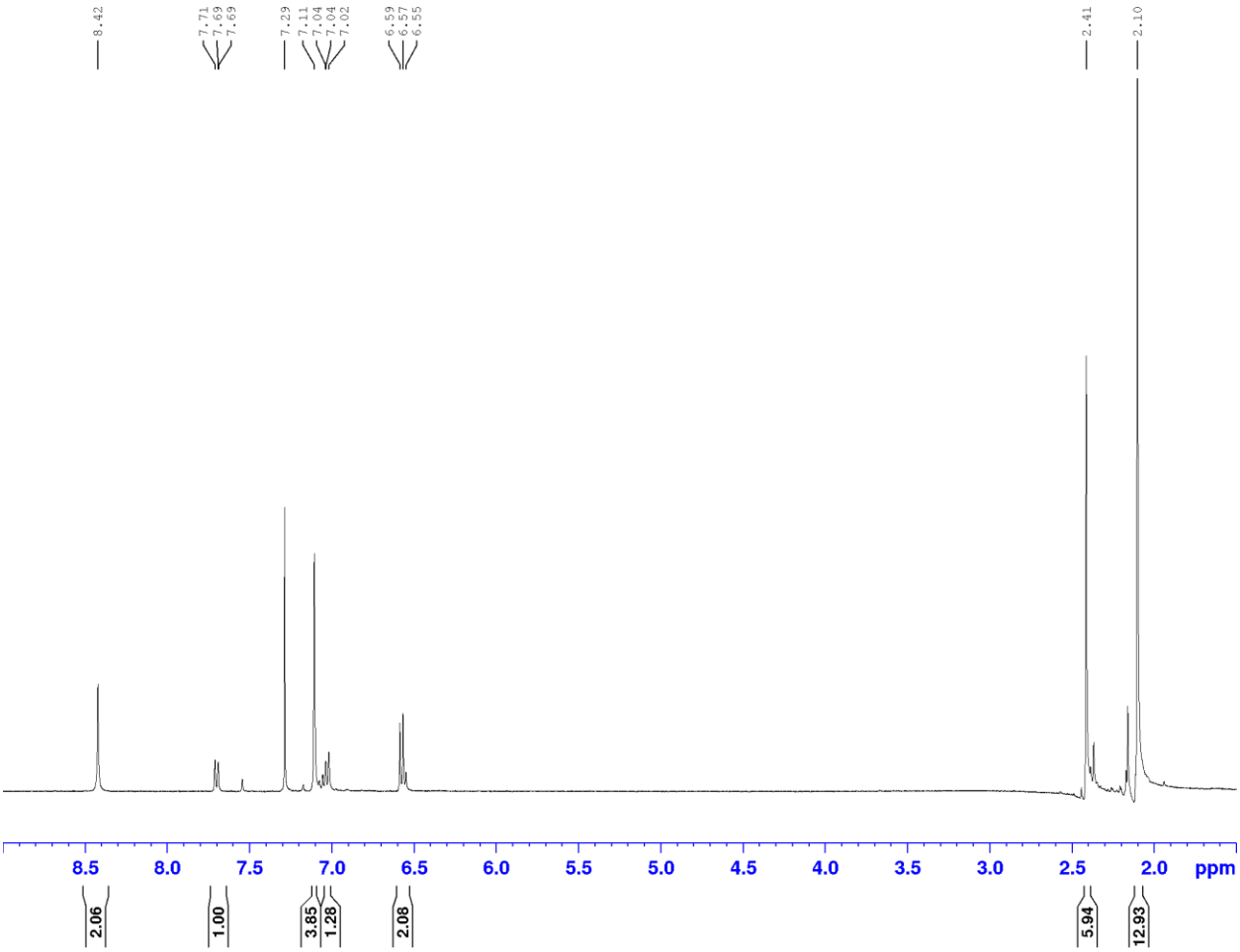

Figure A5. *^{1}H-NMR spectrum of **L3**-H (400 MHz, $CDCl_3$).*

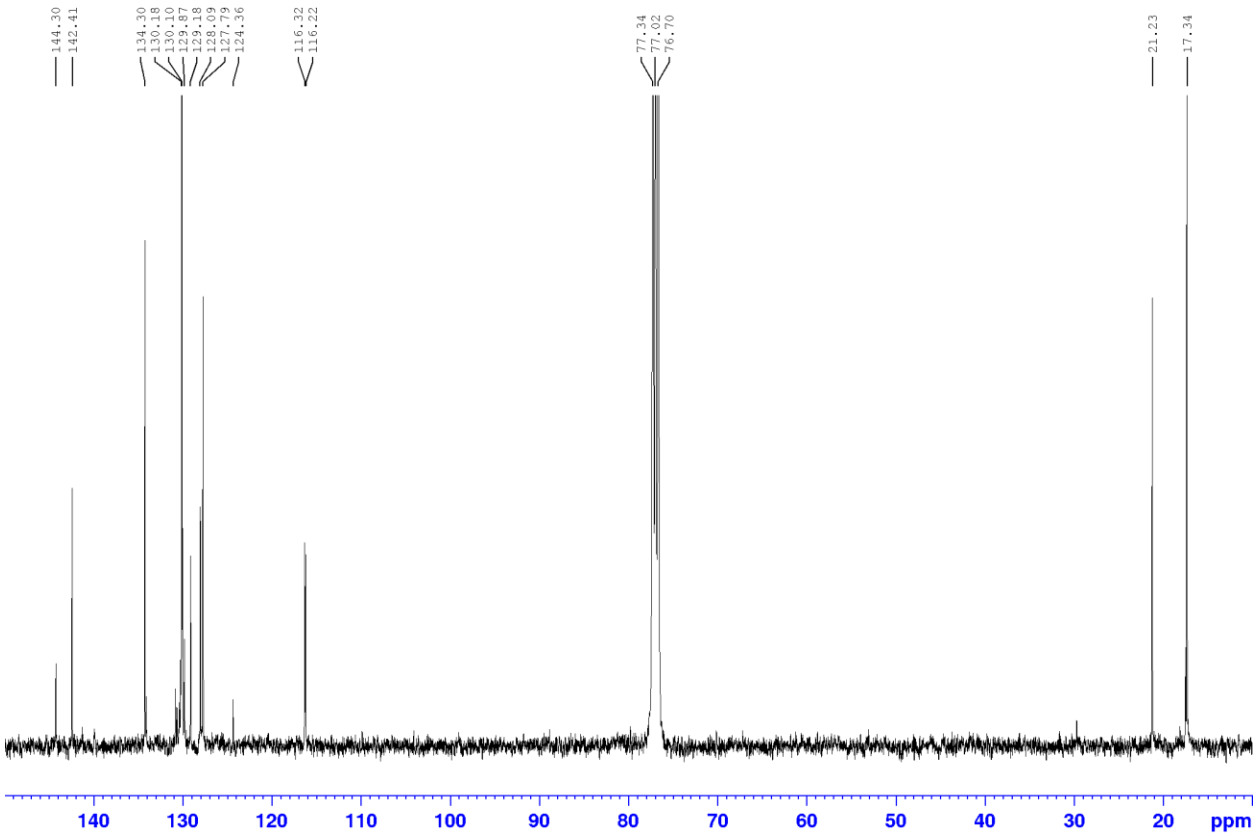

Figure A6. *$^{13}C\{^{1}H\}$ NMR spectrum of* ***L3-H*** *(75.5MHz, $CDCl_3$).*

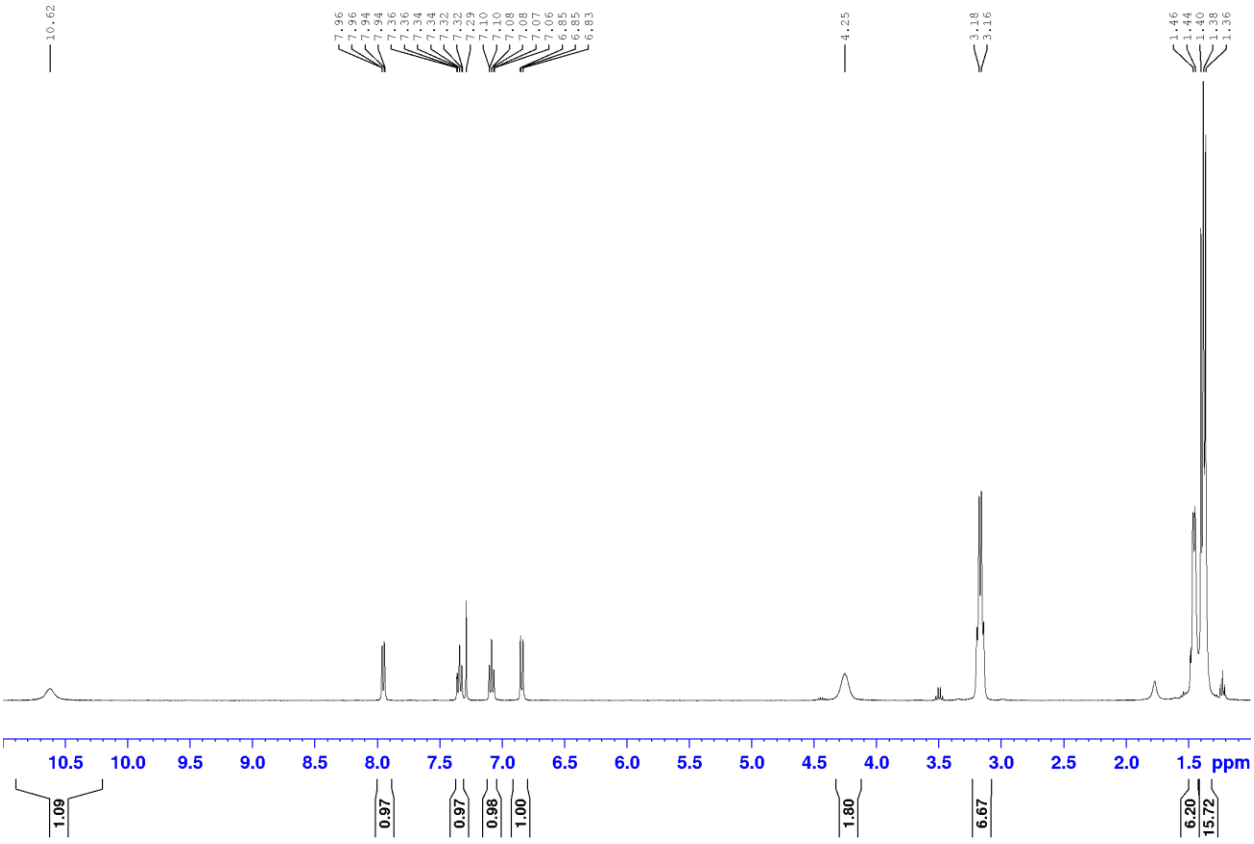

Figure A7. *^{1}H-NMR spectrum of **L4**•$HNEt_3$ (400 MHz, $CDCl_3$).*

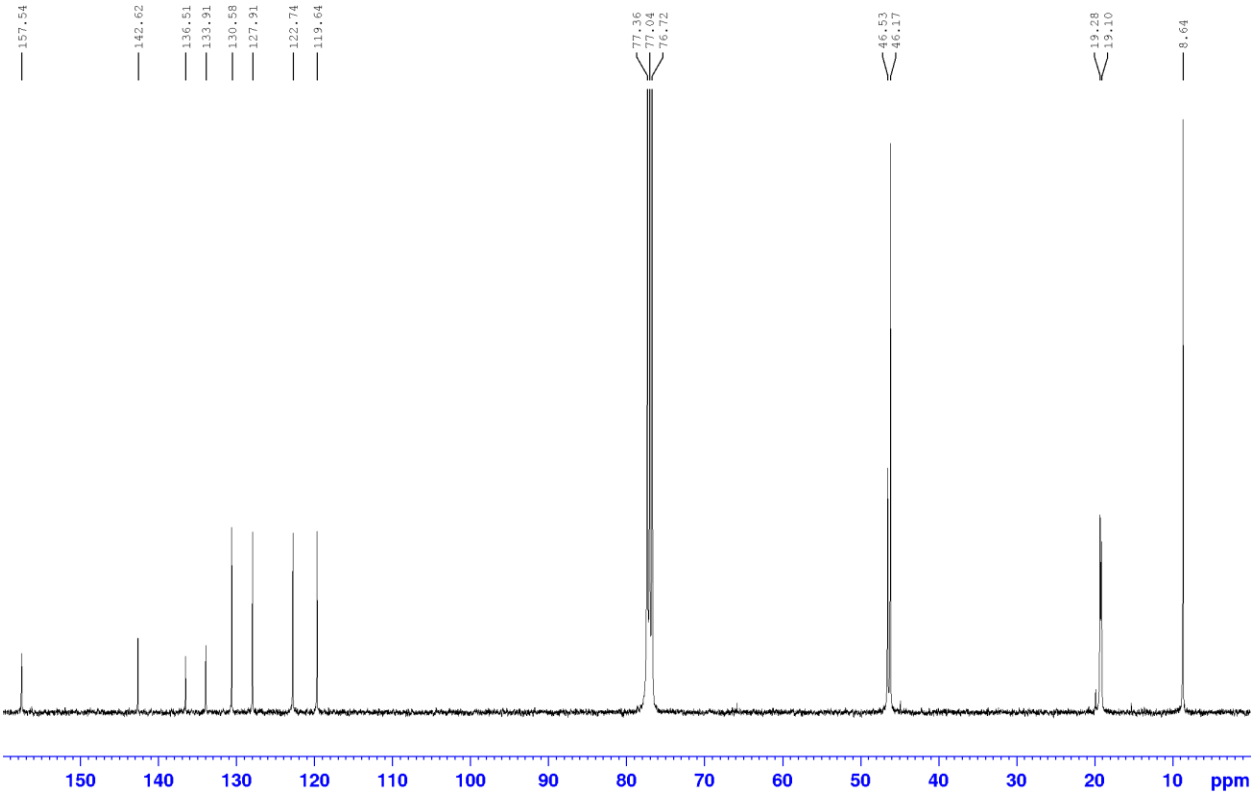

Figure A8. *$^{13}C\{^{1}H\}$ NMR spectrum of* ***L4•****$HNEt_3$ (75.5MHz, $CDCl_3$).*

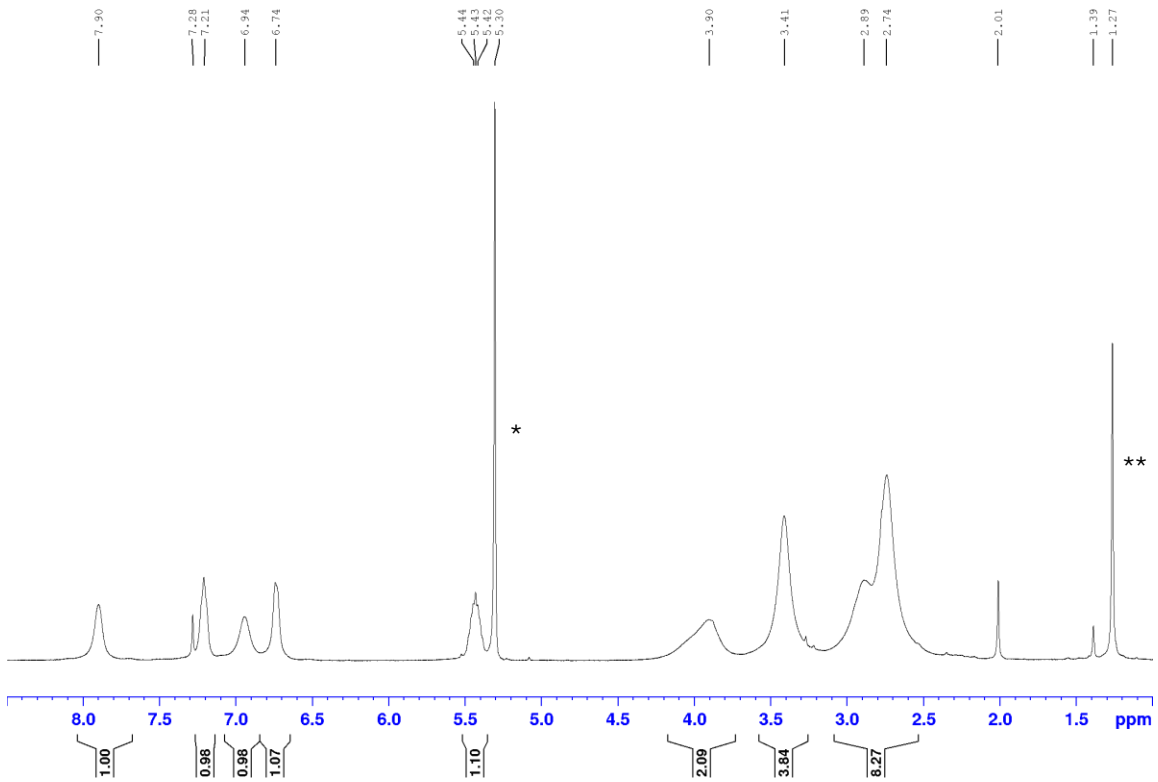

Figure A9. *^{1}H-NMR spectrum of Pd(**L1**)(allyl) (400 MHz, $CDCl_3$). *Note the resonance at 5.30 ppm is DCM. **Note the resonance at 1.27 ppm is HO^{t}Bu.*

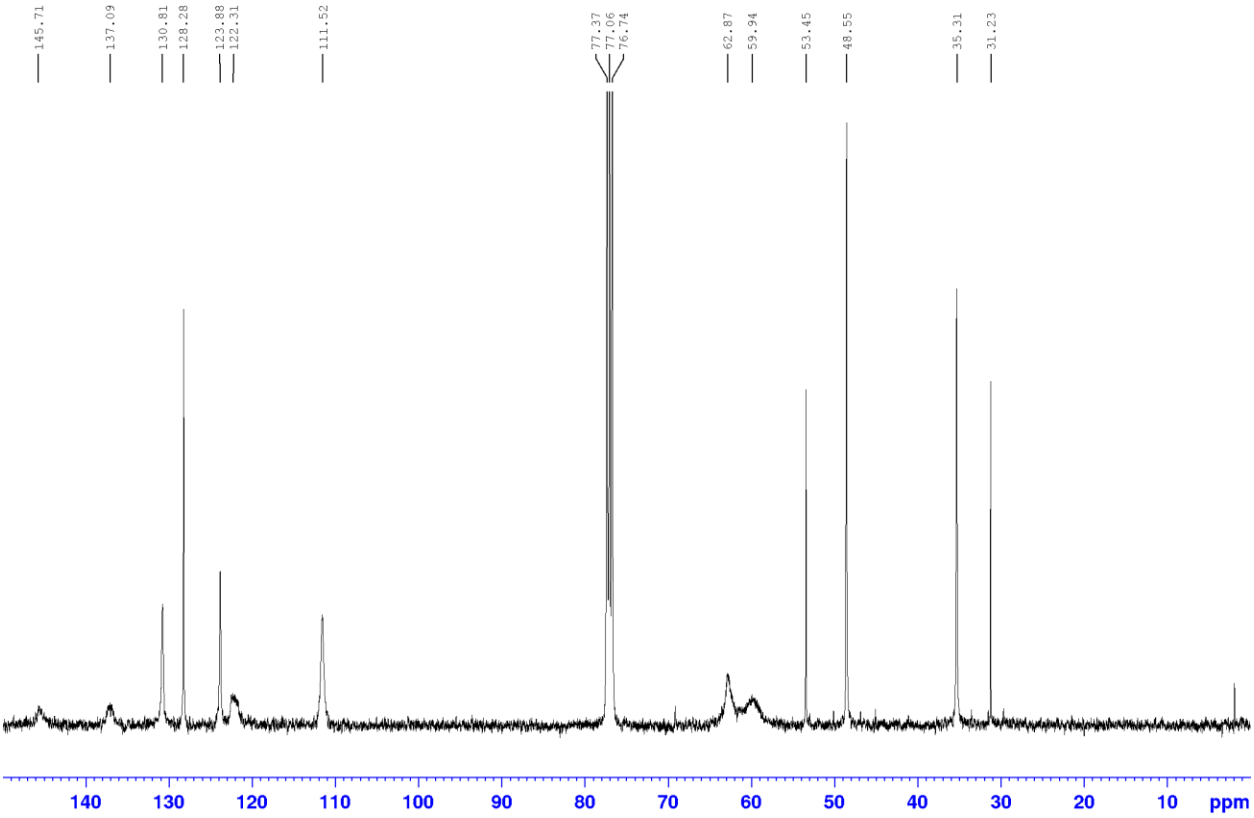

Figure A10. *$^{13}C\{^{1}H\}$ NMR spectrum of Pd(**L1**)(allyl) (75.5MHz, $CDCl_3$).*

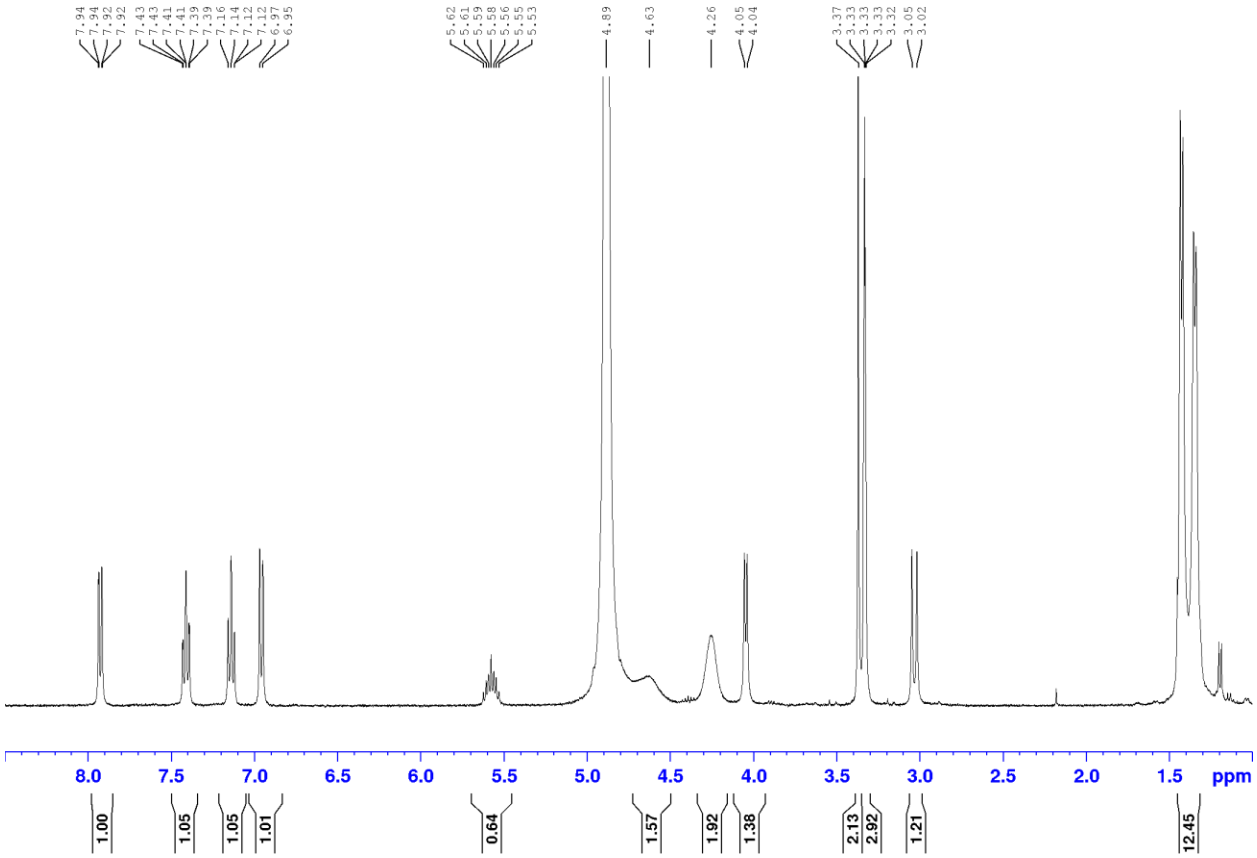

Figure A11. *^{1}H-NMR spectrum of Pd(**L4**)(allyl) (400 MHz, CD_3OD).*

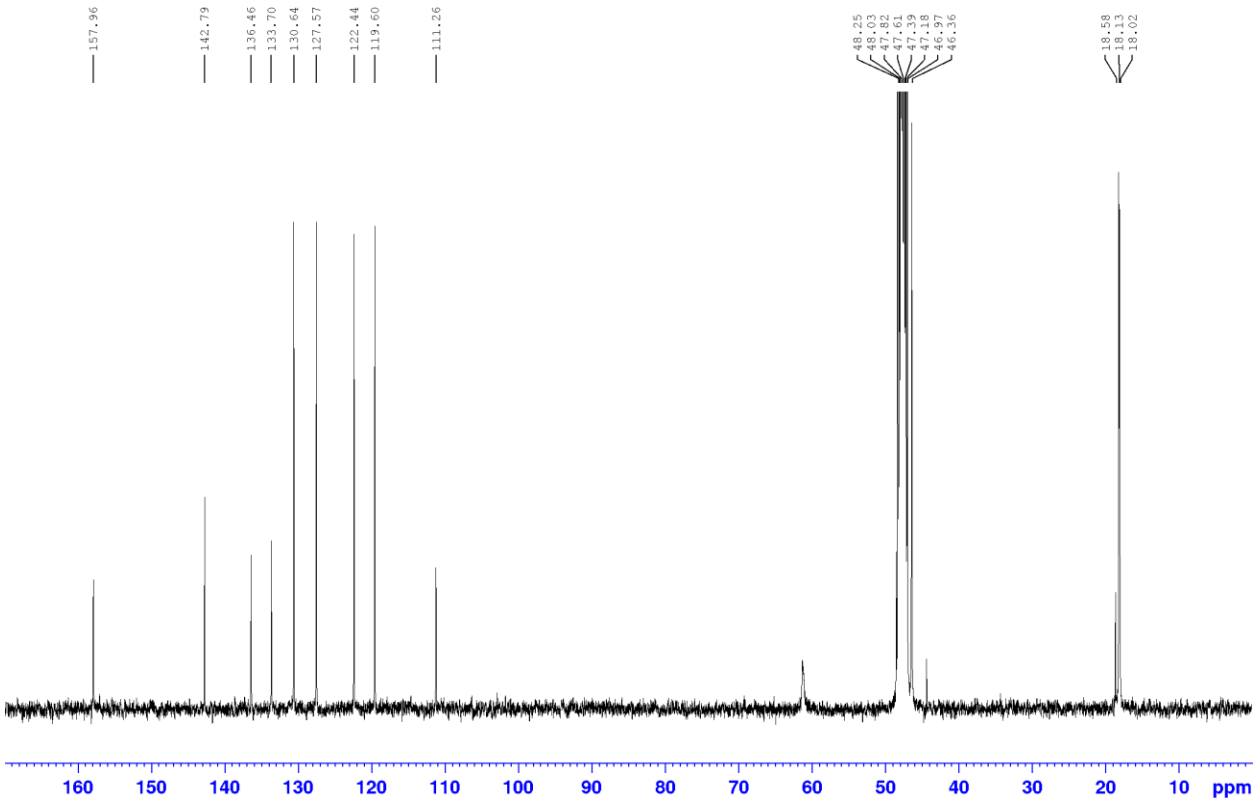

Figure A12. *$^{13}C\{^{1}H\}$ NMR spectrum of Pd(**L4**)(allyl) (75.5 MHz, CD_3OD).*

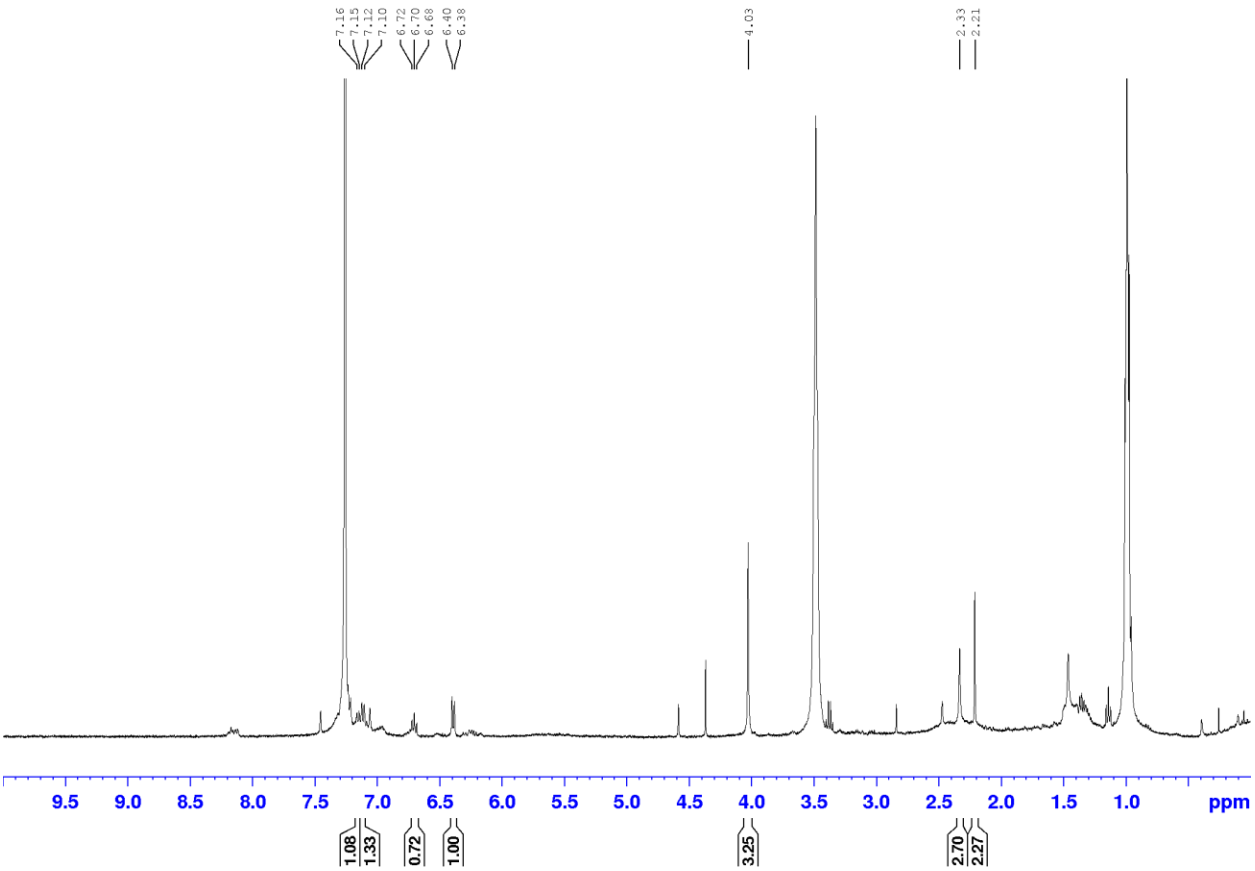

Figure A13. *^{1}H-NMR spectrum of Ni(**L1**)MeLut (400 MHz, C_6D_6).*

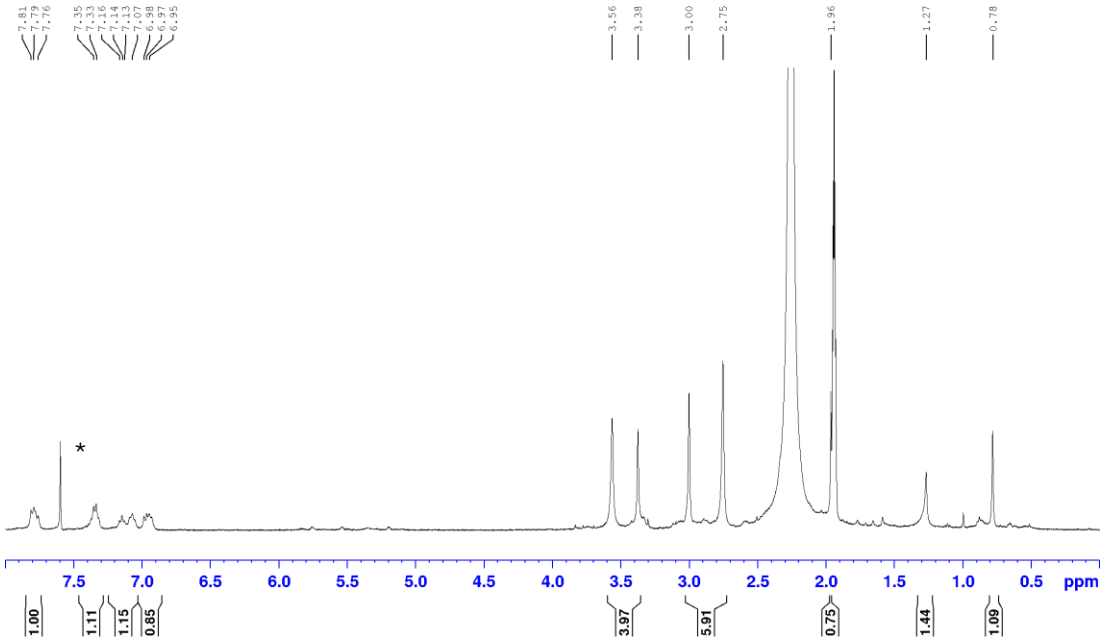

Figure A14. *^{1}H-NMR spectrum of Pd(**L1**)(Me)(MeCN) (400 MHz, CD_3CN). *Note, the signal at 7.60 ppm is $CHCl_3$.*

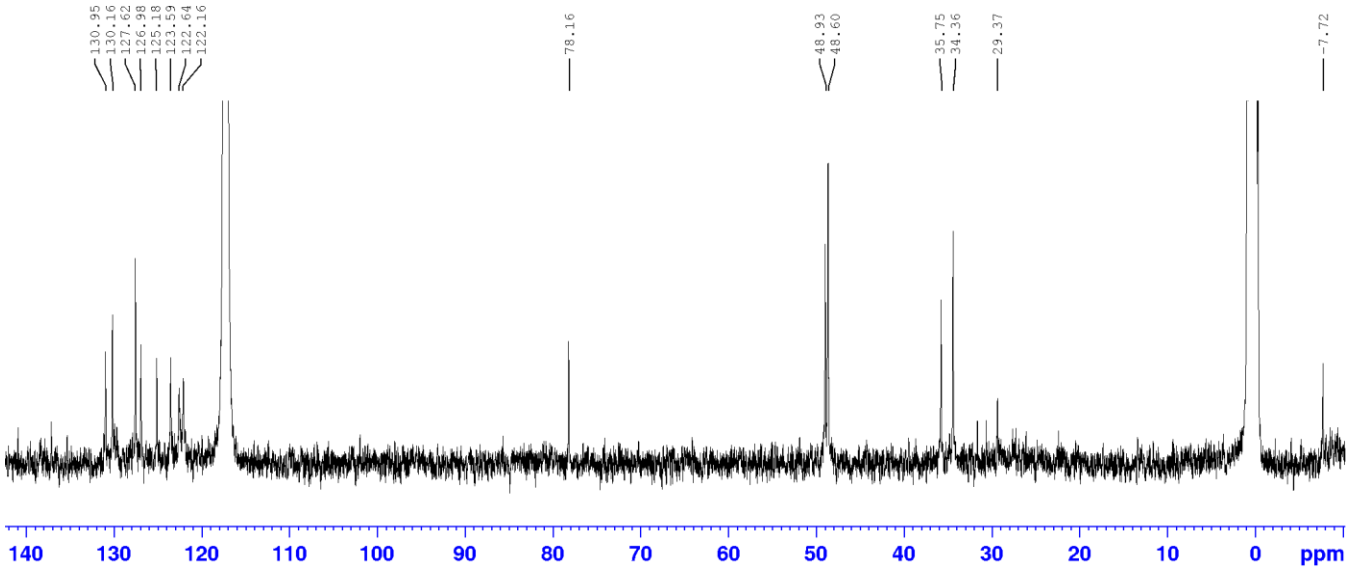

Figure A15. *$^{13}C\{^{1}H\}$ NMR spectrum of Pd(**L1**)(Me)(MeCN) (75.5 MHz, CD_3CN).*

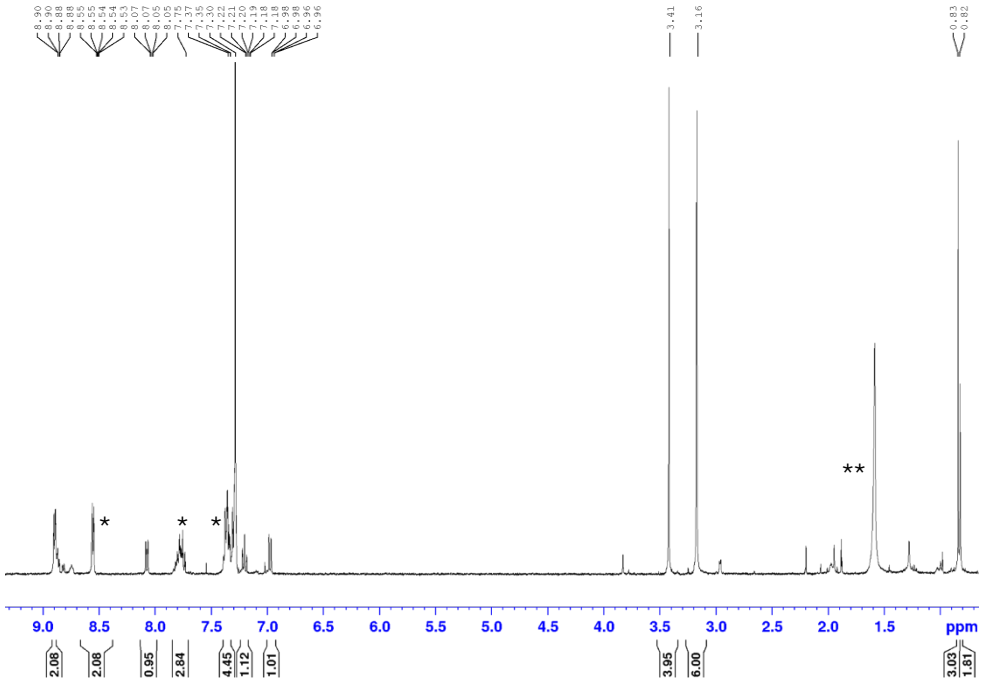

Figure A16. *^{1}H-NMR spectrum of Pd(**L1**)(Me)(py) (400 MHz, $CDCl_3$). Note, the signals at 8.55, 7.76, and 7.22 ppm are remnant pyridine, the signal at 1.57 ppm is H_2O solvent impurity.*

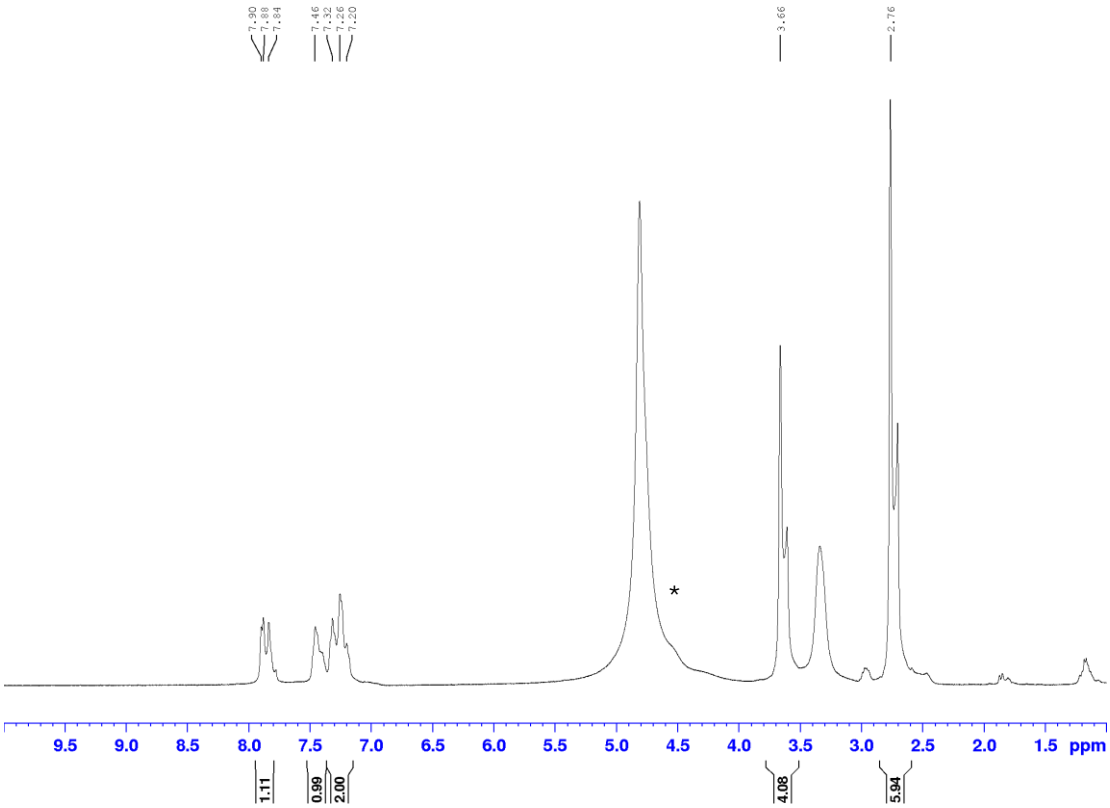

Figure A17. *^{1}H-NMR spectrum of Ni(**L1**)$_2$ (400 MHz, MeOD-d$_4$). *Note, the signal at 4.90 ppm is H_2O.*

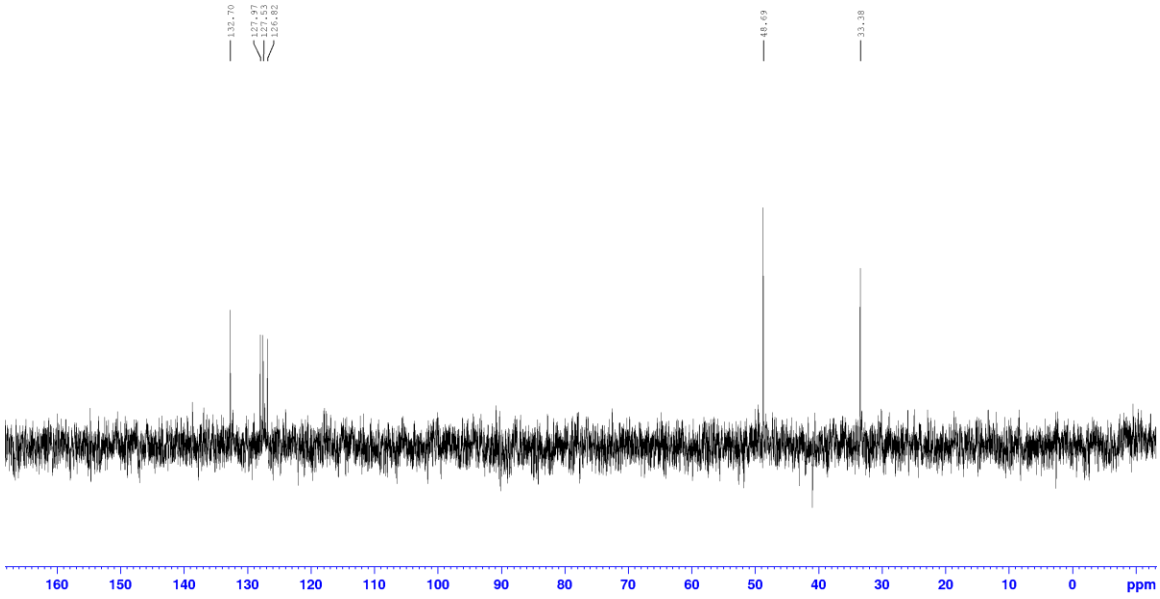

Figure A18. *$^{13}C\{^{1}H\}$ NMR spectrum of Ni(**L1**)$_2$ (75.5 MHz, D_2O)*

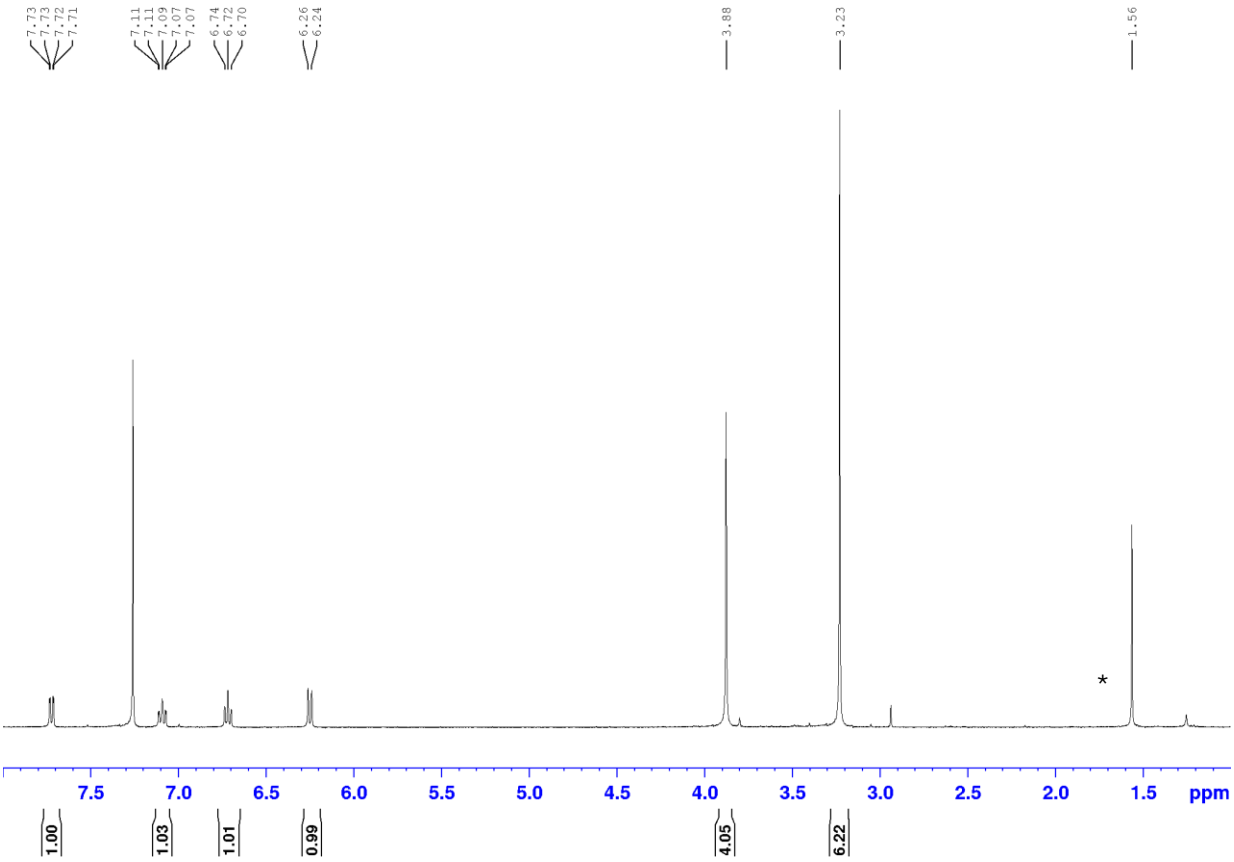

Figure A19. *^{1}H-NMR spectrum of Pd(**L1**)$_2$ (400 MHz, $CDCl_3$). *Note, the signal at 1.56 ppm is H_2O solvent impurity.*

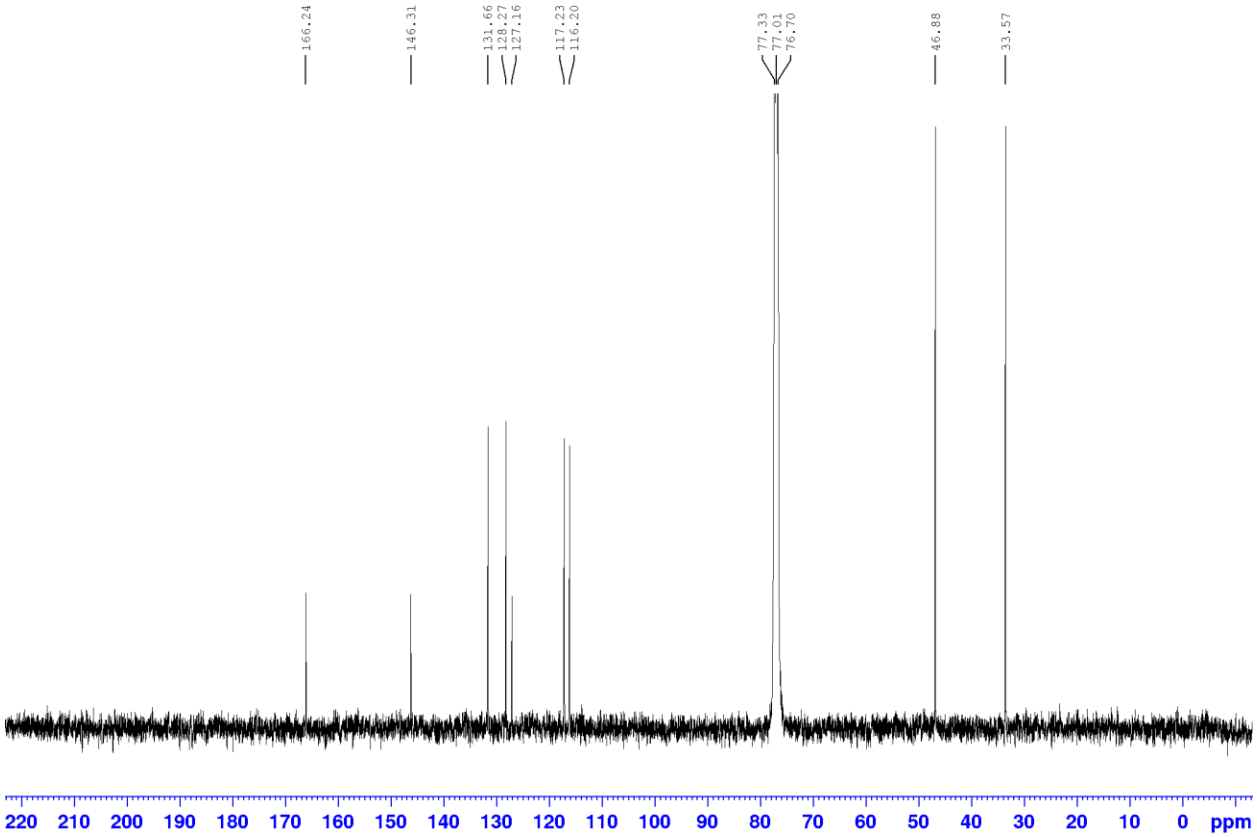

Figure A20. *$^{13}C\{^{1}H\}$ NMR spectrum of Pd(**L1**)$_2$ (75.5 MHz, $CDCl_3$).*

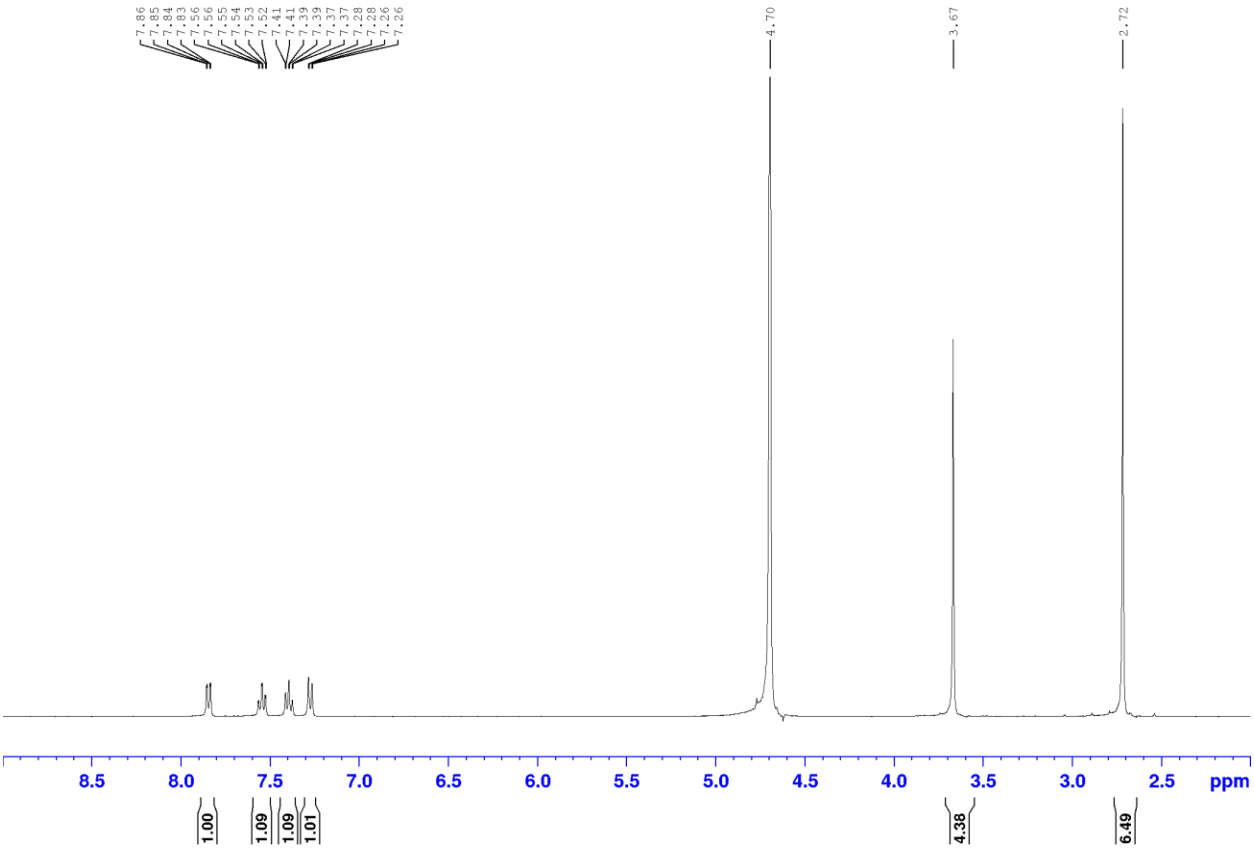

Figure A21. *^{1}H-NMR spectrum of Zn(**L1**)$_2$ (400 MHz, D_2O).*

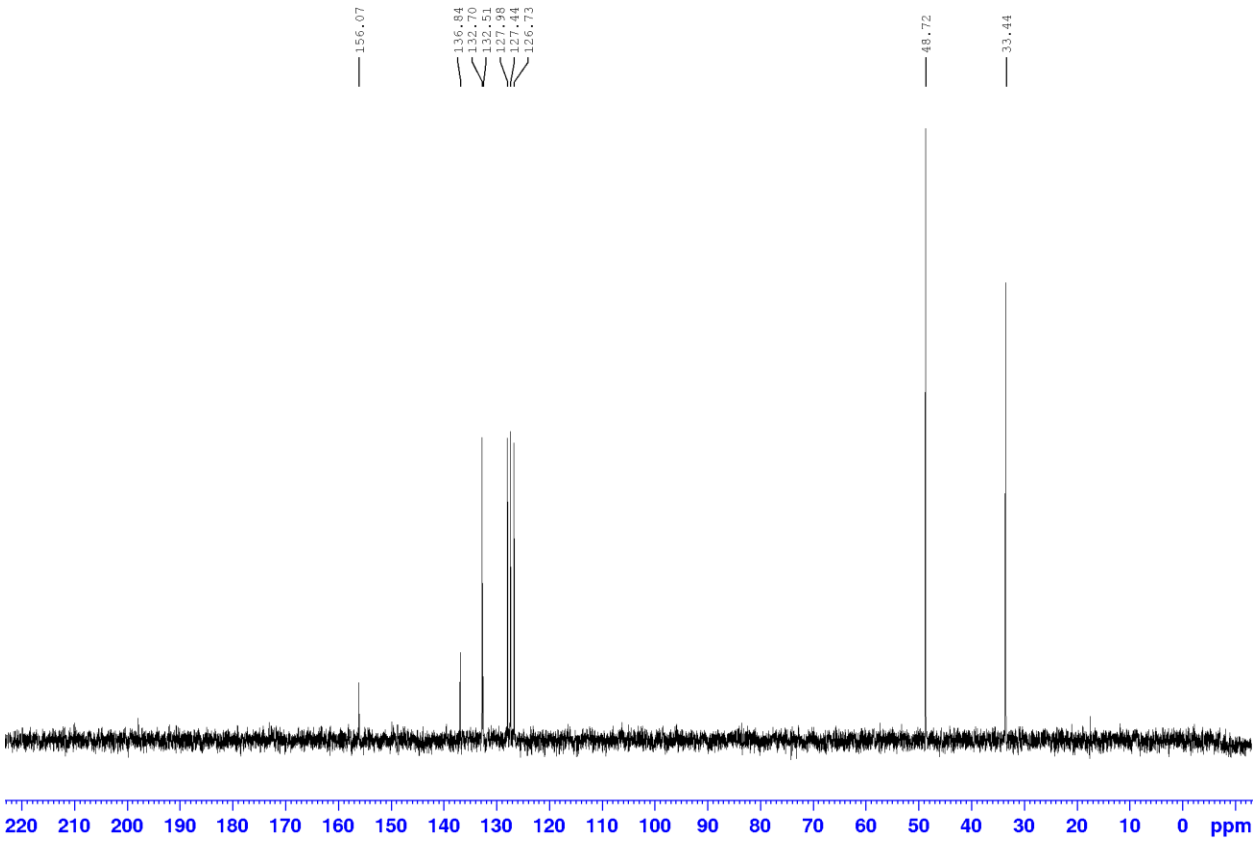

Figure A22. *$^{13}C\{^{1}H\}$ NMR spectrum of Zn(**L1**)$_2$ (75.5 MHz, D_2O).*

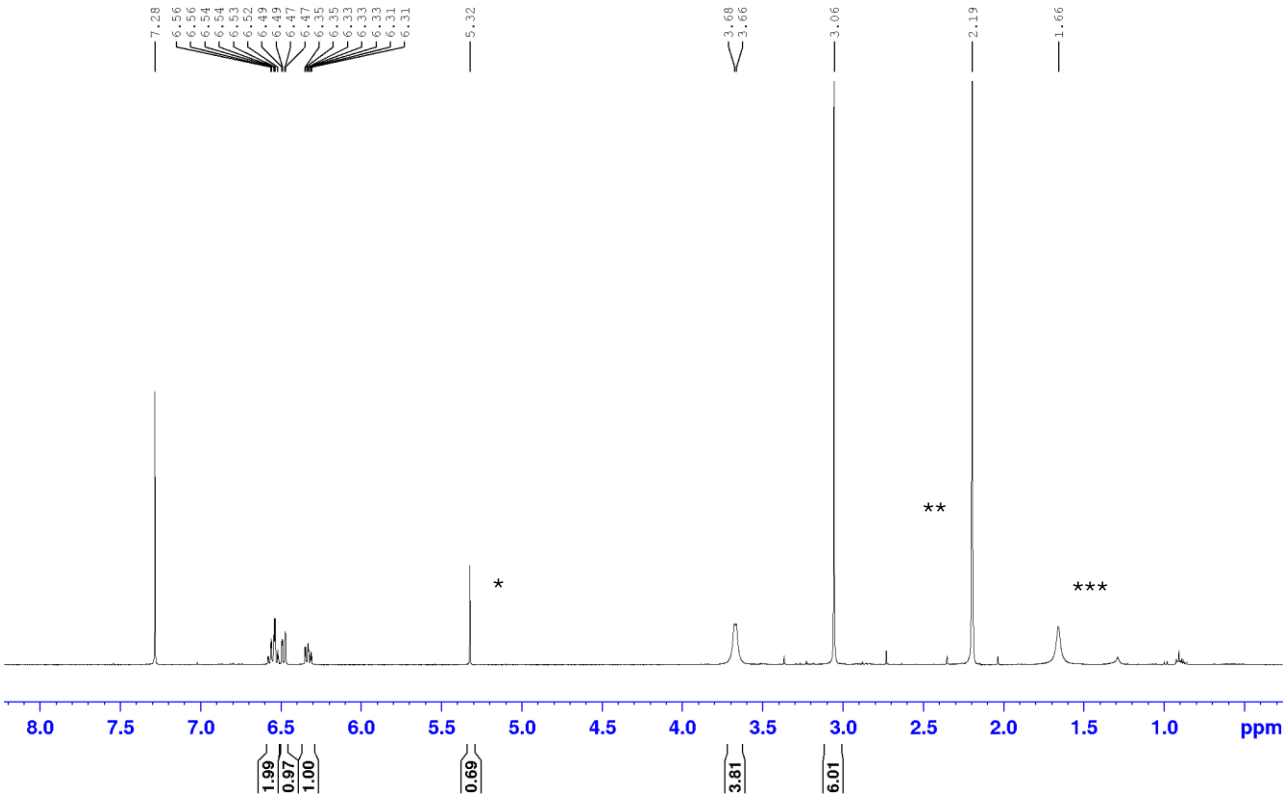

Figure A23. *^{1}H-NMR spectrum of Pd(**phenolate-1**)$_2$. *Note, signal at 5.3 ppm is DCM. **Note, signal at 2.19 ppm is acetone, *** Note, signal at 1.6 ppm is water.*

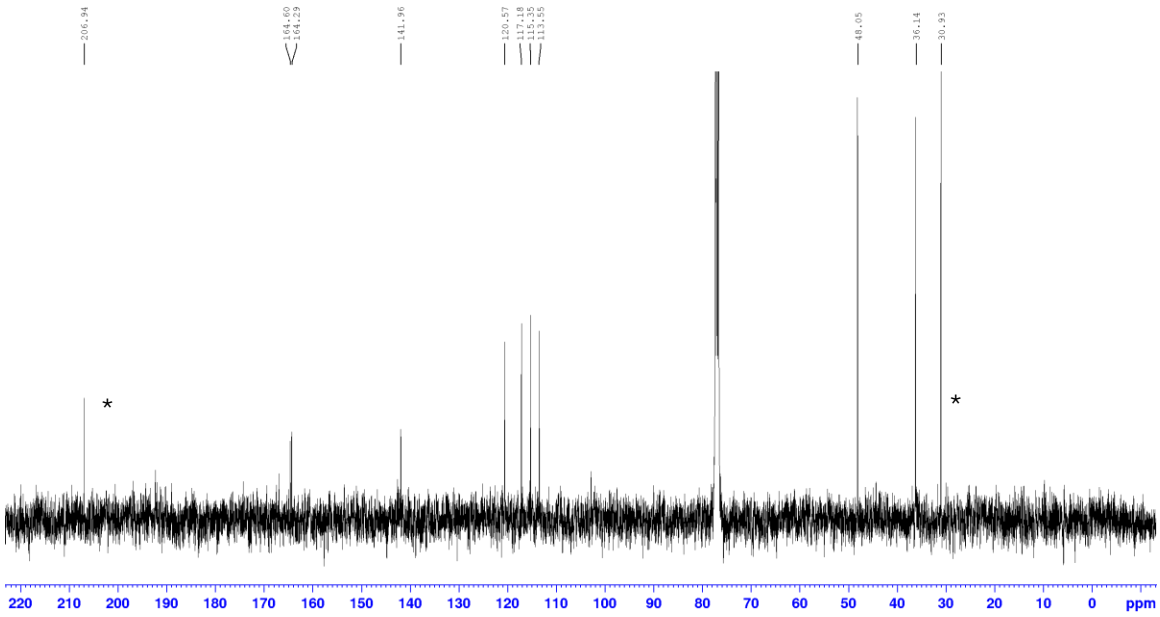

*Figure A 24. $^{13}C\{^{1}H\}$ NMR spectrum of Pd(**phenolate-1**)$_2$ (75.5 MHz, $CDCl_3$). *Note, signals at 206.9 and 30.9 ppm are from acetone.*

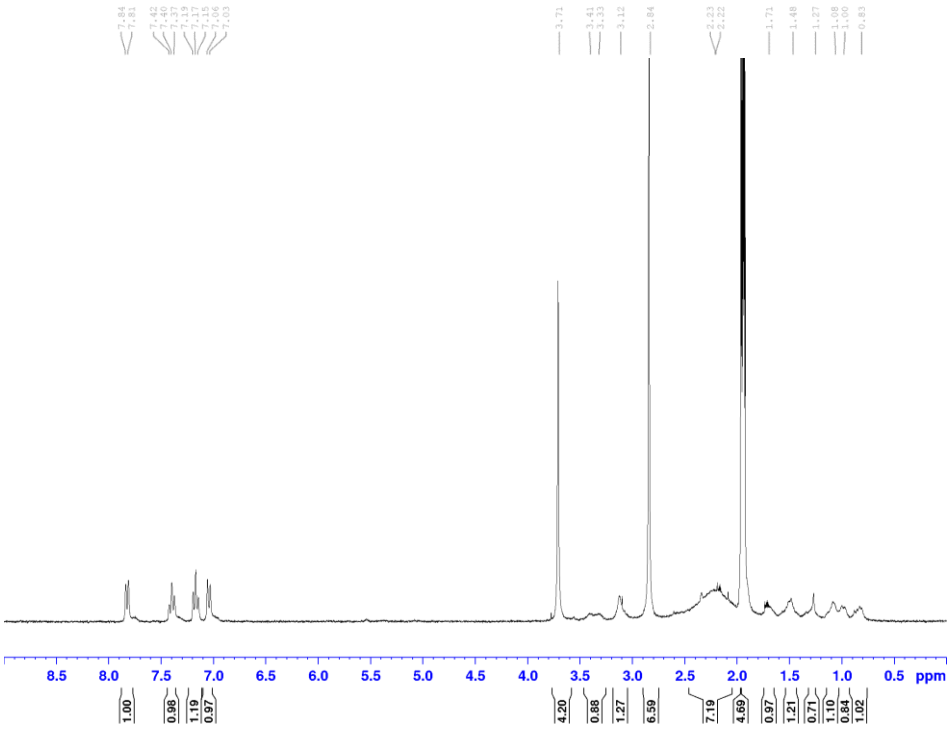

Figure A25. *^{1}H-NMR spectrum of Pd(**L1**)(MeCN)(C_8H_{13}) (400 MHz, CD_3CN).*

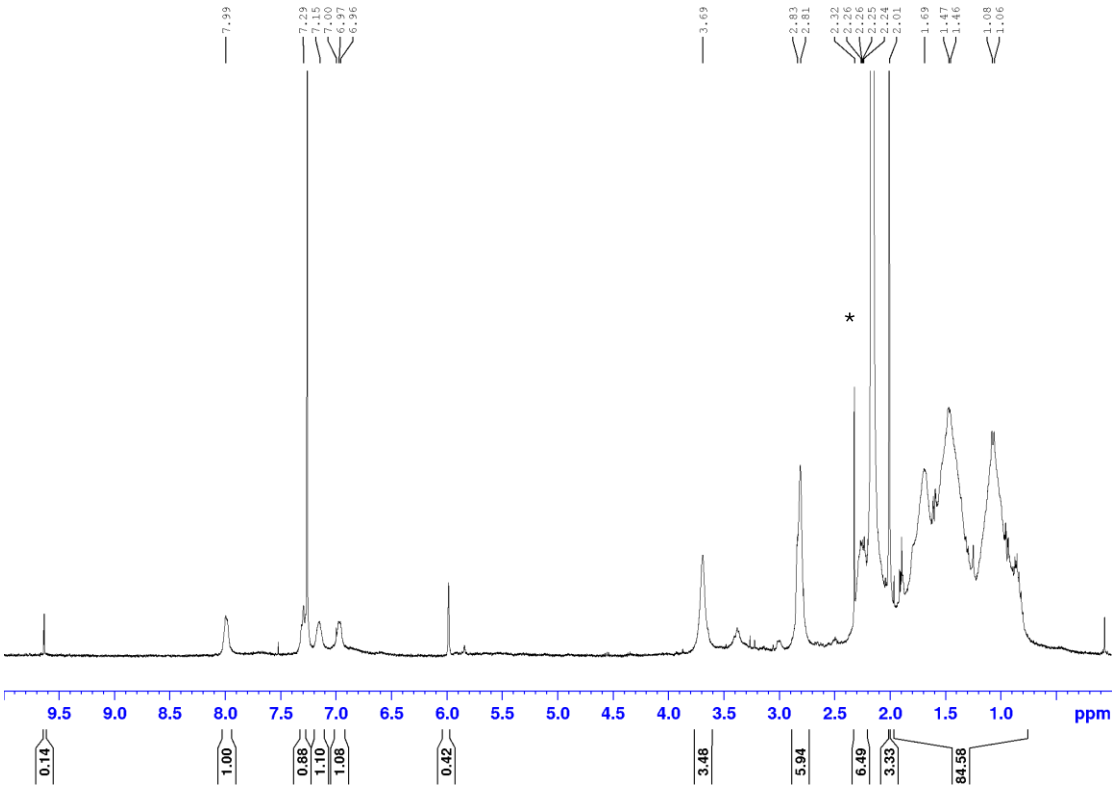

Figure A26. *^{1}H-NMR spectrum of mixture of 10:1 norbornene:Pd(**L1**)(Me)(MeCN) (400 MHz, $CDCl_3$). *Note, signal at 2.16 ppm attributed to acetone.*

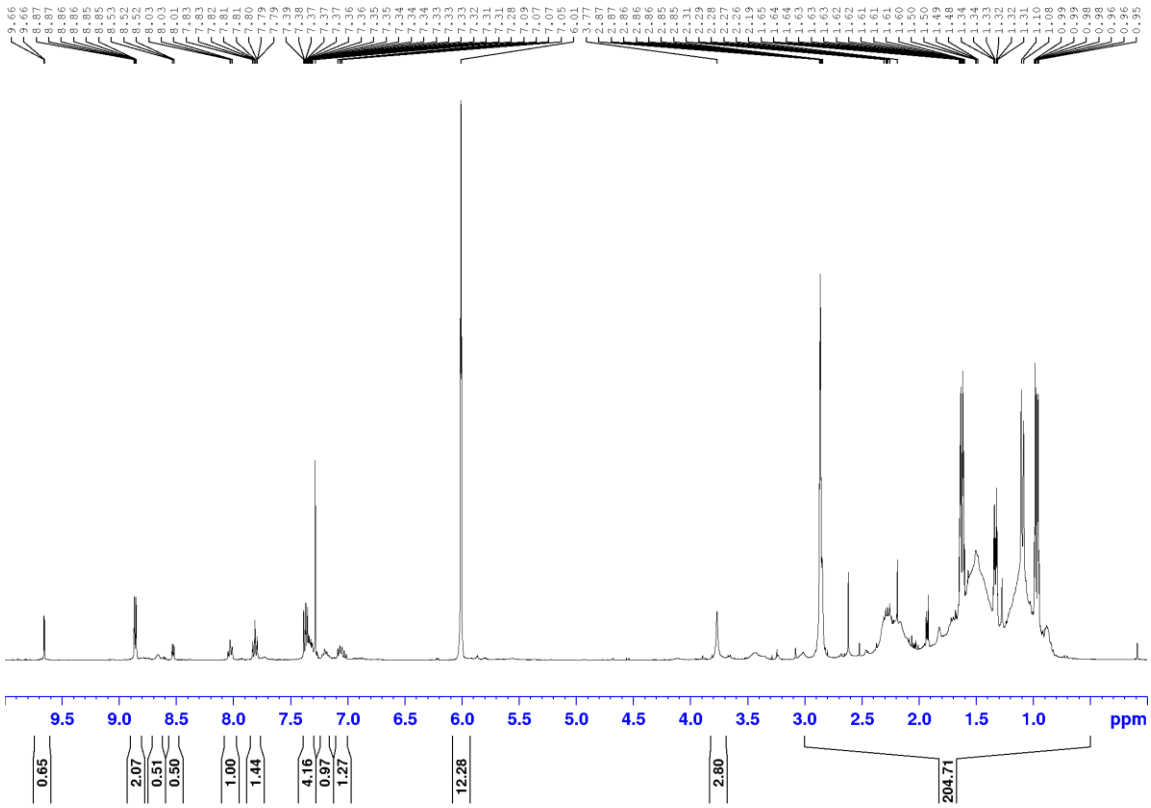

Figure A27. *^{1}H-NMR spectrum of mixture of 20:1 norbornene:Pd(**L1**)(Me)(py) (400 MHz, $CDCl_3$).*

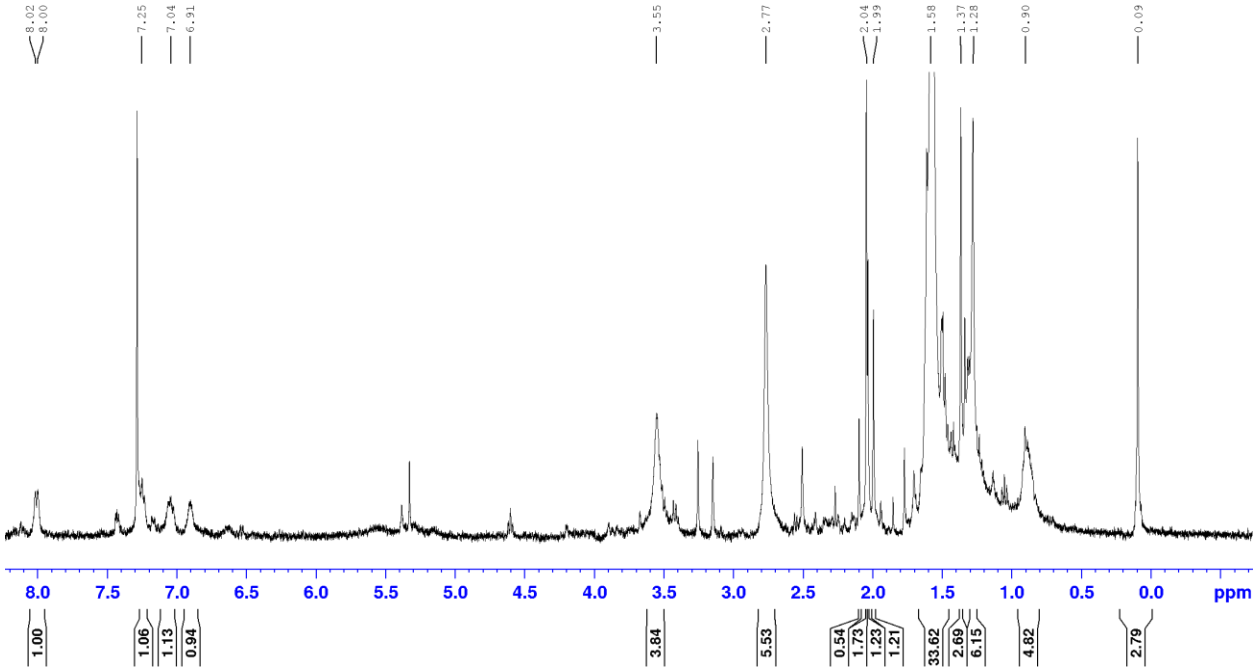

Figure A28. *^{1}H-NMR spectrum of Pd(**L1**)(MeCN)($C_{16}H_{30}N_3$) (400 MHz, $CDCl_3$).*

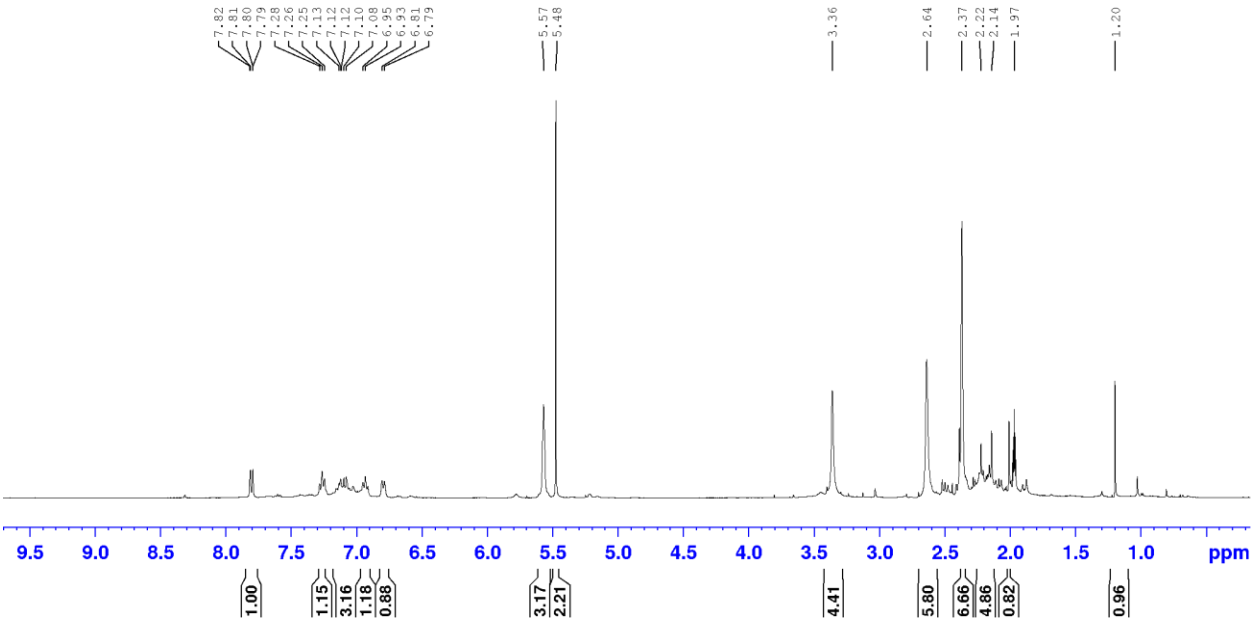

Figure A29. *^{1}H-NMR spectrum of Pd(**L1**)(MeCN)($C_{10}H_{12}N$) (400 MHz, CD_3CN).*

Table A1. *Crystal data and structure refinement for* ***L1****-H*

Empirical formula	$C_{11}H_{15}N_3O_3S$
Formula weight	269.32
Temperature/K	173.00
Crystal system	monoclinic
Space group	C2/c
a/Å	14.3185(6)
b/Å	8.7911(3)
c/Å	20.1292(8)
α/°	90
β/°	103.1760(10)
γ/°	90
Volume/Å^3	2467.07(17)
Z	8
ρ_{calc}g/cm^3	1.450
μ/mm^{-1}	0.267
F(000)	1136.0
Crystal size/mm^3	0.2 × 0.1 × 0.075
Radiation	MoKα (λ = 0.71073)
2Θ range for data collection/°	5.478 to 66.358
Index ranges	-22 ≤ h ≤ 22, -13 ≤ k ≤ 13, -30 ≤ l ≤ 30
Reflections collected	41764
Independent reflections	4713 [R_{int} = 0.0452, R_{sigma} = 0.0266]
Data/restraints/parameters	4713/0/223
Goodness-of-fit on F^2	1.065
Final R indexes [I>=2σ (I)]	R_1 = 0.0400, wR_2 = 0.0951
Final R indexes [all data]	R_1 = 0.0596, wR_2 = 0.1106
Largest diff. peak/hole / e Å^{-3}	0.38/-0.40

Table A2. *Fractional Atomic Coordinates (×10^4) and Equivalent Isotropic Displacement Parameters (Å^2×10^3) for* ***L1****-H.* U_{eq} *is defined as 1/3 of the trace of the orthogonalised* U_{IJ} *tensor.*

Atom	***x***	***y***	***z***	**U(eq)**
S1	1830.9(2)	4399.2(3)	8781.8(2)	18.32(8)
O1	1045.8(7)	4226.1(12)	8175.8(5)	24.0(2)
O2	2100.8(9)	5974.3(12)	8925.4(7)	34.6(3)
O3	1654.4(7)	3567.8(12)	9363.8(5)	26.4(2)
N1	2205.4(9)	3752.0(15)	7353.3(5)	24.0(2)
N2	3000.8(9)	4499.1(13)	6483.0(6)	22.5(2)
N3	1523.8(8)	3607.4(14)	6181.9(6)	22.7(2)
C1	2263.1(9)	3931.7(14)	6695.4(6)	19.4(2)

Atom	*x*	*y*	*z*	U(eq)
C2	2940.7(9)	3259.9(14)	7902.6(6)	18.2(2)
C3	3812.2(12)	5320.2(17)	6884.3(8)	28.8(3)
C4	3729.2(10)	2450.1(15)	7786.2(7)	23.6(2)
C5	4440.0(10)	1953.8(17)	8329.3(8)	27.1(3)
C6	4367.3(10)	2228.7(18)	8995.8(8)	29.3(3)
C7	1778.4(11)	3894.2(17)	5527.8(7)	26.3(3)
C8	2794.1(11)	4530.5(17)	5733.1(7)	26.4(3)
C9	731.6(11)	2612(2)	6222.2(9)	33.9(3)
C10	2843.9(9)	3489.1(14)	8574.5(6)	17.7(2)
C11	3563.6(10)	2963.6(17)	9116.9(7)	24.5(3)

Table A3. *Crystal data and structure refinement for* ***L4•HNEt3***

Empirical formula	$C_{42}H_{68}N_8O_{10}S_2$
Formula weight	909.188
Temperature/K	243.00
Crystal system	monoclinic
Space group	P21/n
a/Å	20.721(3)
b/Å	11.2836(17)
c/Å	21.957(4)
α/°	90
β/°	113.529(5)
γ/°	90
Volume/Å3	4706.9(13)
Z	4
ρcalcg/cm3	1.283
μ/mm-1	0.176
F(000)	1954.2
Crystal size/mm3	0.2 × 0.2 × 0.2
Radiation	Mo Kα (λ = 0.71073)
2Θ range for data collection/°	4.14 to 61.2
Index ranges	-29 ≤ h ≤ 29, -16 ≤ k ≤ 16, -31 ≤ l ≤ 31
Reflections collected	242126
Independent reflections	14446 [Rint = 0.1664, Rsigma = 0.0817]
Data/restraints/parameters	14446/0/573
Goodness-of-fit on F2	1.005
Final R indexes [I>=2σ (I)]	R1 = 0.0557, wR2 = 0.1095
Final R indexes [all data]	R1 = 0.1308, wR2 = 0.1351

Largest diff. peak/hole / e Å-3 0.71/-0.69

Table A4. *Fractional Atomic Coordinates (×10⁴) and Equivalent Isotropic Displacement Parameters (Å²×10³) for* ***L4•HNEt₃****. U_{eq} is defined as 1/3 of the trace of the orthogonalised U_{IJ} tensor.*

Atom	*x*	*y*	*z*	U(eq)
S1	6729.3(2)	6088.8(4)	6252.8(2)	24.43(11)
S2	6712.7(2)	286.0(4)	1379.6(2)	25.33(11)
O1	7022.9(8)	6248.1(12)	6963.3(7)	33.9(3)
O2	6964.9(8)	6969.0(12)	5902.2(8)	41.4(4)
O3	5964.5(7)	5987.7(13)	5959.5(7)	37.7(4)
O4	8770.1(7)	4748.4(13)	8951.6(7)	37.3(4)
O5	7474.8(8)	4579.9(13)	9193.3(7)	36.9(3)
O6	8922.1(7)	1465.9(14)	3929.9(7)	37.5(4)
O7	7700.5(8)	1763.1(13)	4282.4(7)	35.6(3)
O8	6684.8(8)	-603.8(12)	895.3(7)	39.7(4)
O9	7203.0(7)	23.3(12)	2051.0(7)	32.4(3)
O10	6010.6(7)	591.7(12)	1346.0(7)	34.5(3)
N1	6878.2(8)	3678.8(13)	6997.7(7)	23.2(3)
N2	8004.8(8)	4222.2(14)	7889.0(8)	24.3(3)
N3	7020.9(8)	3989.3(14)	8086.1(7)	24.8(3)
N4	7184.8(8)	2368.1(14)	3178.8(7)	23.2(3)
N5	6965.0(8)	2690.0(13)	2073.7(7)	21.7(3)
N6	8114.1(8)	2092.8(14)	2905.0(7)	23.3(3)
N7	5351.6(8)	7411.6(14)	4787.3(8)	26.4(3)
C1	7281.3(9)	3932.9(16)	7585.4(9)	22.1(4)
C2	7077.9(9)	3676.2(16)	6453.8(9)	21.7(4)
C3	7283.9(10)	2611.8(17)	6259.7(10)	30.9(4)
C4	7472.7(11)	2569.9(19)	5723.4(11)	34.9(5)
C5	7461.9(10)	3586.5(19)	5371.0(10)	33.1(5)
C6	8509.3(10)	4278(2)	7564.4(10)	33.1(5)
C7	8759.3(13)	5545(2)	7564.6(14)	56.2(7)
C8	7237.9(10)	4642.6(18)	5543.5(9)	28.3(4)
C9	7037.6(9)	4700.0(16)	6079.8(8)	21.3(4)
C10	8193.4(10)	4461.5(17)	8545.8(10)	27.4(4)
C11	7528.2(10)	4349.6(16)	8676.7(9)	26.9(4)
C12	6262.1(10)	3861.1(19)	7933.9(10)	31.4(4)
C13	6148.7(12)	3159(2)	8473.3(11)	40.2(5)
C14	5922.8(13)	5085(2)	7810.1(13)	50.6(7)
C15	9107.5(11)	3407(2)	7883.0(12)	44.4(6)
C16	6103.9(14)	1329(3)	3040.2(16)	63.1(8)
C17	6441.9(10)	2535.8(19)	3074.4(10)	31.8(5)

Atom	*x*	*y*	*z*	U(eq)
C18	7397.8(9)	2416.6(15)	2648.7(9)	20.3(4)
C19	7100.5(9)	2661.2(16)	1493.8(9)	20.5(4)
C20	7009.9(9)	1611.8(16)	1126.0(9)	21.4(4)
C21	7125.9(10)	1616.0(18)	544.0(9)	27.8(4)
C22	7309.9(10)	2652(2)	313.9(10)	33.1(5)
C23	9117.9(12)	3031(2)	2767.3(13)	46.5(6)
C24	8575.5(10)	2055.1(19)	2533.7(10)	30.0(4)
C25	8343.5(10)	1816.6(17)	3562.2(9)	27.1(4)
C26	7713.5(10)	1982.9(16)	3745.6(9)	26.3(4)
C27	7265.1(10)	3706.0(17)	1246.0(10)	28.2(4)
C28	7367.3(11)	3701.8(19)	660.0(10)	33.1(5)
C29	6380.4(13)	3343(2)	3597.8(11)	46.5(6)
C30	8899.8(13)	835(2)	2576.8(14)	52.4(7)
C31	5569.9(15)	8751(3)	3972.2(13)	59.9(8)
C32	5886.6(11)	8072(2)	4613.2(11)	37.0(5)
C33	4944.5(11)	6492.7(19)	4291.6(11)	37.5(5)
C34	5406.6(14)	5636(2)	4121.9(13)	51.8(7)
C35	4869.4(11)	8256.4(18)	4934.9(11)	35.3(5)
C36	4456.3(12)	7676(2)	5282.7(12)	44.3(6)
C37	4347.3(14)	1387(3)	1092.2(15)	68.8(9)
C38	4454.3(12)	1773(2)	472.4(12)	47.3(6)
N39	5139.9(9)	2387.6(16)	656.4(9)	37.8(4)
C40	5207.9(12)	3507(2)	1037.6(11)	43.8(6)
C41	4620.4(13)	4388(2)	702.4(13)	50.5(6)
C42	5314.0(12)	2628(2)	56.3(11)	39.3(5)
C43	5322.6(12)	1528(2)	-321.6(11)	44.8(6)

Table A5. *Crystal data and structure refinement for Pd(**L1**)(Allyl)*

Empirical formula	$C_{14}H_{18.68}N_3O_3PdS$
Formula weight	415.49
Temperature/K	173.00
Crystal system	monoclinic
Space group	$P2_1/c$
a/Å	12.4788(3)
b/Å	8.0737(2)
c/Å	15.4867(4)
α/°	90

β/°	90.8190(10)
γ/°	90
Volume/Å^3	1560.13(7)
Z	4
ρ_{calc}g/cm^3	1.769
μ/mm^{-1}	1.339
F(000)	839.0
Crystal size/mm^3	0.25 × 0.2 × 0.2
Radiation	MoKα (λ = 0.71073)
2Θ range for data collection/°	5.69 to 61.136
Index ranges	-17 ≤ h ≤ 17, -11 ≤ k ≤ 11, -22 ≤ l ≤ 22
Reflections collected	102951
Independent reflections	4779 [R_{int} = 0.0342, R_{sigma} = 0.0106]
Data/restraints/parameters	4779/2/247
Goodness-of-fit on F^2	1.161
Final R indexes [I>=2σ (I)]	R_1 = 0.0230, wR_2 = 0.0574
Final R indexes [all data]	R_1 = 0.0255, wR_2 = 0.0585
Largest diff. peak/hole / e Å^{-3}	0.50/-0.93

Table A6. *Fractional Atomic Coordinates (×10^4) and Equivalent Isotropic Displacement Parameters (Å^2×10^3) for Pd(**L1**)(allyl). U_{eq} is defined as 1/3 of the trace of the orthogonalised U_{IJ} tensor.*

Atom	***x***	***y***	***z***	**U(eq)**
Pd1	3873.3(2)	2142.2(2)	8232.9(2)	23.15(4)
S1	2565.2(4)	297.1(6)	6867.4(3)	28.05(9)
O1	2403(18)	-962(19)	6209(11)	36.5(19)
O2	1916(12)	100(30)	7640(10)	30.5(19)
O3	3706.8(10)	577.0(17)	7130.1(9)	30.9(3)
N1	2692.6(11)	3765.3(19)	7716.4(9)	24.7(3)
N2	2917.7(13)	6203(2)	8562.7(10)	31.0(3)
C1	2322.9(13)	4986(2)	8229.4(10)	24.4(3)
C2	5047.4(19)	700(4)	8894.1(14)	45.6(6)
C3	4252(2)	3137(4)	9456.0(14)	49.7(6)
C4	5143(2)	2222(4)	9145.3(18)	32.8(6)
C5	3994.4(16)	6630(3)	8304.4(13)	36.2(4)
C6	2294.9(18)	7280(3)	9124.3(12)	34.2(4)
C7	1150.8(17)	6675(3)	8964.8(14)	38.2(4)
N8	1307.1(12)	5120(2)	8492.4(10)	31.4(3)
C9	446.6(16)	4003(3)	8275.3(15)	39.8(5)
C10	2206.6(12)	3676(2)	6897.7(10)	22.0(3)

Atom	*x*	*y*	*z*	U(eq)
C11	2144.2(13)	2199(2)	6417.0(10)	22.7(3)
C12	1733.2(15)	2194(2)	5573.9(11)	28.9(3)
C13	1347.5(16)	3634(3)	5194.5(12)	33.9(4)
C14	1370.0(16)	5083(3)	5671.7(12)	33.1(4)
C15	1803.0(15)	5120(2)	6501.1(12)	28.2(3)
C8	4448(5)	1752(9)	9487(4)	37.9(14)
O1A	2640(30)	-860(40)	6152(16)	43(4)
O2A	1879(17)	-220(40)	7550(15)	34(2)

Table A7. *Crystal data and structure refinement for Pd(**L1**)$_2$*

Empirical formula	$C_{22}H_{28}N_6O_6PdS_2$
Formula weight	643.02
Temperature/K	173.00
Crystal system	monoclinic
Space group	$P2_1/c$
a/Å	10.5108(3)
b/Å	11.6098(3)
c/Å	20.7431(6)
α/°	90
β/°	93.1820(10)
γ/°	90
Volume/Å^3	2527.34(12)
Z	4
ρ_{calc}g/cm^3	1.690
μ/mm^{-1}	0.951
F(000)	1312.0
Crystal size/mm^3	0.2 × 0.2 × 0.015
Radiation	MoKα (λ = 0.71073)
2Θ range for data collection/°	3.882 to 66.4
Index ranges	$-16 \leq h \leq 15$, $-17 \leq k \leq 17$, $-31 \leq l \leq 31$
Reflections collected	64279
Independent reflections	9643 [R_{int} = 0.0743, R_{sigma} = 0.0566]
Data/restraints/parameters	9643/0/341
Goodness-of-fit on F^2	1.088
Final R indexes [I>=2σ (I)]	R_1 = 0.0431, wR_2 = 0.0914
Final R indexes [all data]	R_1 = 0.0785, wR_2 = 0.1089
Largest diff. peak/hole / e Å^{-3}	0.67/-1.11

Table A8. *Fractional Atomic Coordinates (×10⁴) and Equivalent Isotropic Displacement Parameters (Å²×10³) for Pd(**L1**)₂. U_{eq} is defined as 1/3 of the trace of the orthogonalised U_{IJ} tensor.*

Atom	***x***	***y***	***z***	**U(eq)**
Pd1	2561.9(2)	5070.4(2)	7322.4(2)	13.35(5)
S1	4370.7(6)	4906.0(6)	6210.2(3)	19.92(13)
S2	930.5(7)	5672.1(6)	8392.6(3)	19.75(13)
O1	4257.0(17)	5120.6(15)	6924.1(9)	19.1(4)
O2	5680(2)	5070(2)	6066.8(11)	33.9(5)
O3	3806(2)	3822.9(17)	6012.0(10)	27.5(4)
O4	878.1(18)	5100.0(15)	7738.7(8)	18.7(4)
O5	-351(2)	5797.2(19)	8597.0(10)	32.3(5)
O6	1691(2)	6708.5(16)	8401.6(10)	27.6(4)
N1	1676(2)	5765.7(19)	6518.0(10)	17.2(4)
N2	-483(2)	6296.3(19)	6679.2(11)	21.3(5)
N3	-142(2)	4674(2)	6182.3(13)	25.1(5)
N4	3428(2)	4397(2)	8150.1(10)	20.7(5)
N5	5085(2)	3222(2)	7777.2(12)	25.7(5)
N6	5651(2)	4671(2)	8404.6(13)	28.5(5)
C1	3469(3)	6002(2)	5813.6(12)	19.1(5)
C2	2221(2)	6251(2)	5981.4(11)	16.4(5)
C3	391(2)	5595(2)	6460.0(11)	16.5(5)
C4	-245(3)	7328(2)	7056.3(15)	31.2(7)
C5	-1754(3)	5772(3)	6607.3(16)	29.5(6)
C6	-1539(3)	4757(3)	6157.4(17)	31.1(7)
C8	525(3)	3762(3)	5869.4(17)	33.2(7)
C9	1518(3)	7048(2)	5586.4(13)	23.6(6)
C10	2046(3)	7554(3)	5060.6(13)	29.8(7)
C11	3280(3)	7301(3)	4905.8(14)	35.6(8)
C12	3982(3)	6525(3)	5280.2(13)	27.6(6)
C13	1722(3)	4651(2)	8900.6(12)	19.5(5)
C14	2881(3)	4161(2)	8734.7(12)	18.5(5)
C15	4672(2)	4097(2)	8117.8(12)	18.7(5)
C17	4293(4)	2441(3)	7383.2(15)	38.2(8)
C18	6467(3)	3281(3)	7739.8(18)	42.6(9)
C19	6842(3)	4054(3)	8317(2)	46.2(10)
C21	5540(4)	5528(3)	8905.6(16)	47.8(10)
C22	3446(3)	3366(2)	9178.8(13)	23.6(6)
C23	2894(3)	3097(3)	9750.6(13)	28.7(6)
C24	1745(3)	3591(3)	9902.2(13)	28.2(6)

Atom	*x*	*y*	*z*	U(eq)
C25	1160(3)	4354(2)	9467.2(13)	25.0(6)

Table A9. *Crystal data and structure refinement for Pd(**L1'**)(MeCN)$_2$*

Empirical formula	$C_{14}H_{17}N_5O_3PdS$
Formula weight	441.78
Temperature/K	173.00
Crystal system	monoclinic
Space group	$P2_1/n$
a/Å	10.4228(3)
b/Å	7.3231(2)
c/Å	22.5371(6)
α/°	90
β/°	97.6430(10)
γ/°	90
Volume/Å^3	1704.91(8)
Z	4
ρ_{calc}g/cm^3	1.721
μ/mm^{-1}	1.234
F(000)	888.0
Crystal size/mm^3	0.2 × 0.1 × 0.075
Radiation	MoKα (λ = 0.71073)
2Θ range for data collection/°	4.56 to 63.14
Index ranges	-15 ≤ h ≤ 15, -10 ≤ k ≤ 10, -33 ≤ l ≤ 33
Reflections collected	86676
Independent reflections	5703 [R_{int} = 0.0445, R_{sigma} = 0.0199]
Data/restraints/parameters	5703/0/220
Goodness-of-fit on F^2	1.074
Final R indexes [I>=2σ (I)]	R_1 = 0.0316, wR_2 = 0.0779
Final R indexes [all data]	R_1 = 0.0412, wR_2 = 0.0826
Largest diff. peak/hole / e Å^{-3}	1.09/-0.74

Table A10. *Fractional Atomic Coordinates (×10^4) and Equivalent Isotropic Displacement Parameters (Å^2×10^3) for Pd(**L1'**)(MeCN)$_2$. U_{eq} is defined as 1/3 of the trace of the orthogonalised U_{IJ} tensor.*

Atom	*x*	*y*	*z*	U(eq)
Pd1	3665.2(2)	3010.1(2)	2102.6(2)	26.08(5)
S1	7294.6(6)	2267.6(9)	4277.9(3)	36.25(13)

Atom	*x*	*y*	*z*	U(eq)
O1	7180(3)	3811(4)	4660.6(10)	67.6(7)
O2	6430(3)	798(4)	4371.9(11)	75.4(9)
O3	8616(2)	1667(4)	4300.1(11)	70.8(8)
N1	4625.3(18)	2064(3)	3502.3(9)	29.5(4)
N2	2825.0(17)	3039(2)	2841.5(9)	27.1(3)
N3	2489.3(19)	1845(3)	3725.9(9)	32.8(4)
N4	1916(2)	2462(3)	1536.5(10)	39.7(5)
C1	3350(2)	2340(3)	3348.6(10)	26.0(4)
C2	5331.2(19)	3497(3)	2615.1(10)	25.1(4)
C3	5590.4(19)	2874(3)	3207.8(10)	25.3(4)
C4	1401(2)	3032(3)	2844.3(12)	34.5(5)
N5	4571(2)	2810(3)	1364.8(10)	37.0(4)
C6	1260(2)	2723(4)	3500.1(13)	37.9(5)
C7	2829(3)	1580(5)	4363.8(12)	47.3(7)
C8	6317(2)	4432(3)	2376.1(11)	32.0(4)
C9	7533(2)	4673(3)	2697.5(12)	36.4(5)
C10	7798(2)	3957(3)	3267.2(12)	35.2(5)
C11	6842(2)	3058(3)	3528.3(11)	28.9(4)
C12	5085(3)	2604(4)	956.7(12)	37.9(5)
C13	5765(3)	2349(5)	440.6(13)	50.1(7)
C14	1077(3)	2178(4)	1175.6(13)	42.2(6)
C15	15(4)	1835(5)	698.1(17)	60.8(9)

Table A11. *Crystal data and structure refinement for Pd(**phenolate-1**)*$_2$.

Empirical formula	$C_{14}H_{17}N_5O_3PdS$
Formula weight	441.78
Temperature/K	173.00
Crystal system	monoclinic
Space group	$P2_1/n$
a/Å	10.4228(3)
b/Å	7.3231(2)
c/Å	22.5371(6)
α/°	90
β/°	97.6430(10)
γ/°	90
Volume/Å^3	1704.91(8)
Z	4

ρ_{calc}g/cm^3	1.721
μ/mm^{-1}	1.234
F(000)	888.0
Crystal size/mm^3	0.2 × 0.1 × 0.075
Radiation	MoKα (λ = 0.71073)
2Θ range for data collection/°	4.56 to 63.14
Index ranges	-15 ≤ h ≤ 15, -10 ≤ k ≤ 10, -33 ≤ l ≤ 33
Reflections collected	86676
Independent reflections	5703 [R_{int} = 0.0445, R_{sigma} = 0.0199]
Data/restraints/parameters	5703/0/220
Goodness-of-fit on F^2	1.074
Final R indexes [I>=2σ (I)]	R_1 = 0.0316, wR_2 = 0.0779
Final R indexes [all data]	R_1 = 0.0412, wR_2 = 0.0826
Largest diff. peak/hole / e Å^{-3}	1.09/-0.74

Table A12. *Fractional Atomic Coordinates (×10^4) and Equivalent Isotropic Displacement Parameters (Å^2×10^3) for Pd(**phenolate-1**)$_2$. U_{eq} is defined as 1/3 of the trace of the orthogonalised U_{IJ} tensor.*

Atom	***x***	***y***	***z***	**U(eq)**
Pd1	10000	5000	5000	19.44(9)
Pd2	5000	5000	0	18.75(9)
O1	9789(3)	6346(3)	4404(2)	27.5(5)
O2	3363(3)	3833(2)	-1149(2)	28.0(5)
O3	4432(7)	9635(4)	2497(6)	80(2)
O4	7602(4)	10694(2)	3666(2)	33.7(7)
N0	8705(4)	5308(4)	1927(3)	34.9(7)
N1	11227(3)	4481(3)	3850(2)	23.2(5)
N2	11906(3)	6006(3)	2876(3)	27.5(6)
N3	11158(3)	4058(3)	1773(3)	28.3(6)
N4	5514(3)	6353(3)	-795(2)	22.8(5)
N5	4388(3)	5463(3)	-2729(3)	26.7(6)
N6	4304(4)	7289(3)	-1783(3)	30.8(6)
C1	11412(3)	4816(3)	2873(3)	22.3(6)
C2	8945(5)	8014(4)	4855(4)	35.7(9)
C3	8181(6)	8617(4)	5506(4)	41.9(10)
C4	12434(5)	1809(4)	3595(4)	41.2(10)
C5	12239(4)	2815(4)	3341(3)	31.2(7)
C6	11442(4)	3406(3)	3977(3)	22.9(6)
C7	9122(4)	6982(3)	5076(3)	25.7(6)
C8	12628(5)	7057(4)	3879(4)	35.5(8)
C9	10151(4)	2805(4)	1396(4)	37.5(9)

Atom	***x***	***y***	***z***	**U(eq)**
C10	11422(5)	4778(4)	939(3)	37.2(9)
C11	11986(5)	6109(4)	1689(4)	38.7(9)
C12	2822(4)	2754(3)	-901(3)	27.5(7)
C13	1658(5)	1800(4)	-1601(4)	43.1(11)
C14	1111(5)	688(4)	-1340(4)	49.3(13)
C15	8293(5)	9495(4)	378(4)	40.9(10)
C16	7157(4)	8545(3)	-345(3)	29.9(7)
C17	6584(3)	7424(3)	-91(3)	23.7(6)
C18	4769(3)	6374(3)	-1718(3)	22.1(6)
C19	4946(4)	4498(4)	-3085(3)	33.1(8)
C20	3710(5)	5802(4)	-3612(4)	37.2(9)
C21	3408(5)	6912(4)	-2903(4)	44.6(11)
C22	3954(5)	8034(5)	-750(5)	44.7(11)
C23	4960(30)	9448(9)	2450(12)	340(19)
C24	6254(15)	10036(9)	3930(7)	130(5)